




University of
Stavanger

Faculty of Science and Technology

MASTER'S THESIS

Study program/Specialization: MSc. Petroleum Engineering Well Engineering	Spring semester, 2016 Open access
Writer: Felipe Rios	 (Writer's signature)
Faculty supervisor: Dr. Jan Aasen External supervisor(s):	
Thesis title: Clean-up of horizontal well using ICD	
Credits (ECTS): 30	
Key words: Horizontal well Clean-up Inflow control devices, ICD Stand alone screen, SAS NETool Return permeability Influx rate Drawdown Damage zone	Pages: 81 + Appendix: 15 Stavanger, Jun 15 th - 2016

ACKNOWLEDGMENTS

... Dios es Amor ...

God is love. The glory and victory is to the Lord, thanks to the Almighty for guide me in this way to reach such a great goal.

I want to thank my beautiful and wonderful wife for her courage, patience and for teaching me the wise meaning of a constructive love. Similarly, this milestone is dedicated to my little two daughters; they are God's blessings and angels of infinite happiness.

I would like to dedicate this project to my Family, the greatest treasure and inspiration of my whole life. Thanks mother to embrace grace, love and bounty on my heart. Thanks to my father for teaching me courage, work passion and the real meaning of happiness by enjoy simple details at time goes. Thanks to my adorable sister for the pure fraternal love. Gratitude to all angels I met on this way.

Special thanks to my supervisor Dr. Jan Aasen for her wise guidance, support and technical orientation during the course of the project. Likewise, I want to thank Dr. Arild Lohne from IRIS-International Research Institute of Stavanger for his support and approval on using the lab experimental simulator.

Finally, I want to thank Norway for the opportunity to learn from such a great culture. Thanks Stavanger for the green, calm and safe inspiration and also for being the birthplace of my little baby. Thanks UiS for the innovative orientation and thanks to the entire Faculty of Petroleum Engineering for the great educational curriculum and professional staff.

.....

Dios es Amor. La Gloria y la Victoria son para el Señor, gracias al Altísimo por guiarme en este camino para alcanzar tan grande objetivo.

Quiero agradecer a mi hermosa y maravillosa esposa por su coraje, paciencia y por enseñarme el sabio significado del amor constructivo. Igualmente, este gran triunfo es dedicado a mis dos pequeñas hijas; ellas son bendiciones de Dios y ángeles de infinita felicidad.

Me gustaría dedicar este proyecto a mi Familia, el más grande tesoro y la inspiración más grande en mi vida. Gracias Madre por sembrar un abrazo de gracia, amor y bondad en mi corazón. Gracias Padre por enseñarme el coraje, la pasión por el trabajo y el real significado de la felicidad mientras se disfruta de los detalles simples a medida que pasa el tiempo. Gracias a mi adorable hermana por su amor puro y fraternal. Gratitud a todos esos ángeles que encontré en el camino.

ABSTRACT

An efficient clean-up process is a key factor determining horizontal wells productivity. Numerous factors cause formation damage around wellbore vicinity and numerous treatments have been developed to mitigate each damaging factor. In this project the main damage contributing elements are associated to polymer and particle trapping during drilling stage. Likewise, we set the return permeability as the key factor to define the clean-up process efficiency in horizontal wells completed with ICD-inflow control devices.

Knowing the drilling fluid properties, lab experimental simulations of return permeability are upscale to field conditions under a geometrical damage region established as a truncated cone. Reported dynamic filtration data from a very long horizontal well located in the Norwegian Continental Shelf, is used to define the geometrical damage region; and it is subsequently subdivided into small segments along the horizontal section for improved interpretation. Cumulative flow passing through each segment determines the return permeability and therefore, the clean-up efficiency.

Influx simulations of the horizontal well segments are coupled with the lab experimental simulations to evaluate the evolution in time of the return permeability and its effect at the heel and toe section of the well. In order to impose the drawback of static simulations, we incorporate a transient flow regime analysis into the horizontal well productivity equation.

An iterative process of modelling lead us to find that return permeability recovery is very high at the beginning of the clean-up process while maintaining a slightly increase at late times. The benefit of using ICD-Inflow Control Devices for clean-up process compared to SAS-Stand Alone Screens is demonstrated by the evolution in time of the return permeability at the toe, solving one of the most common concerns in horizontal wells productivity.

This model can be used to determine the time it takes to obtain a certain value of return permeability at the heel and toe of the horizontal section. Likewise, flow rate sensitivity analysis can be performed to obtain the optimum clean-up flow rate for the process. Its great advantage for the well planning stage lies on the fact that no lab experiments needs to be performed and it can be used when no data from production logging is available.

TABLE OF CONTENT

1. Introduction	9
1.1. Background and Problem statement	9
1.2. Scope	9
1.3. Outline of the Chapters	10
2. Modeling the Clean-up process on ICD completions	12
2.1. Formation damage and Well Clean-Up basic theory	12
2.1.1. Formation damage: dynamic filtration during drilling	14
2.1.2. Clean-up: Return permeability	16
2.1.3. Clean-up: Return permeability decay function	18
2.1.4. "Maximize" software tool	18
2.2. ICD basic theory	21
2.2.1. ICD definition and flow path	21
2.2.2. ICD classification and benefits	22
2.2.3. ICD physics	24
2.3. Horizontal well productivity, Joshi Model	25
2.4. Transient flow in horizontal wells	31
2.5. NETool™ software model and simulation method	34
3. Simulation and results	37
3.1. Modeling process structure	37
3.2. Well definition	39
3.3. Completion type – SAS	40
3.4. Transient flow incorporated into Initial case	42
3.5. Completion type – ICD	44
3.6. Formation damage and clean-up	47
3.6.1. Radius of invasion	47
3.6.2. Damage permeability – "Maximize simulation tool"	50
3.6.3. Return permeability – "Maximize simulation tool"	53
3.6.4. Upscaling the return permeability and clean-up process	56
4. Discussion	66
4.1. SAS vs. ICD drawdown and influx rates	66
4.2. Flow regimes and transient pressure	68
4.3. Final model analysis and benefits of ICD during clean-up	69

5. Conclusions and recommendations	74
6. References	76
Appendix A	80
Appendix B	82
Appendix C	90
Appendix D	91

LIST OF FIGURES

Figure 1. Solid particles size and plugging tendency (adapted from Bellarby, 2009)	12
Figure 2. Clean-up in high permeable horizontal sections (Bellarby, 2009)	13
Figure 3. Inflow control device, ICD (Aadnoy & Hareland, 2009)	21
Figure 4. Inflow control devices classification	23
Figure 5. Drainage volume: Vertical well (left) & Horizontal well (right)	26
Figure 6. Horizontal well drainage, 2D simplified solution.....	27
Figure 7. Horizontal well flow regimes.....	31
Figure 8. Modeling process structure.....	38
Figure 9. Horizontal well definition.....	39
Figure 10. SAS Completion – Pressure results	40
Figure 11. SAS Completion – Influx results	41
Figure 12. ICD Completion – Pressure results.....	45
Figure 13. ICD Completion – Influx rate	46
Figure 14. Dynamic and static losses.....	47
Figure 15. Time - dynamic and static losses.....	48
Figure 16. Filtrate flux.....	49
Figure 17. Radius of invasion.....	49
Figure 18. Pore volume injected during mud flooding	51
Figure 19. Reduction in permeability over time	52
Figure 20. Reduction in permeability vs. Pore volume injected.....	52
Figure 21. Pore volume injected during flow back.....	53
Figure 22. Return permeability variation during flow back.....	54
Figure 23. Return permeability variation vs. Pore volume.....	55
Figure 24. Damage region - Truncated cone.....	56
Figure 25. K_{return} upscaling process	57
Figure 26. PV produced, evolution @ early times.....	58
Figure 27. Return permeability evolution @ early times.....	59
Figure 28. PV produced, evolution @ late times.....	60
Figure 29. Return permeability evolution @ late times.....	60
Figure 30. Clean-up time @ heel and toe based on K_{return}	61
Figure 31. Drawdown evolution during clean-up: ICD vs. SAS.....	63
Figure 32. Influx rate evolution during clean-up: ICD vs. SAS.....	64
Figure 33. Detailed Influx rate evolution during clean-up: ICD.....	65
Figure 34. ICD and SAS Drawdown pressure	67
Figure 35. ICD vs. SAS Completion – influx rate.....	68
Figure 36. Clean-up time for SAS and ICD completion	71
Figure 37. Skin removal during clean-up	72

LIST OF TABLES

Table 1. Geometric factors for Joshi model 29
Table 2. Well & Reservoir properties 39
Table 3. Calculated horizontal flow regime limits 44
Table 4. Drilling fluid properties 50
Table 5. Time steps and reservoir width..... 63

LIST OF EQUATIONS

Equation 1, Dynamic filtration.....	15
Equation 2, Radius of invasion.....	15
Equation 3, Trapping rate.....	16
Equation 4, Permeability (Carman-Kozeny)	17
Equation 5, Effective pore diameter.....	17
Equation 6, Return permeability decay function	18
Equation 7, Pore throat porosity Equation 8, Specific surface.....	20
Equation 9, Effective permeability Equation 10, Coefficient a.....	20
Equation 11, Nozzle pressure drop	24
Equation 12, Flow coefficient	24
Equation 13, Potential function.....	26
Equation 14, Horizontal plane production rate.....	27
Equation 15, Vertical plane production rate	27
Equation 16, Horizontal well production rate – Joshi model.....	28
Equation 17, Drainage radius.....	28
Equation 18, Drainage radius – Ellipse.....	29
Equation 19, Horizontal well production - Anisotropy.....	29
Equation 20, Effective wellbore radius	30
Equation 21, Horizontal skin.....	30
Equation 22, LRF pressure transient.....	32
Equation 23, LRF Time limit in pressure transient.....	33
Equation 24, Apparent skin	33
Equation 25, Pseudo skin - LRF	33
Equation 26, Flow rate model	35
Equation 27, Pressure gradient.....	35
Equation 28, Pressure transient adjustment.....	43
Equation 29. Return permeability functions.....	54
Equation 30. K_{return} @ Heel, evolution in time.....	61
Equation 31. K_{return} @ Toe, evolution in time.....	61
Equation 32. Volume of truncated zone (Segmented damage region)	62
Equation 33, ILF pressure transient.....	80
Equation 34, ILF Time limit in pressure transient.....	80
Equation 35, ILF condition.....	81
Equation 36, Pseudo skin – ILF	81

1. Introduction

1.1. Background and Problem statement

Clean-up process of a well is a critical stage that determines and/or influence productivity of the well, which indeed motivate this study. It is performed as the start-up sequence once the well has been drilled and completed and consists basically into cake removal around the wellbore and backflow of filtrate and debris that cause nearby and reservoir damage.

Due to the increased areal exposure of horizontal wellbores to the reservoir section compared to vertical wells, this clean-up stage is subsequently more extensive in time, resources and complexity. In addition, permeable horizontal wells experience increased pressure drop from heel to toe due to friction, which may affect the effective drawdown applied to each part of the horizontal section. Irregular or uneven drawdown across the horizontal section will lead to zones not been cleaned up properly and consequently to less production.

Inflow control devices or ICD have been used since more than two decades as type of completion for horizontal wells in order to balance the drawdown across the entire section. So, by using them is claimed that clean-up process is improved and less concerns are imposed to the productivity reduction as given by Al-Khelaiwi et al., (2009).

The objective of this project is to develop a model to simulate this phenomenon in horizontal wells completed with inflow control devices by using Maximize software (lab return permeability modeling) and NETool™ software (a micro-nodal analysis tool that integrates reservoir properties and completion architecture in the wellbore vicinity) incorporating segmented, time-dependent skin analysis and transient flow to improve results. The primary aim of the thesis is that the presented model will help to understand and simulate the clean-up process for such wells under planning stage where not production data neither lab data are available; and it could help to predict how long it takes to obtain a given value of return permeability at the heel and the toe sections, similarly it may benefit to evaluate the best cumulative flow values to be used during clean-up stage, and furthermore improve productivity.

1.2. Scope

The thesis scope is to purpose a hydraulic model to simulate the clean-up phenomenon in ICD completions including fluid invasion and pore throat trapping as

mainly contributors to formation damage. It is important to mention that emulsions, clay swelling, phase trapping, wettability effects, chemical adsorption and biological activities are also contributing factors for this process as given by Civan, (2007, pp. 5-7); nevertheless they are not covered under this study. Similarly, ICD are also used into heterogeneous reservoirs to balance zonal drawdowns, where high permeable zones are cleaned up preferentially. However, the study is more focused into ICD utilization to offset heel to toe effect on isotropic reservoirs.

1.3. Outline of the Chapters

This project is mainly structured as follow:

- Literature revision about formation damage and clean-up process, dynamic filtration and return permeability modeling in “Maximize” software tool, as well as ICD definition, classification and benefits. It also includes Joshi horizontal well productivity model, transient flow and physics behind the micro-nodal analysis, all topics covered in Chapter 2.
- Simulations and results are covered in Chapter 3. It starts with an explanation of the modeling process structure or in other words, the methodology adopted to develop this model, then the initial model set up, adjustment to transient flow, ICD model and nozzle design. Furthermore, it shows the return permeability simulation and final influx estimation comparing initial model and ICD model.
- Discussions of basic and final model results are covered in Chapter 4. It also includes the benefits and application of the proposed model.
- Conclusion and recommendations are covered in Chapter 5.

In the preparative work, a very long horizontal well is defined. Well geometry and reservoir properties are established for this particular well. Structure of the study is based on an initial model of a stand-alone screen completion or SAS until model is adjusted for transient flow. A skin model is then incorporated into the initial model and escalated to an inflow control devices or ICD completion. Sensitivities studies are performed in order to optimize the model and analyze results.

NETool™ software (Halliburton) is used to simulate influx in the wellbore by coupling fluid flow through porous media and hydraulic flow into nozzle type ICD completion architecture. This detailed micro-nodal analysis benefits to study the Clean-Up process by establishing segmented skin and formation damage and analyzing wellbore inflow when using ICD completions.

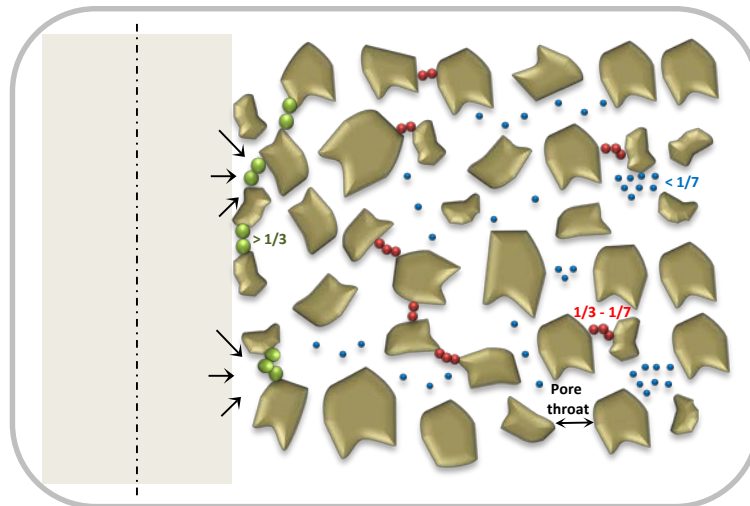
Maximize software (IRIS – International Research Institute of Stavanger) is used to simulate return permeability experiments from lab and then upscale them to the field case to evaluate clean-up. Its output is used as input for NETool™ simulation of the influx rate and cleans-up processes.

2. Modeling the Clean-up process on ICD completions

In this chapter the main literature and mathematical formulations used in the model are presented. They cover three main topics: formation damage and well clean-up, ICD or inflow control devices physics and finally transient flow. The two software general mathematical models used develop the project are also covered in the chapter.

2.1. Formation damage and Well Clean-Up basic theory

Well clean-up process corresponds to the stage of drilling debris removal including drilling fluids, filtrate and mud cake coming out of the formation while production is started on a well, as defined by Schlumberger oilfield glossary, (2016). During drilling and completion stage, mud filtrate penetrates the formation causing formation damage or reduction in permeability in the wellbore vicinity. Mud cake is built up around the wellbore creating an impermeable layer that regulate the invasion of the filtrate. Fluids contents solids are designed to bridge the formation and reduce invasion. Figure 1 adapted from Bellarby, (2009, p. 44) shows the internal and external cake caused by particles, in which particle size is compared to pore throat size.



$$\left(\begin{array}{c} > \frac{1}{3} \text{ Pore throat} & \left| \frac{1}{7} \text{ to } \frac{1}{3} \text{ Pore throat} \right. & < \frac{1}{7} \text{ Pore throat} \\ \text{Form external cake} & \text{Form internal cake} & \text{Pass through formation} \\ \text{Easy to back produce} & \text{PLUGGING tendency} & \text{Easy to back produce} \end{array} \right)$$

Figure 1. Solid particles size and plugging tendency (adapted from Bellarby, 2009)

It is suggested that particles sizes between $1/7$ to $1/3$ of the pore throat size have a plugging tendency and are difficult to back produce. During well clean-up process we aim to remove the internal and external cake across formation.

Removal of the internal filter cake and external cake is done by producing the well at specific rates during first well flow or well testing period, being the latest a very frequent stage in exploratory and new wells. External filter cake experience a lift-off pressure that needs to be offset by the zonal drawdown pressure. These effects will define the effective or poor clean-up process of specific zone across the horizontal section, and then, the productivity of well according to Bellarby, (2009, p. 43). Other models consider flow rate and local velocity as clean-up contributors as mentioned by Egerman et al., (2002).

One of the main concerns in high permeable horizontal wells, and generally speaking in most of horizontal wells, is the limited production through the entire horizontal section. In other words, parts of the horizontal section do not flow at all due to cake lift-off pressure being higher than the sectional drawdown. As mentioned previously, frictional pressure drop along wellbore and high influx due to high permeability aggravate it and create irregular flow contribution for isotropic cases, leading to a poorer clean-up process at the toe as shown in Figure 2 adapter from Bellarby, (2009, p. 45). In the other hand, heterogeneous reservoirs have a tendency to better clean-up in high permeable formations.

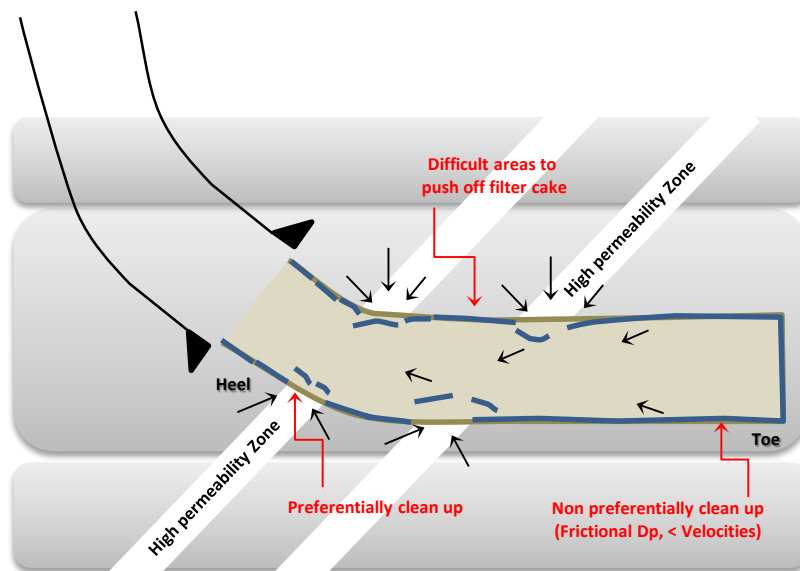


Figure 2. Clean-up in high permeable horizontal sections (Bellarby, 2009)

Before analyzing clean-up process, the formation damage is mainly established in the model due to dynamic filtration during drilling, and then the return permeability is chosen as the key parameter to obtain an efficient clean-up process after the well is

flow back during production. So, these two factors are chosen into the model as they are the main quantitative and qualitative contributors to formation damage and clean-up process of this particular case.

A more detailed analysis of the factors affecting the clean-up process additional to the cake lift-off pressure mentioned by Bellarby, (2009) is presented in this project.

External cake lift-off pressure is different to the FIP-Flow initiation pressure. The lift off pressure is more related to the pressure need to remove the cake, while the FIP depends on solids invasion according to Suri & Sharma, (2005). External filter cake and FIP-flow initiation pressure are another parameters used to evaluate clean-up process, however is well reported that external cake has not role in the flow initiation pressure neither in the return permeability as given by Suri & Sharma, (2005, pp. 11-17). FIP has more influence in low permeability formations (<10 mD) as given by David et al., (2014) and it represents a very short time in the transient flow period of clean-up, so it is not the case of our study which include later periods and higher permeability formations.

Our main focus are the dynamic filtration and solids invasion as formation damage factors in order to estimate the reduction in permeability, then we analyze the improvement of the permeability during flow back considering the cumulative flow that pass over an specific surface area as given by Ding et al., (2002) and Lohne et al., (2010). It represents a clean-up model that considers the amount of fluid produced in a specific area (cumulative influx rate/area) of the well rather than only the differential pressure to lift the cake as considered by other mentioned models. It is important to mention that flow rate only accelerate or decelerate the process, while the cumulative flow represents the efficiency of the clean-up process.

The model uses formation damage and return permeability simulator that mimics the lab experiments, and it is called Maximize software tool. It is combined with the near wellbore flow simulation across horizontal well using NETool™ software. This project analyze clean-up process using internal filter cakes by defining skin factor from invasion depth and damage permeability ratio, and they are better covered in the simulation method described in Chapter 3.1

2.1.1. Formation damage: dynamic filtration during drilling

Formation damage is defined by Bennion, (1999) as “The impairment of the invisible, by the inevitable and uncontrollable, resulting in an indeterminate reduction of the unquantifiable”. It clearly states the complexity to quantify and represent formation damage. In our case, dynamic filtration is the main formation damage contributor.

Dynamic filtration of the fluid into the formation causing a radius of invasion and pore throat trapping due to particle sizes are covered in this project to represent the damage zone. Return permeability values from laboratory experiments are evaluated dynamically to model the clean-up efficiency.

During drilling, mud filtrate invades the porous formation while forming a filter cake at the wellbore face. Initially, spurt losses are experienced into the formation until particles sizes accumulate in front of the wellbore to form a filter cake. In no circulating conditions, only static losses invade a short radial distance in the wellbore. Yet, during circulating periods or dynamic conditions the filtrate invade a higher distance in the wellbore causing an increased damage zone. Filtration stages are modeled by Equation 1 that represents the accumulated dynamic filtration volumes as given by van der Zwaag et al., (2012).

$$V_d = \underbrace{V_{sp}}_{\text{Static filtration}} + A\sqrt{t} + B.t$$

Equation 1, Dynamic filtration

Where,

$V_d \rightarrow$ *Dynamic filtration*

$V_{sp} \rightarrow$ *Spurt losses*

$A, B \rightarrow$ *Coefficients*

$t \rightarrow$ *Time*

A semi-empirical mathematical model for estimate invasion rate and invasion depth was introduced by Breitmeyer et al., (1989) in a basic leaky piston form as shown in Equation 2. This method allows us to relate the dynamic filtration volume and the radius of invasion to determine the damage zone extension along the horizontal wellbore length as it is better explained next chapter in results section. If we know the losses in the well, we can estimate the dynamic fluid filtration and radius of invasion.

$$r_i = \left\{ r_w^2 + \frac{2r_w}{\phi S_i} \int C_m dt \right\}^{0,5}$$

Equation 2, Radius of invasion

Where,

$r_i \rightarrow$ Radius of invasion

$r_w \rightarrow$ Wellbore radius

$\emptyset \rightarrow$ Porosity

$S_i \rightarrow$ Average filtrate saturation

$C_m \rightarrow$ Filtrate flux or mud cake constant

2.1.2. Clean-up: Return permeability

Return permeability (k_{return}) is defined as the ratio of the final formation permeability k_d over initial formation permeability k , after oil is flushed back ($k_{\text{return}}=k_d/k$). It is key parameter to evaluate clean-up process efficiency. The final formation permeability k_d can also be interpreted as the damage permeability at certain moment. The return permeability then, varies from 0 to 1. Today, this value is mainly obtained after various lab experiments. In general terms, mud particles invade the formation causing a reduction in permeability called damage permeability. Main purpose of a good clean-up is to reach the return permeability in an efficient manner and in short time as reasonable possible. During filtration, mud particles are trapped into the formation pore throat or filter cake depending of particles size and filter cake permeability. Pore throat trapping and pore lining retention are considered two physical factors for particle accumulation during filtration process as given by Lohne et al., (2010). Equation 3 summarizes the trapping rate for every particle size. We do focus our analysis on pore throat trapping as main contributor of the effect.

$$\frac{d\sigma_i}{dt} = \lambda_i C_i u$$

Equation 3, Trapping rate

Where,

$i \rightarrow$ Subcomponent, each particle size

$\lambda_i \rightarrow$ Detrapping term [1/Length]

$C_i \rightarrow$ Concentration of component i

$u \rightarrow$ Darcy velocity

In a dynamic process, mud particles of different sizes based on a particle size distribution or PSD are transported into the formation pore throats after spurt losses, and then a filter cake is built up at wellbore surface. Looking at this process in time steps, the pore throats get smaller as particles are deposited and similarly the filter cake permeability and porosity change due to deposition of large particles size. This process is modeled using Equation 4 as given by Lohne et al., (2010). It is called the

Carman-Kozeny approach that includes the properties of trapped particles through specific surface area and relate permeability to porosity simulating porous media as bundle of tubes. Smaller particles (mainly polymer components) are allowed to pass through the filter cake and reduced formation pore throat. This process forms the called external filter cake and the internal filter cake. During drilling and fluid circulation the filter cake is constantly eroded and refilled, so filter cake remains almost in few millimeters of thickness while the invasion of particles and losses increase during drilling and fluid circulation.

$$k = \frac{\phi^3}{2\tau(1 - \phi)^2(S_o)^2}$$

Equation 4, Permeability (Carman-Kozeny)

Where,

$k \rightarrow$ Permeability

$\phi \rightarrow$ Porosity

$\tau \rightarrow$ Tortuosity, effective flow path

$S_o \rightarrow$ Specific surface area, for spheres: $6/D_p$

$D_p \rightarrow$ Particle diameter

The bundle of tubes approach used by Carman-Kozeny considers the specific surface area (surface to volume ratio) of each component (particle size) and includes the effective pore diameter as shown in Equation 5. Combining Equation 3, 4 and 5 at different time steps we can obtain the permeability change in time during damage and backflow.

$$D_\phi = \sqrt{\frac{32\tau k}{\phi}}$$

Equation 5, Effective pore diameter

Where,

$D_\phi \rightarrow$ Tube diameter, all tubes have same diameter

It is important to mention that clean-up efficiency can be evaluated from different factors similarly to the diverse numbers of elements causing formation damage, for instance: relative permeability K_r , flow initiation pressure or cake lift-off as given by Rana & Sharma, (2001) and Zain & Sharma, (2001). Our analysis is based on return permeability as a holistic factor, and through the model we do simulate lab experiments for better interpretation. Others damage mechanisms and clean-up factors are out of scope in this project.

2.1.3. Clean-up: Return permeability decay function

Similarly Han et al., (2005) presented a simplified profile for return permeability based on a dimensionless invasion depth for cores analysis. An exponential decay function described in Equation 6 is used for this purpose, and it is presented in this project to compare the lab experimental simulations. Coefficients a and b are obtained from laboratory experiments if at least two pressure measurements are known. An average of this simplified function is estimated integrating the decay function and it corresponds to an input being used for NETool™ simulations.

$$RP_x = 1 - ae^{-bx}$$

Equation 6, Return permeability decay function

Where,

$RP_x \rightarrow$ Return permeability as function of x

$a \rightarrow$ Coefficient, damage at mud surface due to invasion

$b \rightarrow$ Coefficient, distribution of damage

$x \rightarrow$ Dimensionless invasion depth $\left(\frac{x}{L}\right)_{core}$

An interesting similarity of the return permeability is found between the current model and the decay function and it is better covered in the discussion chapter.

2.1.4. "Maximize" software tool

A simulation tool called "Maximize" from IRIS-International Research Institute of Stavanger developed by Lohne et al., (2010) is used to evaluate particle transportation during return permeability simulations of laboratory experiments, and it is used as input for the NETool™ software simulation to distinguish influx rate evolution while return permeability change in time, starting at initial damage permeability (after drilling, before clean-up) until complete flow back (after clean-up).

The tool can simulate: filter cake build up under static and dynamic conditions, fluid loss in linear and radial geometry, transport of solids and pore throat plugging, salinity effects and multi-component water base mud. We do focus the study on return permeability evolution in time due to transport of solids, and we upscale

values from lab to field in order to match the evaluation of influx rate and clean-up process.

How it works? The core is represented in grid blocks and solution is moving forward in time by solving changes in time step. IMPES method (implicit pressure, explicit saturation) is used to solve the pressure equation in the flow model. Dissolved and dispersed components of the mud are defined, as well as particle size of solids, polymer properties and formation properties. Boundary conditions are established for the outputs.

What does the software model? The filter cake model is based on dynamic filtration and it also uses the Equation 1. Solids and polymers are both analyzed. In polymers, their effects on fluid viscosity and polymer sizes may affect dynamic filtration. In solids, two mechanisms are added into the filter cake model: de-attachment and erosion. Cake permeability model is based on Equation 4 and 5, while compressibility effect is integrated into the calculation. One of the important parameters that is of our focus is particle retention in the formation. It is based on Equation 3 and it covers two mechanism of particle retention: pore throat trapping and pore lining retention. Main focus is on pore throat trapping as higher contributor to the retention effect. Exchange cations are analyzed in the salinity and clay swelling model that affect the pore volume available for flow.

What kind of output is delivered? Diverse scenarios can be analyzed like: polymer particle accumulation in time, phase relative permeability evolution in time, pore volume injected, cake permeability and porosity evolution in time, and so on. We do concentrate our results in the evolution of return permeability at different time steps during flow back. As mentioned previously, those values of return permeability are inputs in NETool™ to simulate and evaluate influx rate/area.

Two methods are used to compute permeability reduction in time over the damage zone:

- a) Effective harmonic average between cake permeability and the original permeability of the rock.
- b) First, pore throat permeability is calculated based on a fraction of total pore space. Then a specific surface area (Volume/Area) is estimated for each solid and polymer particle based on Equation 4. Finally, porosity is corrected due to deposited material and new permeability is calculated based on surface area and corrected porosity. An effective harmonic average within the original permeability of the rock, determine the final permeability reduction as described by Equation 7, 8, 9 and 10 following an iterative routine.

$$\phi_{pore\ throat} = \phi \left(1 - \frac{\sigma_p + \sigma_s}{a} \right)$$

Equation 7, Pore throat porosity

$$S_{0\ pt} = \frac{S_o(1-\phi)a + (S_{0s}\sigma_s + S_{0p}\sigma_p)\phi}{(1-\phi)a + (\sigma_s + \sigma_p)\phi}$$

Equation 8, Specific surface

$$k_{eff} = \left[\frac{a}{k_{pt}(\phi_{pt}, S_{0\ pt})} + \frac{1-a}{k} \right]^{-1}$$

Equation 9, Effective permeability

$$a = \max\left(f_{pt}, \frac{\sigma_s + \sigma_p}{1 - \phi_{ic}}\right)$$

Equation 10, Coefficient a

Where,

ϕ → Porosity

σ → Trapped material

S_o → Specific surface area, for spheres: $6/D_p$

a → $\sigma_s - \sigma_p / (1 - \phi_{internal\ cake})$

$k_{pt}(\phi_{pt}, S_{0\ pt})$ → Permeability based on Equation 4

f → Modification factor

p : polymer, s : solids, pt : pore throat, ic : internal cake

This is mainly the model that the software uses and we will not present details of the mathematical approach. A more systematic methodology of the software can be found as given by Lohne et al., (2010).

The advantage of using this simulation tool into the model can be summarized as follow:

- Integrate lab experiments for different fluid properties
- It models variation of fluid losses and return permeability in time
- Incorporate particle trapping and filtration mechanism to define damage
- Main variables or output are modeled in time and pore volume.
- We can integrate data from lab experiments into an influx simulator to upscale it to field conditions. It adds value due to the limitations to perform real lab experiments and the associated requirements.

2.2. ICD basic theory

2.2.1. ICD definition and flow path

Inflow control devices or ICD are a type of completion tubular or equipment commonly used in horizontal wells on today's. In general terms, we can describe them as a screen having a close inflow path that diverge the entire flow through only a small area in order to induce a pressure drop inside the tool. It is important to mention that not all ICD in the market have a filter media (or screen) around it, but the use of no filter media-ICD type is very limited to consolidated formations.

Similarly to a screen joint, which have a base pipe as the central structure, it also has a filter media, drain layer and protective shroud. From the manufacturing point of view, screen joints have a perforated base pipe (in which no considerable pressure drop is generated) while inflow control devices have a non-perforated base pipe and instead a "choke module" wherein flow is diverted as shown in Figure 3 taken from Aadnoy & Hareland, (2009), creating a favorable pressure drop.

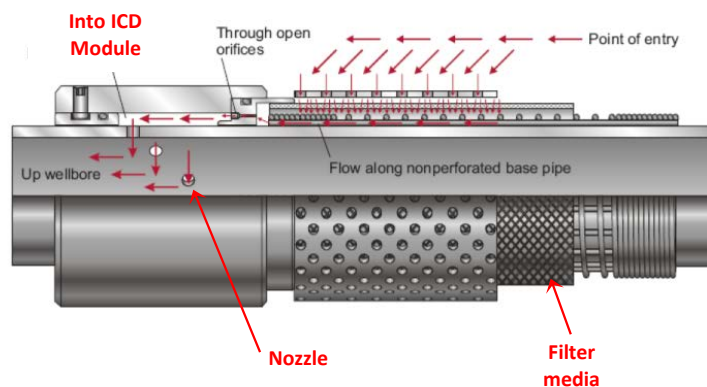


Figure 3. Inflow control device, ICD (Aadnoy & Hareland, 2009)

Flow coming from reservoir arrives to the inflow control device radially entering the protective shroud (small red arrows in Figure 3), and then it continues radially until the filter media where sand control production is restricted. Clean production fluid travels now in axial direction to the ICD module located at the end of the joint. Very fine particles are allowed to flow within the fluid phase as part of the sand control design, so plugging is avoided as particles would not be able to bridge into the restricted area. Once the reservoir fluid arrives to ICD module, it is diverted into the restricted area (< 4 mm) that can be a small tube, nozzle, plate, helical path and so on.

A pressure drop is generated in this module and intrinsically transmitted to the reservoir section. Finally flow pass through the ICD joint restricted area to the inner part of the completion, traveling up to the top of the well via the tubing. A well is completed using many ICD joints and each joint has its own restricted area. Often, segmented compartments are designed into the horizontal section by using packers, so more radial flow is induced into the completion and less annular axial flow is allowed.

Inflow control devices have mainly uses in horizontal wells or highly deviated wells to counteract against heel to toe effect, coning/cresting phenomenon as well as uneven drawdown across entire horizontal section. Different flow geometries are used by service companies like Schlumberger, Halliburton, Baker Hughes, Weatherford, Tendeka, Inflow Control and so on in order to generate the desired pressure drop.

2.2.2. ICD classification and benefits

Previous master thesis projects at UiS have covered an extensive literature of the different types of inflow control devices. Bensnes Torbergsen & Aadnøy, (2010, p. 22) classify them as helical, orifice (nozzle), tube and hybrid types belonging to the passive ICD type. Kasa et al., (2011, pp. 13-16) and Gimre & Aadnøy, (2012, p. 26) incorporate description of the active ICD type or commercially known as autonomous or self-adjusting inflow control devices, in which RCP (rate controlled production), Equiflow autonomous, Bench AFD and autonomous inflow control valves are included.

Figure 4 shows the main types of the ICD: passive and active type. The first type, called passive ICD is described as static or constant area restriction that is installed in the completion and remains the same until it is removed.

Dynamic inflow control devices are also a type of passive ICD that incorporates special features for "shift to purpose" by using well intervention (slickline, coiled tubing, wireline, joint pipe). "Shift to purpose" means the ICD module have extra flow paths for fluid injection, fully production, secondary nozzle type or standard on-off choices to isolate one zone or compartment as given by Absolute Completion Technologies - Inflow control , (2016). It can also incorporate dissolvable ball valves as given by Schlumberger - Inflow control devices, (2016).

In the other hand, active inflow control devices have a variable area restriction that self-regulate or adapt to changes in reservoir pressure or type of fluid flowing through it as described by Al-Kadem et al., (2015). Use of inflow control devices as part of completion design benefits for equalizing the desired pressure drop along the

entire horizontal section, delaying water breakthrough, reducing coning/cresting effects, benefiting the toe part of the well and counteracting heterogeneous influx due to frictional pressure drop and permeability variances. Physical principle of nozzle type ICD is discussed in next chapter.

There are other flow control devices categorized mainly as flow control valves that also graduate a downhole choking area. They are activated from surface via hydraulic control lines and they correspond to the main component of smart completions. Passive ICD nozzle type is the basic design used for analysis in this project. Next chapter presents a comprehensive approach of ICD physics.



Figure 4. Inflow control devices classification

2.2.3. ICD physics

The key parameter regarding of inflow control devices is the generated pressure drop inside the tool and it is governed by the Bernoulli's principle applied to incompressible fluids ($v^2/2 + gz + P/\rho = \text{constant}$) relating velocity v , gravity g , height z , pressure P and density ρ . Pressure drop is calculated as follow:

$$\Delta P = \frac{\rho v^2}{2C^2} = \frac{\rho Q^2}{2A_{valve}^2 C^2} = \frac{8\rho Q^2}{\pi^2 D_{valve}^4 C^2}$$

Equation 11, Nozzle pressure drop

Where, Equation 11 represents pressure drop through an orifice or nozzle:

ΔP → Pressure drop across orifice

ρ → Average fluid density

V → Fluid velocity through orifice

Q → Fluid flow rate through orifice

A → Area of orifice

D → Diameter of orifice

C → Flow coefficient

Flow coefficient is derived for a single orifice and corresponds to:

$$C = \frac{C_D}{\sqrt{1 - \beta^4}} = \frac{1}{\sqrt{K}} \dots \dots \dots \text{where } \beta = \frac{D_2}{D_1}$$

Equation 12, Flow coefficient

Where:

C_D → Discharge coefficient

K → Pressure drop coefficient

Passive ICD follow the principle of $dp \sim q^2$, while autonomous ICD uses $dp \sim q^n$ where $3 \leq n \leq 5$, as mentioned in Landmark NETool Technical Manual, (2014). The smaller the nozzle size the higher is the pressure drop. Different types of ICD use specific equations for particular flow path geometry. For instance, tube or tubular type ICD includes friction factor and minor loss coefficients within tubes and ICD channel type includes same parameters through the channel. Spiral flow path type is

classified experimentally by density and viscosity ranges. Nozzle type is used in this analysis and Equation 11 and 12 describe the pressure drop model. Physics behind other non-nozzle type ICD is out of scope in this analysis and it can be accessible through previously mentioned vendors and their specific models.

An inflow control device may have many nozzles and its corresponding total pressure drop per joint. Equation 11 and Equation 12 are applied to each nozzle and summed up for each joint. Frequently, the horizontal section of the well is compartmentalized by installing isolation packers. Each compartment can contain one or many ICD joints. The desired pressure drop for a specific compartment (or specific ICD joint) is then calculated until balance the frictional pressure drop, and it is better explained in Chapter 2.5. ICD nozzle pressure drop is designed in such way that frictional pressure drop inside tubing is coupled with reservoir pressure drop. Special drainage areas and horizontal well productivity models describe the pressure drop or drawdown between reservoir and wellbore, and they are better describe in next section.

2.3. Horizontal well productivity, Joshi Model

Why is the horizontal well productivity model important? Answer to this question is the motivation of the current project in which we look for a model to improve clean-up in horizontal wells, removing skin factor smartly and totally along horizontal section. So, incorporating skin factor into well productivity model help us to study clean-up process on ICD completions. Skin is then included by defining return permeability values at specific segment of the well. Some of the horizontal well productivity models in the literature are: Joshi, (1988) assuming infinitive conductivity; Babu & Odeh, (1989) assuming uniform flux; Economides, & Frick, (1996) assuming also infinitive conductivity and applicable to multilaterals wells on same plane, and so on for each specific case. They are derived assuming different assumptions, so they are not directly comparable.

In this project, fluid flow from reservoir to a horizontal wellbore is modeled based on Joshi, (1988). Model is established using potential fluid theory, it means that pressure response is compared with an electrical analog and experiments were conducted to validate the model. Joshi model is highly acceptable and accurate in horizontal well productivity calculations on today's. For cases under its boundary conditions and assumptions, it reflects infinitive conductivity or negligible pressure drop at wellbore. NETool™ software also incorporates it into the micro-nodal analysis, so those are reasons to choose this model for the project.

Conventional vertical well drains according to a circular cylinder while horizontal well drains according to an ellipsoid as stated in Joshi model and shown in Figure 5. It describes the pressure function (hyperbolic) in ellipses representing constant pressure (dashed line in Figure 6) while flow velocity function (trigonometric) is presented as hyperbolas (blue arrows in Figure 6). Both are compared and a solution is found to describe the analogy of potential function vs. pressure as described in Equation 13.

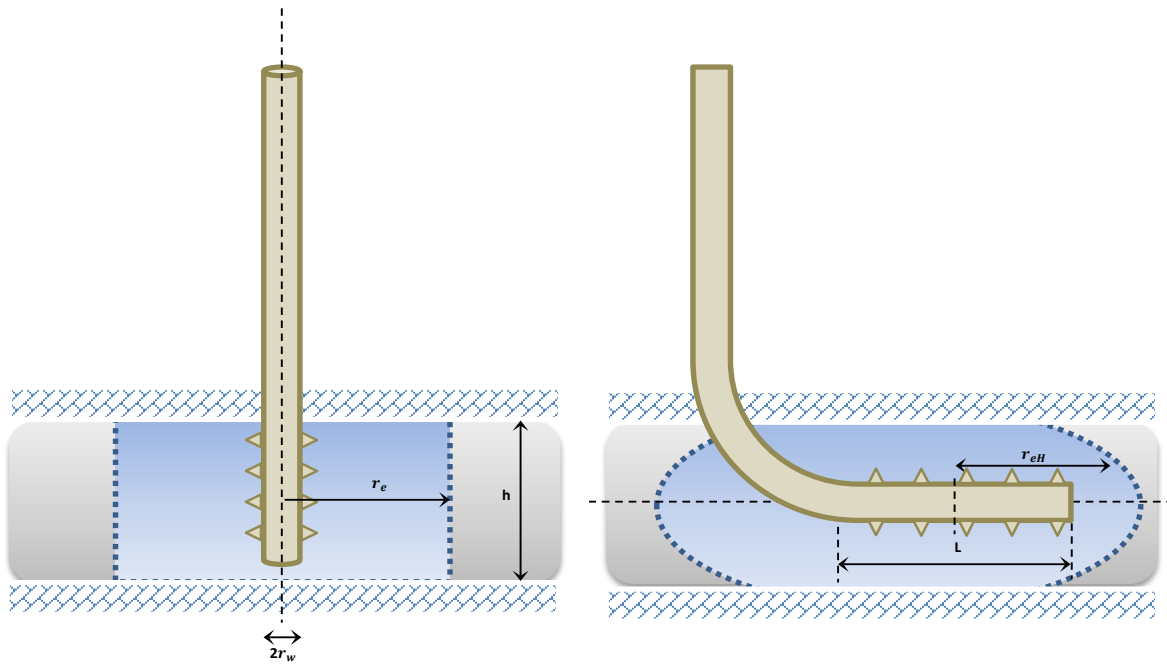


Figure 5. Drainage volume: Vertical well (left) & Horizontal well (right)

$$w(z) = \phi + i\Psi = \cos^{-1}\left(\frac{z}{\Delta r}\right)$$

Equation 13, Potential function

The general equation is then solved establishing boundary conditions to a well of length L , assuming the well located along x axis. In this equation the potential function ϕ is the same as pressure P . This represents the principle of potential fluid theory.

Where:

$z \rightarrow z = x + iy$

$\phi \rightarrow$ Pressure function

$\Psi \rightarrow$ Flow velocity function

$\Delta r \rightarrow$ Half horizontal well length

To calculate the horizontal well production, Laplace equation $\nabla^2 P=0$ is solved in 3D space. In order to simplify it, a 2D analysis is performed assuming oil flow into a horizontal well, in a horizontal plane and vertical plane separately as shown in Figure 6. Pressure distribution within the reservoir is obtained under assumption of constant pressure at the drainage boundary and wellbore. Darcy's law ($Q=KA/\mu \partial P/\partial L$) is used to estimate the oil production rates using the previous calculated pressure distribution.

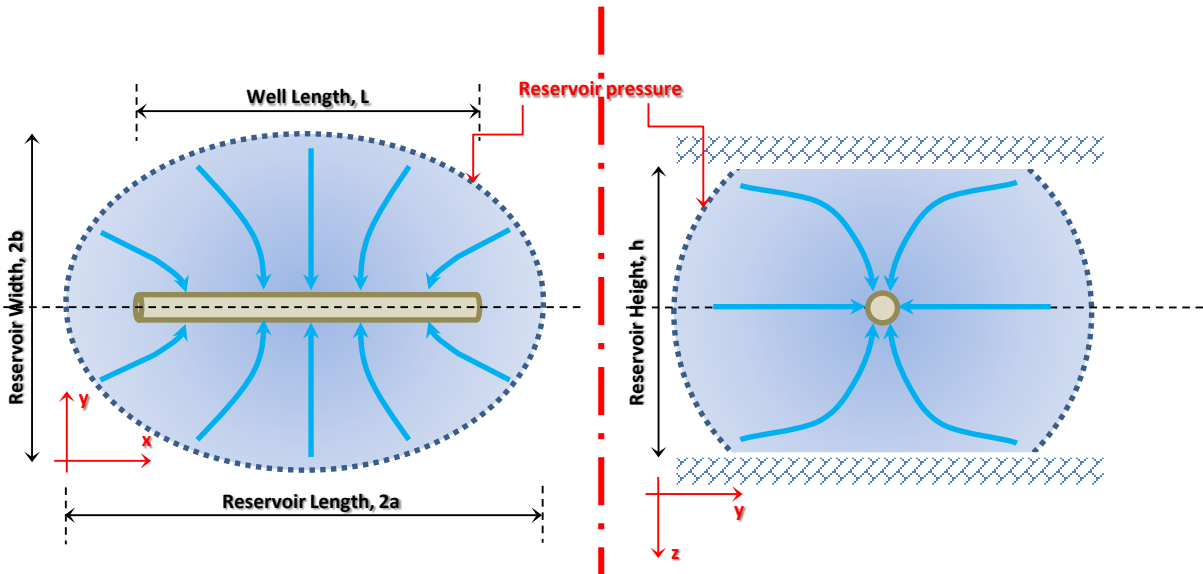


Figure 6. Horizontal well drainage, 2D simplified solution

Applying potential fluid theory for pressure distribution into a horizontal well in a horizontal plane we obtain Equation 14.

$$q_1 = \frac{2\pi\kappa_o\Delta P/\mu B_o}{\ln\left(\frac{a + \sqrt{a^2 - (L/2)^2}}{L/2}\right)}$$

Equation 14, Horizontal plane production rate

Likewise, using potential fluid theory for pressure distribution into a horizontal well in a vertical plane we obtain Equation 15.

$$q_2 = \frac{2\pi\kappa_o\Delta P/\mu B_o}{\ln(h/2r_w)}$$

Equation 15, Vertical plane production rate

Where:

- q_1 → Flow rate in horizontal plane
 q_2 → Flow rate in vertical plane
 k_o → Permeability
 ΔP → Pressure drop
 μ → Fluid viscosity
 B_o → Volumetric factor
 a → Half major axis – drainage ellipse
 L → Horizontal well length
 h → Reservoir height
 r_w → Wellbore radius

Horizontal well productivity (q_H) is calculated adding flow rate in horizontal and vertical planes. Likewise, the terms vertical and horizontal flow resistances are incorporated using an electrical analog concept, resulting in Equation 16.

$$q_H = \frac{2\pi k_o h \Delta P / \mu B_o}{\underbrace{\ln \left[\frac{a + \sqrt{a^2 - \left(\frac{L}{2}\right)^2}}{\frac{L}{2}} \right]}_{\text{Horizontal flow resistance}} + \underbrace{\frac{h}{L} \ln \left(\frac{h}{2r_w} \right)}_{\text{Vertical flow resistance}}}$$

Equation 16, Horizontal well production rate – Joshi model

Equation 16 is used to estimate horizontal well productivity for isotropic reservoirs, considering a well located in the middle of the reservoir and non-skin damage conditions. Boundary conditions are limited to $L > h$ and $L/2 < 0,9 r_{eH}$. These conditions are evaluated and validated in the current model and they are well covered in Chapter 4. Horizontal well drainage radius r_{eH} is found equating areas of ellipse and circle getting Equation 17.

$$r_{eH} = \sqrt{ab}$$

Equation 17, Drainage radius

Where,

- a → Half major axis – drainage ellipse
 b → Half minor axis – drainage ellipse

Analyzing values of (a) and (b) in previous Figure 6, one can determine $+L/2$ and $-L/2$ represent foci of a drainage ellipse. Similarly, r_{eH} can be estimated as per Equation 18 as given by Aasen, (2016).

$$r_{eH} = a[1 - (L/2a)^2]^{1/4}$$

Equation 18, Drainage radius – Ellipse

For boundary conditions of $L/2a \leq 0.5$, it corresponds to $r_{eH} \cong a$, and geometrical factors can be established. Table 1 lists the main geometrical relationships. The inverse of $L/2a$ is used in the proposed model, so in Chapter 3 the results shows the validity of the model while maintaining proportionality of data in Table 1.

Table 1. Geometric factors for Joshi model

Geometric Factors – Joshi Model		
L/2r_{eH}	L/2a	L/r_{eH}
0,1	0,0998	1,002
0,2	0,198	1,010
0,3	0,293	1,024
0,4	0,384	1,042
0,5	0,470	1,064
0,6	0,549	1,093
0,7	0,620	1,129
0,8	0,683	1,171
0,9	0,739	1,218

Influence of anisotropy incorporates the terms β into the Equation 16 resulting in Equation 19. Usually vertical permeability is less than horizontal permeability for many reservoir formations. In horizontal wells, high vertical permeability is an important factor for increasing productivity. So, if vertical permeability is affected or lower, vertical flow resistance increase (right term in denominator of Equation 16) and production (q_H) is affected. Equation 19 is valid for $L > \beta h$.

$$q_H = \frac{2\pi k_H h \Delta P / \mu B_o}{\ln \left[\frac{a + \sqrt{a^2 - \left(\frac{L}{2}\right)^2}}{\frac{L}{2}} \right] + \frac{\beta h}{L} \ln \left(\frac{\beta h}{2r_w} \right)}$$

Equation 19, Horizontal well production - Anisotropy

Where,

$\beta = \sqrt[2]{k_h/k_v} \rightarrow$ Anisotropy coefficient

$k_h \rightarrow$ Horizontal permeability

$k_v \rightarrow$ Vertical permeability

Skin factor also affects horizontal well productivity. Negative skin value gives higher production and increasing positive skin values its opposed effect. r_{we} represents the effective wellbore diameter, which increase or decrease due to skin factor (S) as shown in Equation 20 (upper formula). It denotes an imaginary wellbore diameter affected by near wellbore skin. Rewriting r_{we} in terms of horizontal drainage radius r_{eH} , we obtain Equation 20 (lower formula). In horizontal wells, similar to vertical wells, production rates increase when effective wellbore radius (r_{we}) is increased.

$$r_{we} = r_w e^{-S}$$

$$r_{we} = \frac{r_{eH}(L/2)}{a[1 + \sqrt{1 - (L/2a)^2}][h/2r_w]^{h/L}}$$

Equation 20, Effective wellbore radius

Bellarby, (2009, p. 34) defines the horizontal skin S_h derived from Joshi model as follow:

$$S_h = \ln \left[\frac{a + \sqrt{a^2 - (L/2)^2}}{(L/2)} \right] + \frac{\beta h}{L} \ln \left[\frac{\beta h}{2r_w} \left(1 - \frac{2\ell_\delta}{\beta h} \right)^{-2} \right] - \ln \left(\frac{r_e}{r_w} \right)$$

Equation 21, Horizontal skin

Where,

$\ell_\delta \rightarrow$ distance to mid height

The term ℓ_δ introduces well eccentricity effect into the skin factor, which in turn, also affect the horizontal well production in Equation 16. Hence, in conclusion the anisotropy, skin and eccentricity affect the horizontal well productivity in the Joshi model. These mathematical approach will be used in the analytical model describe in the results covered in Chapter 3.

Clean-up process is a transient flow period happening at production start-up. Next chapter presents the main flow regimes and transient pressure for horizontal wells.

2.4. Transient flow in horizontal wells

In general, flow through porous media as described in the diffusivity equation can be analyzed in three different states or periods: Unsteady or transient flow, pseudo steady state and steady state. Clean-up process is an unsteady or transient state and it means that pressure change with time is different at different locations. This project is concentrated in transient flow, so mathematical formulation is only presented for this period.

Pressure transient characteristics are mainly affected by isotropic or anisotropic ratio (k_v/k_h), formation thickness and well length as given by Kamal, (2009). Horizontal wells exhibit complex flow regimes. Three flow regimes are identified during infinite-acting period as shown in Figure 7: early radial flow (*ERF*), intermediate linear flow (*ILF*) and late radial flow (*LRF*) also known as pseudo radial. Extra flow regimes are included by other authors as given by Kuchuk, (1995); for instance hemi radial flow which appears when well is not centered in the reservoir vertical boundaries. For the purpose of the thesis we do consider the main three groups.

The question arises now is: Why do we need a transient flow equation? In order to adjust the steady state period simulated by NETool™ software, a pressure transient analysis is performed to identify the flow regime of the current well conditions. Usually the clean-up process happens at intermediate linear flow or late radial flow depending mainly on the well length. So, by determining the current flow regime boundaries, the reservoir width of the Joshi PI model in NETool™ is exactly matched for any particular time step. Streamlines or flow velocity functions (blue arrows from Figure 6) in the Joshi model match with streamlines at LRF in Figure 7, so our model is mainly focused on late radial flow.

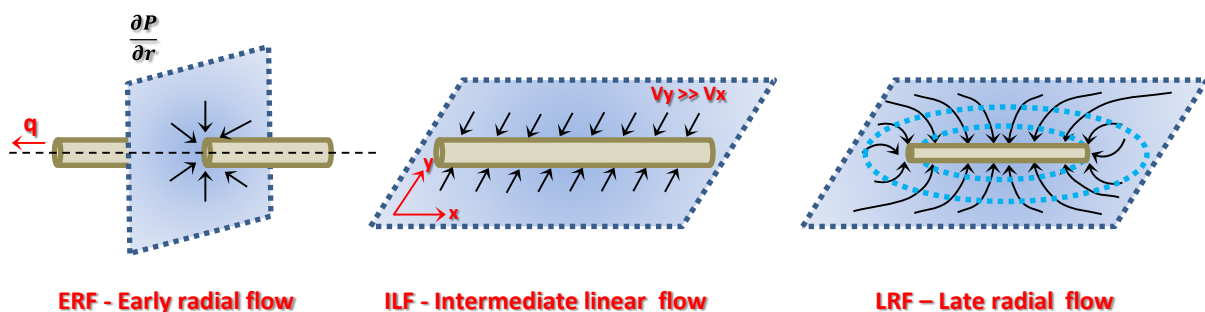


Figure 7. Horizontal well flow regimes

Pressure transient models usually assume uniform flux or infinitive conductivity. Based on the statement that pressure drop inside the wellbore is small compared to the pressure drop in the reservoir, the infinitive conductivity model matches the assumption as given by Ozkan & Raghavan, (1995) and it is presented in Equation 22 for LRF - Late radial flow. It could also lead to consider negligible pressure drop at wellbore, which also fit into previous Joshi model for horizontal well productivity, making this study to be founded under same period and wellbore conductivity. Equation 22 describes the pressure transient model for horizontal wells in terms of dimensionless variables (upper formula), and well flowing pressure difference (lower formula).

$$\sqrt{\frac{k}{k_z}} P_{wD} \approx \frac{1}{2} \left[\ln \left(t_D \frac{L_D^2 \sqrt{k_x k_y}}{r_{wD}^2 k_z} + 0.80907 \right) \right] + S_a$$

$$\Delta P_{wf} = \frac{162.6qB\mu}{\sqrt{k_h k_y} h} \left(\log t + \log \frac{\sqrt{k_x k_y}}{\phi C_t \mu r_{w,eq}^2} - 3.23 + 0.87S_a \right)$$

Equation 22, LRF pressure transient

Where,

- k → Permeability, [mD]
- k_x → Permeability in x direction, [mD]
- k_y → Permeability in y direction, [mD]
- k_z → Vertical permeability [mD]
- P_{wD} → Dimensionless pressure
- t_D → Dimensionless time
- L_D → Dimensionless lenght
- r_{wD} → Dimensionless wellbore radius
- S_a → Apparent skin
- ΔP_{wf} → Pressure drop, [psi]
- q → Flow rate, (bpd)
- B → Volumetric factor, [bbl/STB]
- μ → Viscosity, [cP]
- h → Reservoir thickness, [ft]
- $r_{w,eq}$ → Wellbore radius, [ft]
- t → Time, [hr]

Equation 22 is very important for analysis in this project and it is widely used to match and adjust steady state results from NETool™ software into transient flow. It

is better explained in Chapter 3, where results are presented. Boundary conditions are imposed to pressure transient solution in time scales as follow:

$$t \geq \max \left\{ \frac{988\phi C_t \mu L_h^2}{k_x}; \frac{2.515\phi C_t \mu h^2}{k_z} \right\}$$

Equation 23, LRF Time limit in pressure transient

Hence, the maximum value between both statements is used as the time late radial flow start in the transient pressure scenario. The term S_a or apparent skin in Equation 22 is determined from pseudo skin concept using Equation 24.

$$S_a = S_p + \sqrt{\frac{k}{k_z}} S$$

Equation 24, Apparent skin

Where,

$S \rightarrow$ Formation damage

$S_p \rightarrow$ Pseudo skin

$$k = \sqrt[3]{k_x k_y k_z}$$

Pseudo skin is basically defined as the difference between dimensionless pressure of horizontal and vertical wells after onset of later radial flow. Besson, (1990) presents the following correlation to estimate S_p as stated in Equation 25. It applies when $[(k_z/kL_h)^{0.5}/h] \geq 0.4$

$$S_p \approx \ln \left(\frac{4r_w}{L_h} \right) + \frac{\sqrt{\frac{k}{k_z}} h}{L_h} \ln \left[\frac{2 * \sqrt{\frac{k}{k_z}} h}{2\pi r_w (1 + \sqrt{\frac{k}{k_z}}) \cos \pi * \frac{2Z_w - h}{2h}} \right] - \left(\left(\frac{\sqrt{\frac{k}{k_z}} h}{L_h} \right)^2 * \left(\frac{1}{6} + 2 \left(\frac{2Z_w - h}{2h} \right)^2 \right) \right)$$

Equation 25, Pseudo skin - LRF

Where,

$S_p \rightarrow$ Pseudo skin

$$k = \sqrt[3]{k_x k_y k_z}$$

$k_z \rightarrow$ Vertical permeability, mD

$L_h \rightarrow$ Horizontal length, m

$h \rightarrow$ Reservoir height, m

$Z_w \rightarrow$ Distance to mid height, m

Variables that are not mentioned correspond to same terms in Equation 22. Pressure drop from pressure transient Equation 22 is equated to pressure drop from Joshi model using Equation 16, thereby producing a formula that calculates the flow rate as a function of reservoir parameters. The minimum boundaries in which each model applies are established. Minimum time limits correspond to the time the LRF flow regime start, and minimum time the Joshi model can be used as per boundary conditions. Solution and results are better explained in Chapter 3. In cases ILF-intermediate linear flow is considered, a maximum time limit needs to be included as shown in Appendix section.

The reason for equating pressure transient and Joshi model is to estimate the reservoir width needed for NETool™ software to calculate the drawdown. As mentioned previously, NETool™ uses Joshi model to estimate horizontal well productivity. Next chapter explain the simulation process and method that the software uses to estimate it.

2.5. NETool™ software model and simulation method

NETool™ software (Landmark - Halliburton) is a micro-nodal analysis tool that integrates reservoir properties and completion architecture in the wellbore vicinity. The software is used to simulate influx and pressure drop in the horizontal wellbore by coupling fluid flow through porous media and hydraulic flow into diverse types of completion architecture. In our particular case, ICD nozzle type completion is the main focus. Advantages of using this software for the present project are:

- It couples fluid flow through porous media and flow through screen base pipe. Usually, other tools can simulate them separately.
- It is mainly designed to simulate horizontal wells flow.
- It incorporates detailed completion architecture, for instance inflow control devices and makes the structure of the completion compartmentalized type.
- It integrates formation damage or skin as well as filter cake option around the wellbore, which indeed help to study and model the clean-up process.
- Wellbore vicinity is defined using diverse layers and nodes.

One of the drawbacks of the software's model is the steady state only option. It means that results are expressed as a snapshot of instantaneous occurrence in the well at steady state period. It is solved by coupling Equation 16 and 22.

The software model can be described as follow: First, fluid flow through porous media is modeled using transmissibility and mobility to define the productivity index PI ($PI=Q/\Delta p$) as Equation 26.

$$Q = M * T * \Delta P$$

Equation 26, Flow rate model

Where,

$Q \rightarrow$ Flow rate

$M \rightarrow$ Mobility

$T \rightarrow$ Transmissibility

$\Delta P \rightarrow$ Pressure drop

Mobility represents k_{eff}/μ or permeability over viscosity. The model have three options to estimate mobility: using relative permeability curves k_r , flow fraction or manual definition.

Transmissibility represents kh/μ or mobility by thickness of reservoir. It can be calculated using PI model (productivity index model based on permeability), using coefficients and skin value, and also manual definition of PI .

Secondly, hydraulic flow through completion architecture is modeled assuming all phases travelling with same speed in form of a mixture (*homogeneous mixture*). Laminar and turbulent flow are defined at annulus and in the tubing using friction factor, then pressure gradient (dP/dx) is calculated using Equation 27 as stated in Landmark NETool Technical Manual, (2014).

$$\frac{dP}{dx} = f \frac{\rho v^2}{2D}$$

Equation 27, Pressure gradient

Where,

$f \rightarrow$ Friction factor

$\rho \rightarrow$ Density

$v \rightarrow$ Velocity

$D \rightarrow$ Diameter

Beggs & Brill model as well as LMK-1 model can be used for same purpose. Flow through ICD nozzles is then modeled using Equation 11.

So the software model integrates the pressure drop from Equation 16 (porous media), Equation 27 (pipe flow) and Equation 11 (ICD nozzle) along the reservoir to surface path. In our case, the pressure drop through porous media follows the Joshi PI model and homogeneous mixture.

Simulation method is based on multilayer and nodes concept. As mentioned previously, wellbore vicinity and completion is segmented using layers in radial direction and length defined nodes along axial direction. Type of completion, and consequently its detailed architecture is established in one of the four layers that describe the wellbore as shown in Figure 9. Most external layer is casing liner; sand control and inflow control are the inner layers while stinger and tubing are the inner most layers. Inside each layer a flow path can be defined by using slotted liner, perforated liner, screen, and ICD. Flow path can also be blocked by using blank pipe, cemented liner or packer.

In order to model clean-up process, formation damage is established using segmented skin values along the horizontal section (radial and axial direction). No filter cake is defined around the screen layer in this project. Skin is internally calculated based on Hawkins formula $[S = (K/K_d - 1) \ln(r_d/r_w)]$ where S represents skin, K_d damage permeability, r_d damage radius, and r_w wellbore radius. Based on the return permeability simulation results (k_d/k) obtained from "Maximize tool", we define the segments and damage permeability into NETool™.

This study basically defines the internal cake as formation damage base on return permeability lab results, and a skin value is set for interpretation of the phenomenon. Formation damage (skin and return permeability) removal in time is modeled as the clean-up progress.

3. Simulation and results

This chapter mainly shows the assumptions and results of the model simulations. It is presented as five mainly steps of the methodology used to develop this project thesis, and it is summarized in the modeling process structure explained next chapter.

3.1. Modeling process structure

Let us start with the general explanation on how the problem statement is analyzed. In the following Figure 8 the flow direction and simulation structure of the current thesis is presented. We build a model and prove its benefits to solve the mentioned problem. Five different main levels are defined as follow:

First, a well is defined in NETool™ including reservoir properties and PI model.

Second, completion architecture is defined for the same particular well. It is characterized for a SAS-stand alone completion. All cases, including ICD completions will be compared against SAS completion to validate the benefits of ICDs.

Third, adjustment of the initial model and results are performed. It basically includes a transient solution evaluation to choose the reservoir width in a particular time step (needed in the Joshi model). This procedure amends the drawback of NETool™ software from steady state to transient flow.

Fourth, we set the ICD completion and adjust it to transient flow as well. The best nozzle size and distribution is estimated.

Fifth, formation damage is defined in NETool™ while simulating particle transportation using “Maximize” software tool. It is used to establish a damage permeability value and return permeability value. Radius of invasion is estimated based on reported losses profile. Exponential decay function is also used as simplified model of return permeability.

Finally, in the fifth level an iterative process is performed in NETool™ by permeability variation from initial damage until final return permeability, considering the same time step for reservoir width definition in the Joshi model. This is the key process and added value for an interpretation of the clean-up process in a steady state simulation. Cumulative flow or pore volume injected per area is the determining parameter to check the progress of clean-up and its efficiency. Further detailed results for each level are explained through Chapter 3.2 to Chapter 3.6.



Figure 8. Modeling process structure

Where:

- NETool Software simulation
- Excel calculations
- Maximize software simulation

PI	Productivity index	K_d	Damage Permeability
L	Horizontal wellbore length	K_{return}	Return permeability
PV	Pore volume	K	Formation permeability
r_i	Radius of invasion		

3.2. Well definition

A long horizontal well from the Norwegian continental shelf is chosen as the base case. Public information of the Tyrihans reservoir properties, well characteristics, drilling fluid components and dynamic losses are given by van der Zwaag et al., (2012). Table 2 and Figure 9 show the well configuration and reservoir properties.

Table 2. Well & Reservoir properties

Well Trajectory			Reservoir Properties		
Description	Value	Unit	Description	Value	Unit
MD	7300	m	Reservoir fluid	Oil	
TVD	3592	m	Oil gravity	44,3	API
Open hole	8 ½	in	Gas gravity	0,81	Kg/Sm ³
Inclination	90	deg	Temperature	137	°C
Azimuth	120	deg	Pressure	353	bar
9 5/8" shoe	5200	m	B _o	1,5	Sm ³ /Rm ³
H _z section	2100	m	μ _o , Oil viscosity	0,5	cP
First node	5200	m	Q _o , Flow rate	1589,8	Sm ³ /d
Well segments	50	m each	Thickness	35	m
Heel & Toe segments	1	m each	K _h , H _z permeability	600	mD
			K _v /K _h	1	
			φ, Porosity	0,25	
			C _t , Compressibility	1*10 ⁻⁶	1/psi

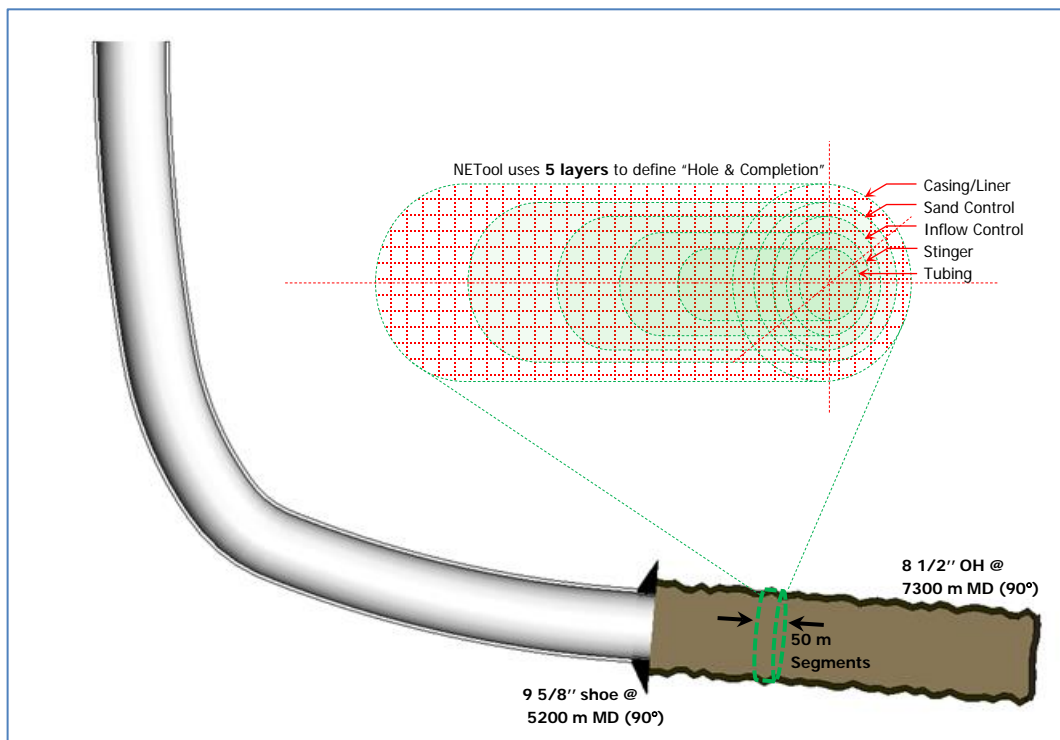


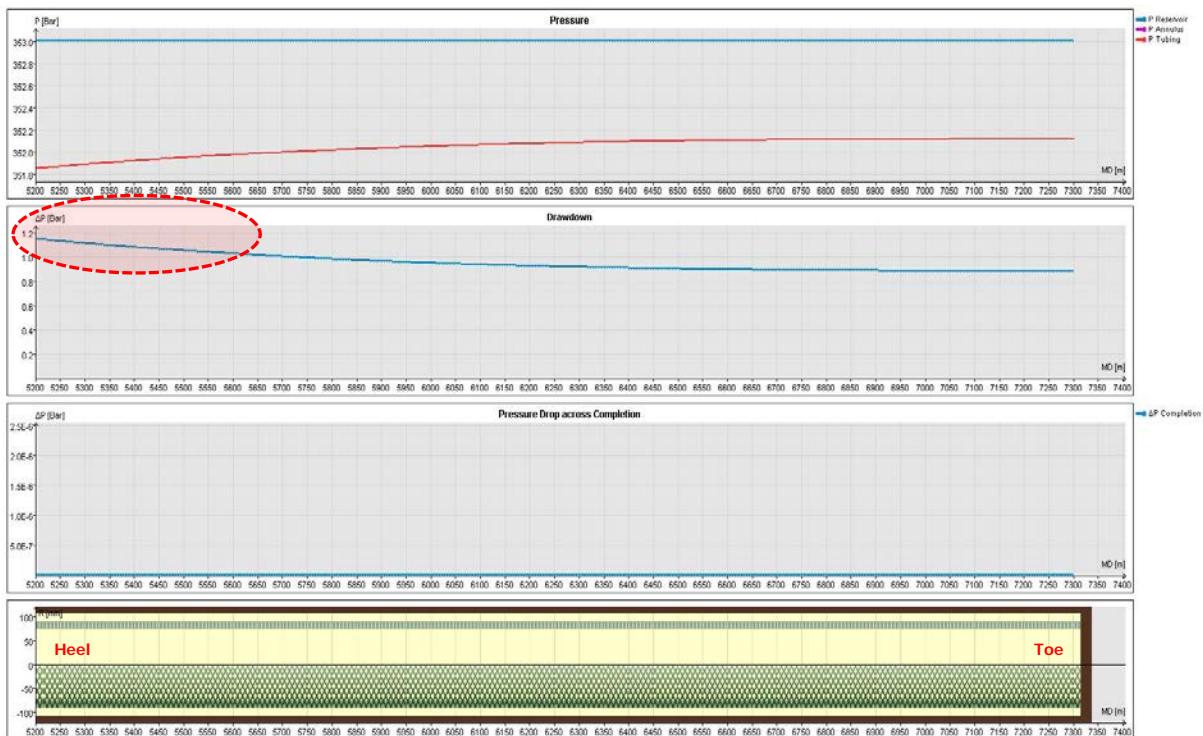
Figure 9. Horizontal well definition

This well is used due to the extensive length and dynamic filtration exposure, making ideal for formation damage analysis. In order to simplify the model, an isotropic condition is established.

3.3. Completion type – SAS

Well architecture is defined as SAS-Stand Alone Screens. Formation roughness of 150µm is defined for the 8 1/2" open hole. 6 5/8" base pipe generic premium screens are used in the second layer defined by NETool™. 7,11" OD Screens with 5,92" ID and 15µm pipe roughness correspond to the completion of the entire horizontal section. Assumption is that no eccentricity is present in the completion neither sand pack around screens. Note that for practical purposes no annular isolation (open hole packers) is installed along the horizontal section due to initial premise of isotropy formation. From operational point of view, the long horizontal section could be divided into compartments to avoid annular flow and favor radial flow; nevertheless for the purpose of this project we do not consider them. Similarly, the blank section of the screens located at both ends (usually few feet for handling purposes) are not considered, so the entire length of screens is assumed to allow flow through it.

Figure 10 (bottom) shows the horizontal section completed with sand screens.



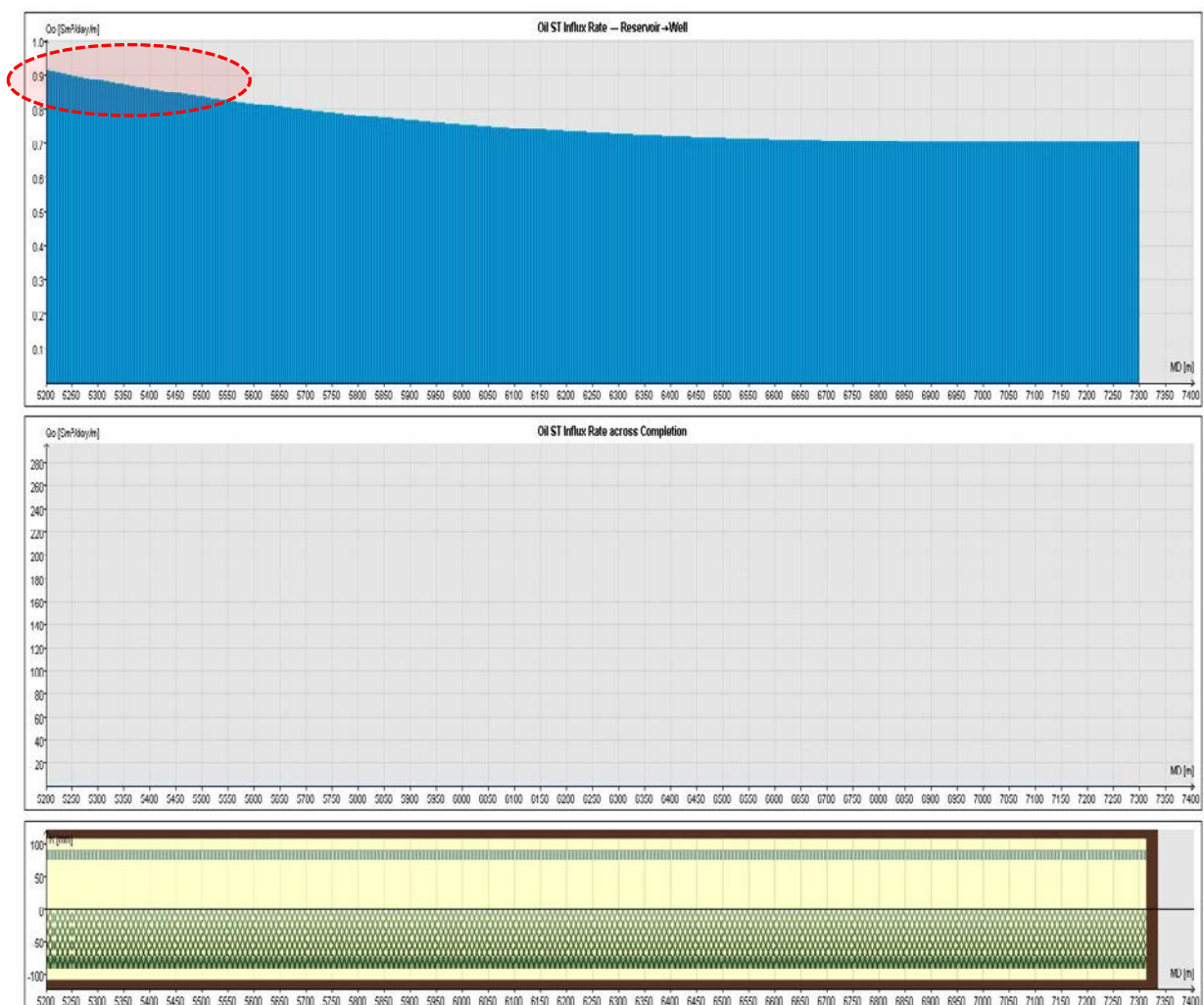
Source: NETool™ 5000.0.4.1 - Halliburton

Figure 10. SAS Completion – Pressure results

50 m length segments are used to discretize the entire section. 1 m length segments are used at the shoe and toe depths to neutralize flow limits effects. As mentioned previously, NETool™ calculate flow and pressure from node to node starting from reservoir through the five layers that define the hole and completion, until it reaches surface. Software setup can be found in Appendix B.

Upper curve in Figure 10 shows a stable reservoir pressure of 353 bar. However, the drawdown pressure (dashed ellipse) is higher at the heel compared to toe due to reduction in tubing pressure caused by frictional losses of 0,22 bar. It will favor higher influx at the heel. Note that annular and tubing pressures are almost identical for SAS. It is important to mention the almost negligible effect of the pressure drop across the screens (lower curve) due to the high open flow area, so completion do not favor any stabilization of the drawdown neither influx rate.

In terms of oil influx rate per length, the higher pressure drop at heel increase the oil influx rate per length (0,91 Sm³/d/m, dashed ellipse) causing a coning effect. Influx rate is reduced at the toe to 0,70 Sm³/d/m as shown by Figure 11 (upper part).



Source: NETool™ 5000.0.4.1 - Halliburton

Figure 11. SAS Completion – Influx results

These findings are the key initial value to be compared with results of ICD completions and the inclusion of skin factor. In fact, influx rates per section are improved by inflow control devices and it is better explained in Chapter 3.5

Before showing the ICD completion results, it is important to mention that influx rates per length are obtained using the Joshi PI Model, which needs the reservoir width as important input. Figure 10 and 11 represents drawdown and influx rates at 5,75 hr (time step) assuming LRF flow, so reservoir width is 1921 m. Calculation procedure for time step 15,90 hr is better explained in next Chapter 3.4.

3.4. Transient flow incorporated into Initial case

Clean-up effects might happen at ILF-Intermediate linear flow or LRF-Late radial flow regimes. In short wells are common to find LRF regime covering the entire effects of clean-up period. In some cases, it may need ILF in the beginning of the clean-up and LRF towards the end.

In our project, clean-up effects are assumed to happen at LRF – late radial flow due to very long well we are considering into. So, ΔP from pressure transient Equation 22 is equated to ΔP from Joshi PI or productivity index model (Equation 16 implicit in NETool™) in order to find the time at which LRF occurs as well as the reservoir width. Why we do it? Idea is to find the exact time for better interpretation of the transient period into a steady state simulator like NETool™. In other words, it solves the drawback of the snapshot simulation provided by the software. Excel is used for this calculation and be able to adjust the model. Equating both ΔP , we get:

$$\frac{162.6qB\mu}{\sqrt{k_h k_y} h} \left(\log t + \log \frac{\sqrt{k_x k_y}}{\phi C_t \mu r_{w,eq}^2} - 3.23 + 0.87S_a \right) = \frac{2\pi k_o h q q_H / \mu B_o}{\ln \left[\frac{a + \sqrt{a^2 - \left(\frac{L}{2}\right)^2}}{\frac{L}{2}} \right] + \frac{h}{L} \ln \left(\frac{h}{2r_w} \right)}$$

K_h is equal to k_y in our case, so it is reduced to k . For practical system units purposes, the term 141.2 must be included as denominator in the left equation. Rewriting the bold values in terms of $2a/L$, and making $\lambda=2a/L$, $S=0$, we get:

$$\ln(\lambda + \sqrt{\lambda^2 - 1}) + \frac{h}{L} \ln \left(\frac{h}{2r_w} \right) = \underbrace{\mathbf{1,15} \left(\mathbf{\log t + \log \frac{\sqrt{k_x k_y}}{\phi C_t \mu r_{w,eq}^2} - 3.23 + 0.87S_a} \right)}_{\tau}$$

The right term is called τ , and equation is solved to obtain:

$$\underbrace{(\lambda + \sqrt{\lambda^2 - 1})}_{\text{LHS}} = \underbrace{e^{\tau - \frac{h}{L} \ln(\frac{h}{2r_w})}}_{\text{RHS}}$$

Equation 28, Pressure transient adjustment

An iterative process is performed assuming a value of *Lambda* λ from maximum and minimum values in Table 1, until LHS-left hand side is the same as RHS- right hand side of the Equation 28.

This approach has two boundaries conditions. First, the lower limit obtained using Equation 23 and data from Table 2. It represents the time in which LRF works. The second limit is related to the Joshi condition $L_h/2 < 0,90 r_{eH}$, where r_{eH} is calculated based on Equation 18 and also Equation 23. It represents the limit to use the Joshi productivity model. So, basically the assumption of *Lambda* λ value should be assumed between the two limits.

Assuming *Lambda* $\lambda = 2,018$ (time step 15,9 hr) we obtain $S_p = -8,42$ using Equation 25, $\tau = 1,41$; $LHS = RHS = 3,77$. Replacing it we get: a , r_{eH} and b for Joshi model:

$$a = \frac{\lambda * L}{2} = \frac{2,018 * 2100}{2} = 2118,5 \text{ m}$$

$$r_{eH} = a[1 - (L/2a)^2]^{1/4} = 2118,5 \left[1 - \left(\frac{2100}{2 * 2118,5} \right)^2 \right]^{1/4} = 1974,2 \text{ m}$$

Using Equation 17 about the drainage radius, we get b as follow:

$$b = \sqrt{a^2 - (L/2)^2} = \sqrt{2118,5^2 - (2100/2)^2} = 1840 \text{ m}$$

Values of a and b represents the half major and minor axis of the Joshi ellipses as shown by Figure 6 and 7. Finally, the reservoir width is obtained as follow:

$$\text{Reservoir width} = 2b = 1840 * 2 = 3680 \text{ m}$$

This is the reservoir width input data defined for the Joshi horizontal well productivity model in NETool™. The iterative process is performed for every time step. Similarly the reservoir thickness is input into the Joshi PI model. A well multiplier of 1 is used,

so no PI manual adjustment is done. Basically, these parameters help to define the PI model used to calculate influx rate per node at specific time.

Table 3 shows results for the main horizontal flow regimes limits in which they appear. This project only present results for LRF – Later radial flow that happens during clean-up process according to the well and reservoir properties. For further studies, equations for flow regime limits can be found in literature as given by Kamal, (2009). Equation for ILF flow regime is presented in Appendix A.

Table 3. Calculated horizontal flow regime limits

Horizontal well - Flow regime boundaries		
Flow regime	Value	Unit
ERF – Early radial flow	$t < 0,0047$	hrs
ILF – Intermediate linear flow	$0,0012 < t < 1,58$	hrs
LRF – Late radial flow	$t > 9,77$	hrs

The two boundary conditions of the model are established using the LRF limit of Equation 23, and the lower limit of Joshi model ($L_h/2 < 0,90 r_{eH}$, in our case any value of $r_{eH} > 1167$ m). Late radial flow starts after 9,77 hr (using Equation 23) as shown in the lower part of Table 3. Flow periods between the mentioned flow regimes are considered transition periods.

At time step 9,77 hr, $r_{eH} = 1538,5$ m and $\lambda = 1,645$, so the Joshi model condition are not reached yet. An important assumption is now used in the project. We do extrapolate the r_{eH} limit of the Joshi model until *time step* = 5,75 hr, in which $r_{eH} = 1169$ m and $\lambda = 1,355$. It demonstrates that Joshi conditions are still reached at time step 5,75hr; for instance lambda values between $1,35 < \lambda < 10,02$ (calculated from Table 1).

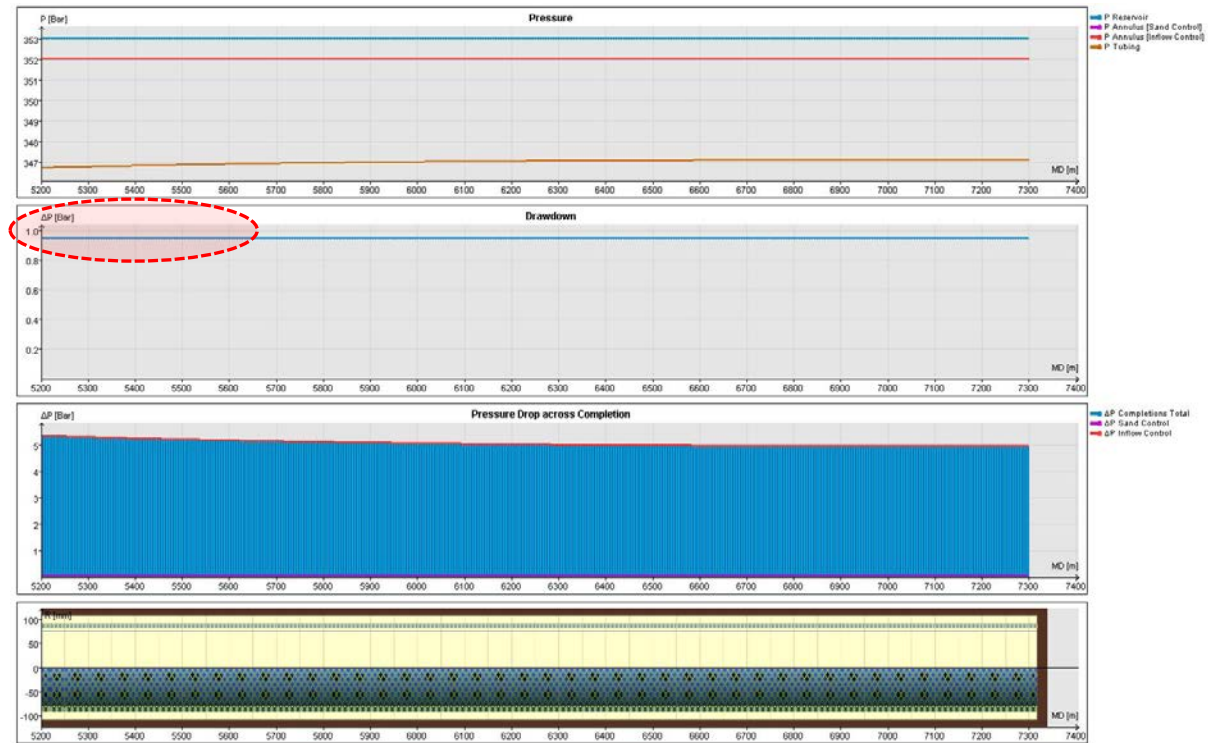
We are moving backward the LRF limits until the Joshi model limits integrating the transition period ($5,75 > t > 9,77$) into late radial flow. In conclusion, our LRF analysis and clean-up period is modelled after $t > 5,75$ hrs. For shorter horizontal wells, the model is valid at much early times. As mentioned previously, the streamlines (blue arrows from Figure 6) in the Joshi model match with streamlines at LRF in Figure 7, so our model is mainly focused on late radial flow.

3.5. Completion type – ICD

Based on the well definition parameters and the initial SAS-Stand alone screen completion defined in the previous chapter, we add to the screens ICD-inflow control devices along the horizontal well section as per Figure 12 (lower part). 6 5/8" OD base pipe screen joints with 7,11" OD and 6,5" ID are used. ICD module is assumed

to have 6,00" OD and 5.92" ID. This configuration makes similarity with SAS Completion. Nozzle type ICD similar to those shown in previous Chapter 2.2.1 (Figure 3 and 4) are installed.

Likewise, no annular isolation in the well neither blank section of the joint are considered. Software setup can be found in Appendix C.



Source: NETool™ 5000.0.4.1 - Halliburton

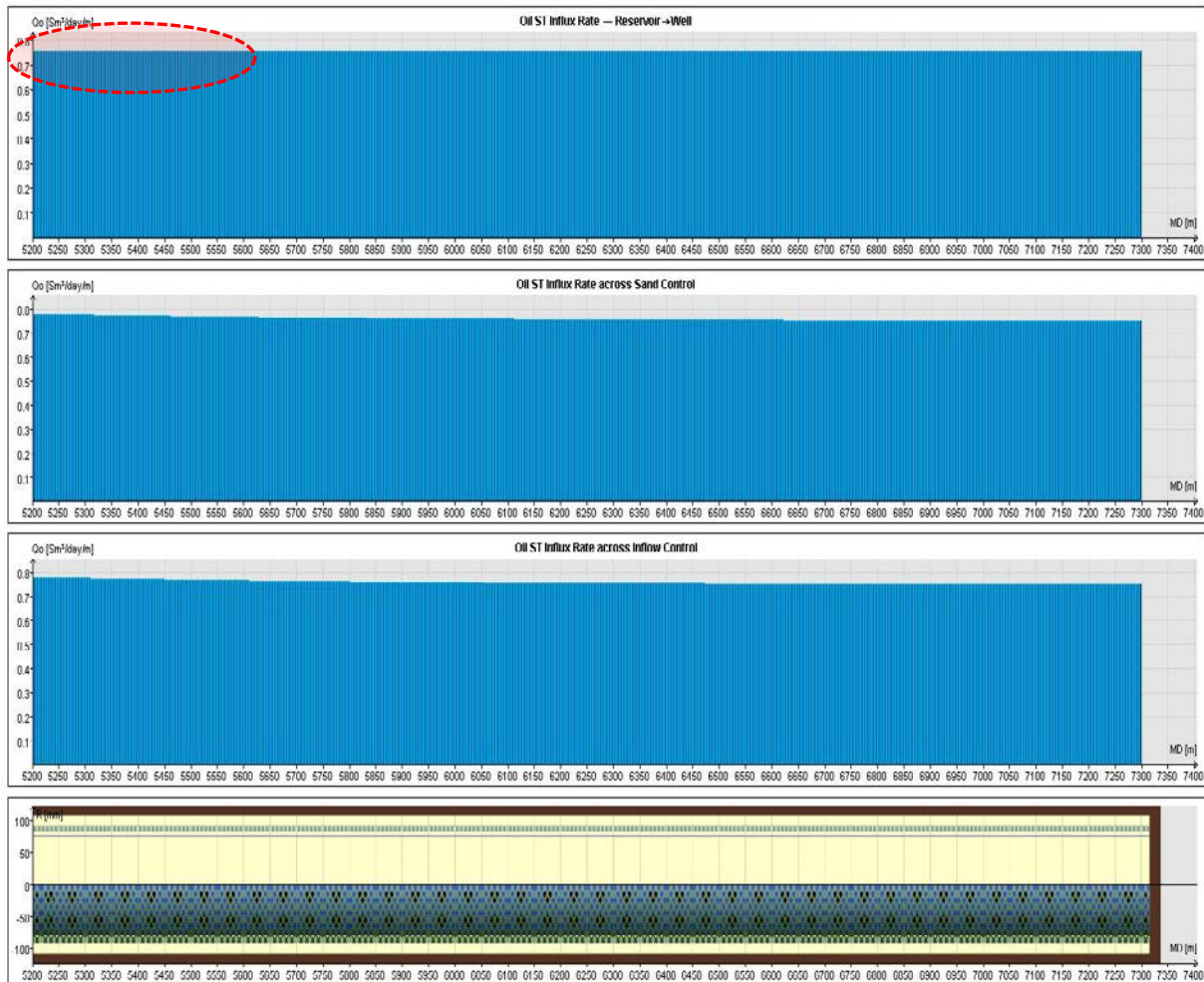
Figure 12. ICD Completion – Pressure results

Assumption is that each ICD joint has maximum four (4) parallel places radially located to install nozzles per joint, so multiple flow areas are considered in the design until we obtain an almost stable *influx rate/Length* with minimum pressure drop at the nozzle ICD.

Final ICD design results show 3 nozzles per joint with an aperture of 1,3 mm each. Same nozzle size and distribution is chosen for the entire well. Upper curve in Figure 12 shows a stable reservoir pressure of 353 bar. Annular pressure is now maintained stable at 352,05 bar and tubing pressure slightly varies from 346,73 at heel to 347,12 bar at toe compared to SAS completion. Middle curve (dashed ellipse) shows the drawdown pressure almost stable at 0,948 bar, so it corresponds to the greatest benefit of inflow control devices and its advantage over SAS completion. Why? Because it will not favor the higher influx rate at the heel so the influx will tend to be stable along the horizontal section and better clean-up at the toe can be reached as

well as less tendency for coning at heel. The frictional pressure loss from toe to heel is also neutralized by the zonal chocking effect of the ICDs.

An average pressure drop at the inflow control device of 5,0 bar is obtained. Different sizes of nozzles, in our case, less than 1,3 mm could also be used on the design but local pressure drop will increase, and the latter is not desired at all. So, during design of the best nozzle size, it is a parameter to be considered within a range of options.



Source: NETool™ 5000.0.4.1 - Halliburton

Figure 13. ICD Completion – Influx rate

Reservoir influx rate per length is shown in Figure 13 (upper curve). A stable value of 0,75 $[\text{Sm}^3/\text{d}/\text{m}]$ is obtained along the well. This value is the ideal value obtained if we divide total flow rate by wellbore length, for instance 1589 $[\text{m}^3/\text{d}] / 2100 [\text{m}]$, so we get 0,75 $[\text{Sm}^3/\text{d}/\text{m}]$. It represents the expected influx rate to maintain constant productivity of each zone in the wellbore length.

The model is also adjusted to transient period as the SAS completion, so a reservoir width of 1921 m (time step 5,75 hr) is used on Figure 12 and Figure 13 results.

3.6. Formation damage and clean-up

Now, formation damage is included in the reservoir to study its effect on drawdown and influx rates. Results are explained in Chapter 3.6.1 and 3.6.2. Then, the evolution of damage removal in time is evaluated for clean-up efficiency into ICD completions in Chapter 3.6.3 and Chapter 3.6.4. A very long well with reported dynamic filtration information is chosen due to high exposure time during drilling and consequently high radius of invasion.

3.6.1. Radius of invasion

Initially, we assume one fluid type and its properties, then we evaluate its damage effects into the reservoir. It means, the radius of invasion and damage permeability are calculated to define the damage zone. Field data from static and dynamic losses are used as given by van der Zwaag et al., (2012), and they are shown in Figure 14 and 15. This data adapts to same wellbore and reservoir properties presented in Table 2 and fit into purpose of the project analysis. Note that we have modified the x axis in order to express it as "MD- measured depth".

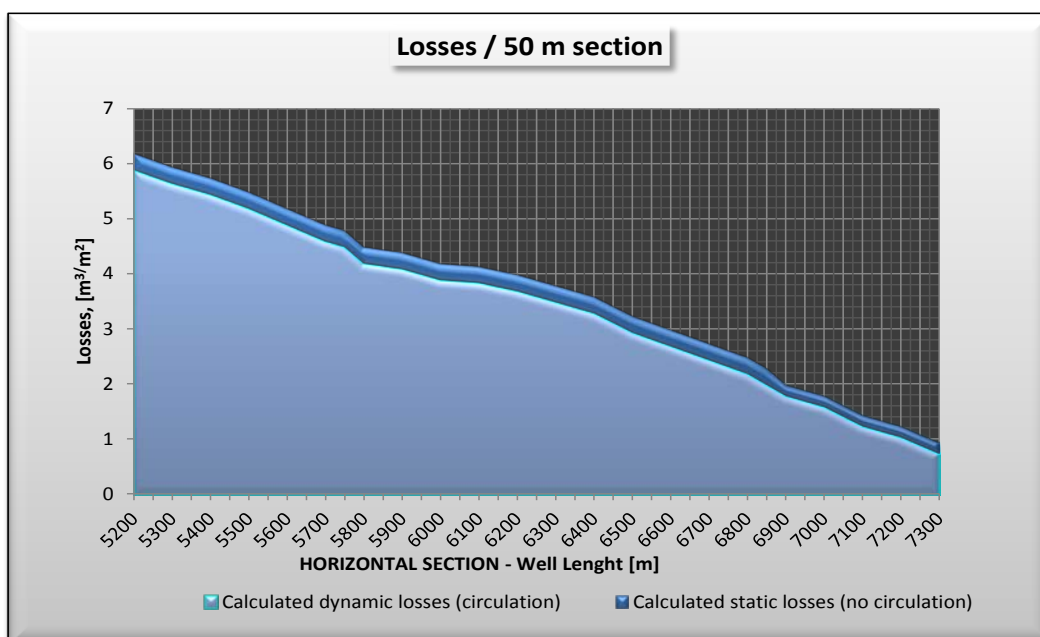


Figure 14. Dynamic and static losses

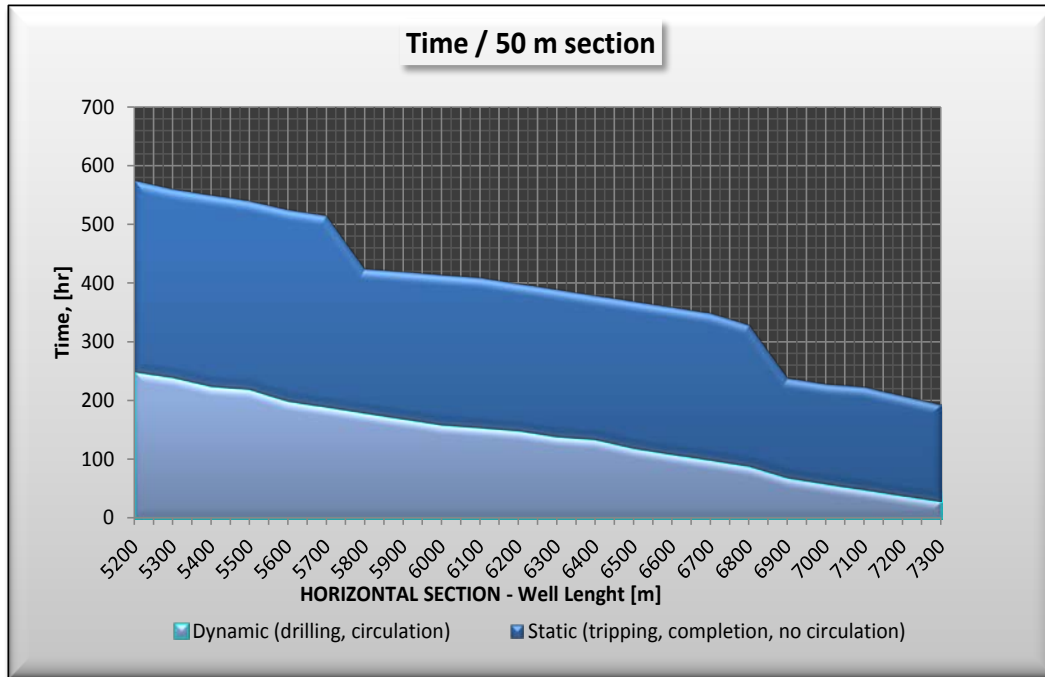


Figure 15. Time - dynamic and static losses

Reported losses from Figure 14 are based on calculation using Equation 1. An important finding here is the higher effect of dynamic losses over the total losses expected during drilling as concluded by van der Zwaag et al., (2012). We do focus our estimation of radius of invasion based on dynamic losses only. We neglect the effects of static losses. Using Equation 2, assuming an average filtrate saturation $S_i=20\%$ as given by Breitmeier et al., (1989), we obtain the radius of invasion as follow:

$$r_i = \left\{ r_w^2 + \frac{2r_w}{\phi S_i} \int C_m dt \right\}^{0,5} = \left\{ 0,108^2 + \frac{2 * 0,108}{0,25 * 0,20} * 0,1739 \right\}^{0,5} = 0,8734 \text{ m @ heel}$$

Dynamic losses at the heel are $5,90 \text{ m}^3$. $C_m dt$ or filtrate flux is calculated dividing dynamic losses / area. Our analysis is based on 50 m well segments, so superficial area is obtained as $A=2\pi r_w * h=33,93 \text{ m}^2$. We obtain filtrate flux as follow:

$$\int C_m dt = \frac{5,90}{33,93} = 0,1739 \text{ m}^3/\text{m}^2$$

Figure 16 shows the variance of $C_m dt$ along the horizontal section. An important finding is observed at the almost stable red line, which corresponds to an average value of $0,00073 \text{ m}^3/\text{m}^2/\text{hr}$. It is obtained dividing *dynamic losses/area/time*. It represents the filtrate rate and we interpret as the filtrate invades the formation at constant rate. This finding is also used as part of the assumption into the model.

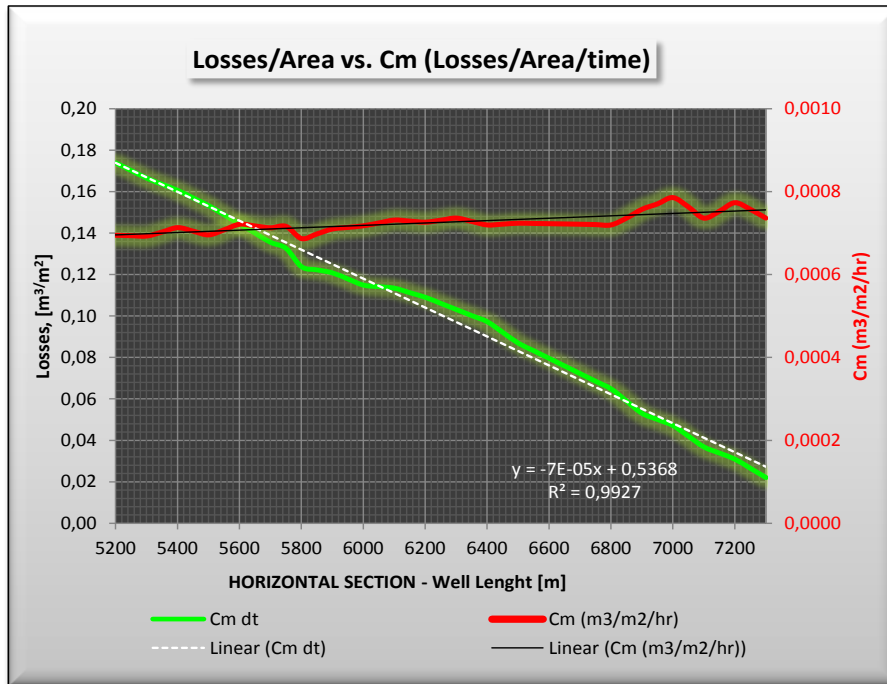


Figure 16. Filtrate flux

Radius of invasion is obtained along the wellbore section replacing data into Equation 2. Results are plotted in Figure 17 showing a truncated cone effect as expected due to presented losses distribution. Longer circulation times at heel create longer damage zone compared to toe. It denotes the shape and limit of the damage zone for our model. Next step, we determine the damage zone permeability.

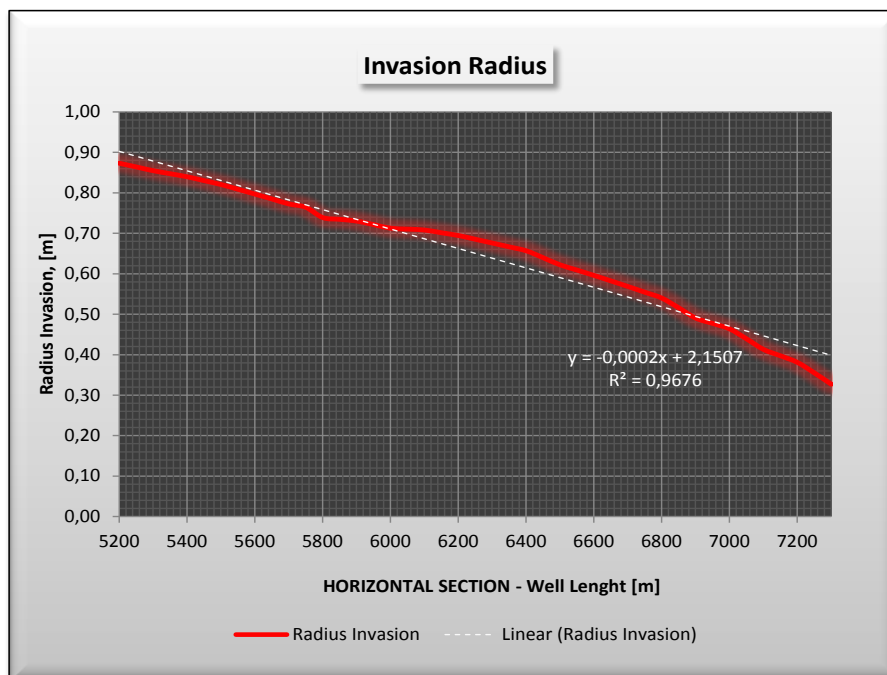


Figure 17. Radius of invasion

3.6.2. Damage permeability – “Maximize simulation tool”

The “Maximize” simulation tool is now used to capture the damage permeability, right after drilling have finished and before clean-up process initiate. Drilling fluid properties as given by van der Zwaag et al., (2012) are listed in Table 4. Core properties are assumed as default values for this kind of test. We do simulate return permeability test at lab conditions and then upscale to field conditions. Initially we do focus on mud (solids and polymers) PSD-particle size distribution and pore throat trapping to obtain the damage permeability. Note that we define two drilling fluid (solids particles) that affect the permeability near wellbore (Mean size of the numbers of particles Mud A: $\approx 10 \mu\text{m}$; Mud B: $\approx 7 \mu\text{m}$;) in order to better explain the clean-up mechanism. In reality, non-damage fluids as shown in Table 4 (PSD terms, based on volume of particles instead of numbers of particles) are reported and used to obtain higher K_{return} in short time, for instance 90-95%.

Table 4. Drilling fluid properties

Drilling fluid properties			Core Properties		
Description	Value	Unit	Description	Value	Unit
Density	1,15	SG	Core type	Linear	
PSD, D_{10}	2	μm	Core length	8	cm
PSD, D_{50}	20 - 29	μm	Core diameter	3,8	cm
PSD, D_{90}	59 - 143	μm	Filter cake diameter	3,4	cm
Xanthan concent	0,005		K, abs permeability	600	mD
Starch concent	0,015		ϕ , porosity	0,25	
Brine concent	0,95		Si, initial saturation	0,2	
Solids concent	0,03		T, temperature	20	$^{\circ}\text{C}$
Mud A - Particle diameter - Mean, Solids	10	μm	Ct, compressibility	0,0001	1/Bar
Mud A – Shape factor	1.24	μm			
Mud B- Particle diameter - Mean, Solids	7	μm			
Mud b – Shape factor	1.12				
Standard deviation	1,5				
Shape factor	1,2				
Grain density	2,65	g/ml			
Tortuosity	3				

The general trapping rate defined as $d\sigma_i = \lambda_i C_i u$ in Equation 3 is solved for each solid and polymer particle size. Note that polymer PDS data is not shown in Table 4. Basically, the software simulate mud is injected into the brine saturated core using a pressure of 15 bar during 90 min or until reaching 1 pore volume. A permeability reduction in time over the core is performed based on Equations 4 and 5 as well as the routine simulation showed by Equation 7 through 10. Time step detailed calculations are not presented here, instead pore volume injected and permeability

reduction results are shown in next Figures 18, 19 and 20 (results from Maximize software). Software setup can be found in Appendix D.

Variation of pore volume injected in time is shown in Figure 18. This behavior is basically resulting of spurt losses, static and dynamic losses. Once the spurt and static losses are reached in the beginning, the dynamic losses tend to be constant. It validates the data presented previously in Figures 15, 16 and 17.

Pore volume is a key parameter to consider in this project. We basically upscale the cylindrical core pore volume to the well segment pore volume of the truncated cone that represents the damage zone. Next Chapter 3.6.3 emphasizes the pore volume approach in terms of damage removal or return permeability.

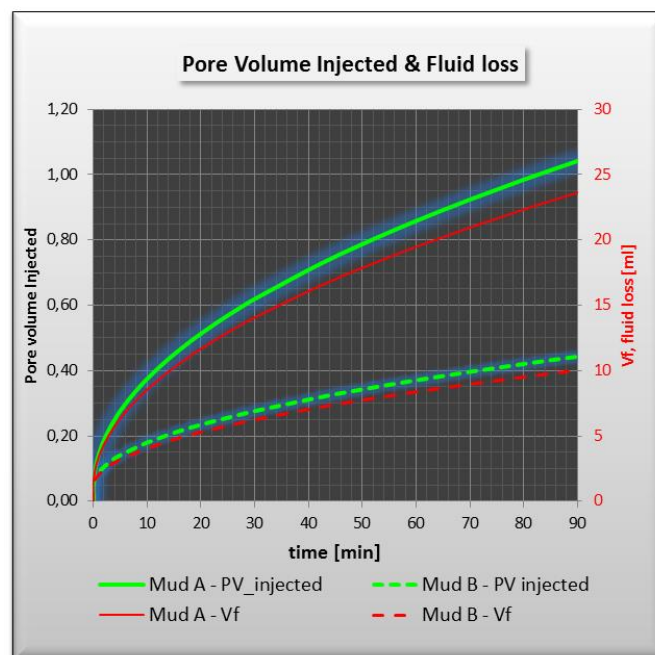


Figure 18. Pore volume injected during mud flooding

The damage permeability of the core after flooding one core pore volume is obtained from Figure 19 and 20. Note that after 30 minutes of the experiment under the established conditions, the damage permeability become constant and around 0,6 pore volumes are injected until this point as shown in Figure 20. Simulation is extended until injecting one pore volume. So the final reduction in permeability (k_d/k) after injecting the Mud A is around 0,41. Considering the initial value of $k=600$ mD, the resultant average damage permeability k_d is 246 mD.

An important assumption here is that obtained value corresponds to an average damage permeability of the entire core. Same assumption is upscale to field condition, in which this value corresponds to a harmonic average between wellbore

radius until the radius of invasion. We do use average damage permeability value in order to input this data into NETool™ simulator at each segment (50 m).

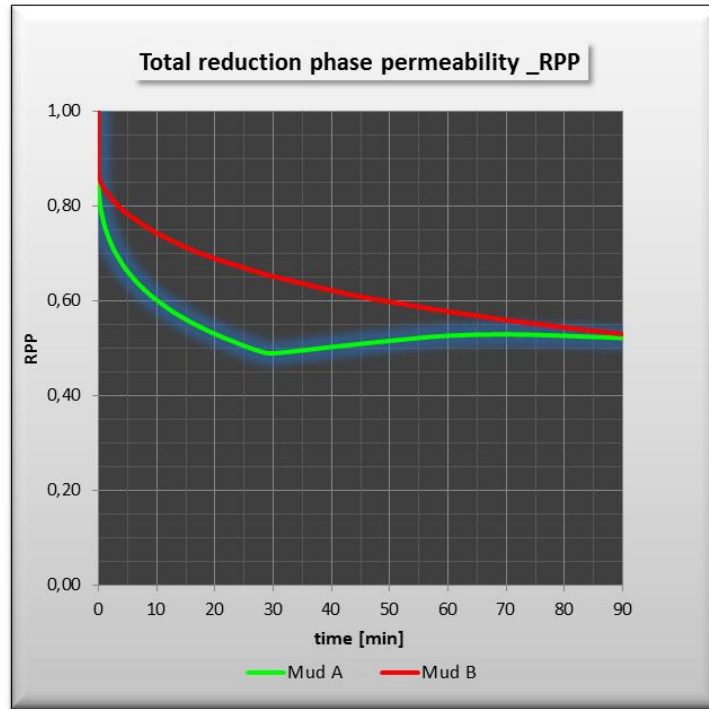


Figure 19. Reduction in permeability over time

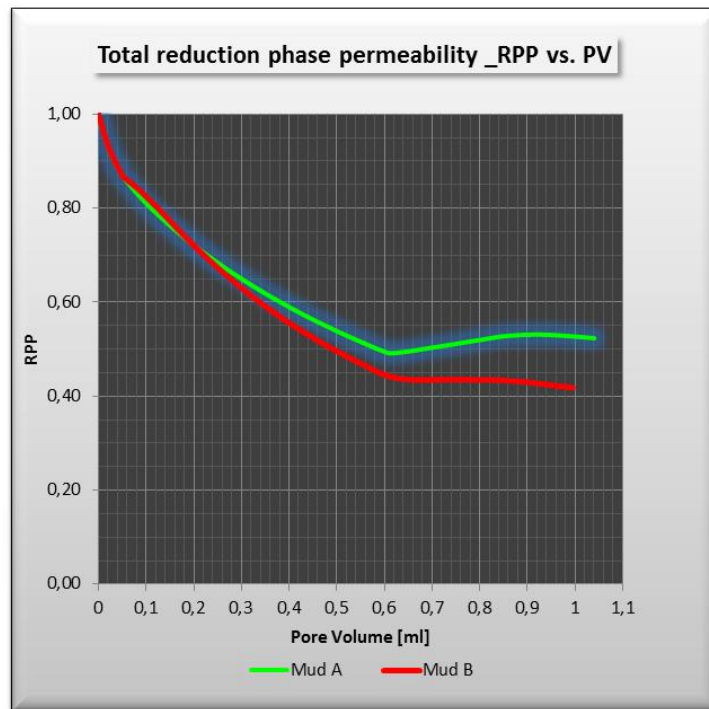


Figure 20. Reduction in permeability vs. Pore volume injected

3.6.3. Return permeability – “Maximize simulation tool”

Return permeability (final k_{damage}/k) is obtained after flow back of oil into the cylindrical core emulating real conditions during clean-up operations. So, the initial average return permeability of the core is 0,52 for Mud A and 0,41 for Mud B, defined as the damage permeability before flow back. Now, oil is flow back at constant rate of 10 ml/m meaning a rate control operation. We do simulate many periods which corresponds to diverse pore volumes injected in an extended time period. Core pore volume injected is constant over time as presented in Figure 21 (results from Maximize software).

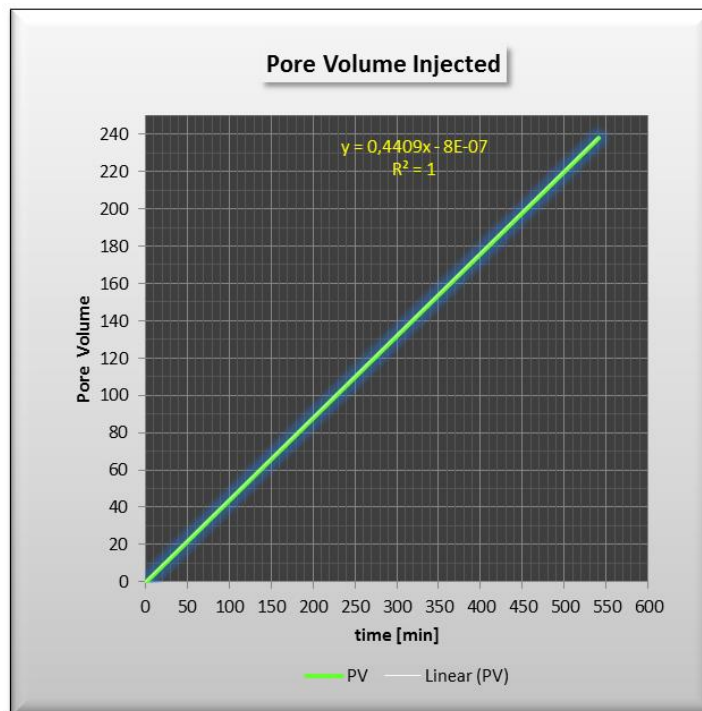


Figure 21. Pore volume injected during flow back

The evolution of damage removal in time is shown in Figure 22 (results from “Maximize” simulation tool).

Clearly we observe that return permeability during flow back follows a tendency similar to a logarithmic or polynomial behavior. It means, during very early time the return permeability follows a very rapid recovery until it gets constant recovery rate after 100 minutes or 60 pore volumes injected. Note that initial damage permeability in Figure 22 and 23 shows 0,41 as initial value for the two fluids, nevertheless we still consider 0,52 as the initial damage permeability for Mud A and no alterations are observed.

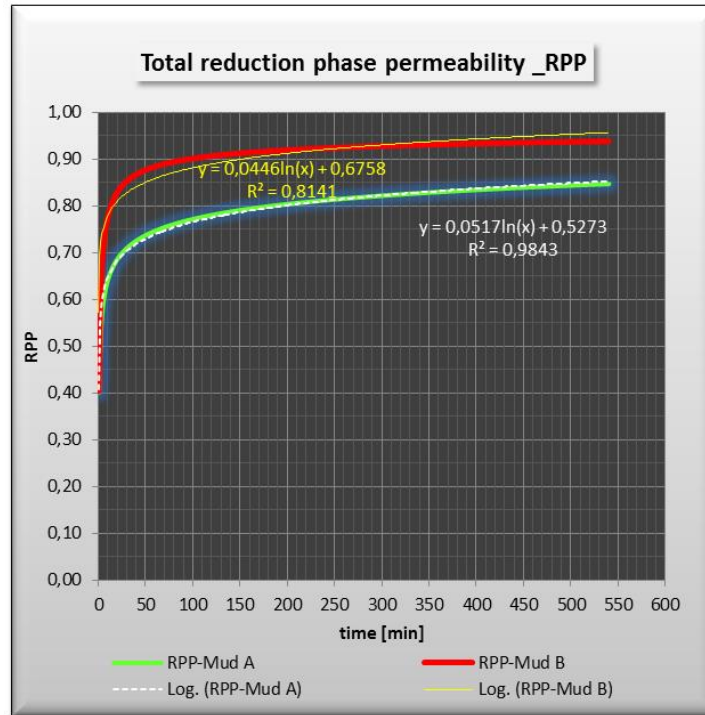


Figure 22. Return permeability variation during flow back

A trend line is established in Figure 22 and Figure 23 in order to obtain a function of the return permeability (k_{return}) versus time, and k_{return} vs injected pore volume (PV), and we get Equations 29:

$$\langle \text{Mud A: } K_{ret} = a_1 \ln(t) + b_1 \rangle \quad \langle \text{Mud B: } K_{ret} = a_2 \ln(t) + b_2 \rangle$$

$$\langle \text{Mud A: } K_{ret} = a_3 \ln(PV) + b_3 \rangle \quad \langle \text{Mud B: } K_{ret} = a_4 \ln(PV) + b_4 \rangle$$

Equation 29. Return permeability functions

Constant values of a_1 , a_2 , a_3 , b_1 , b_2 , b_3 are shown in Figure 22 and Figure 23; nevertheless we observe that not always the logarithmic behavior is approached to lab results, especially for less damaging muds like Mud B (comparing yellow line and red line). In the regression process, the outcome of R^2 is around 0,81 showing a higher discrepancy on the modeled data. For this reason, a different approach is used for Mud B data as shown in Figure 23 (results from Maximize software).

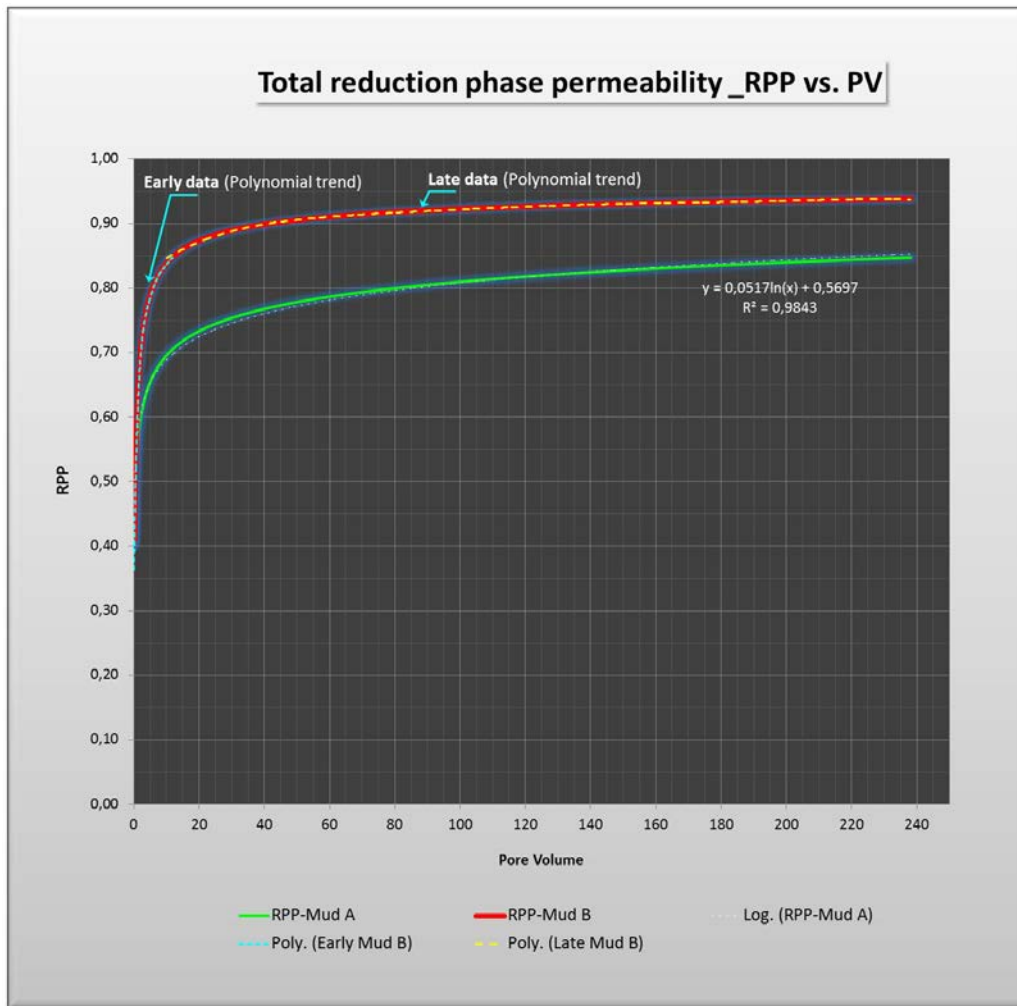


Figure 23. Return permeability variation vs. Pore volume

Figure 23 represents an important finding regarding of return permeability variation due to changes in pore volume. Mud B is used in this study due to higher return permeability values compared to Mud A. The logarithmic function describe very well data from Mud A; however, in order to improve accuracy of the model using Mud B, data is split into early and late time having a cut off pore volume of 12. A six grade polynomial approach ($K_{\text{return}} = a PV^6 + b PV^5 + c PV^4 + d PV^3 + e PV^2 + f PV^1 + g$) is used on each data set to estimate return permeability based on pore volume flushed (cyan and yellow dashed lines). It is important to mention that data adjustment is performed for early values ($3 < PV < 10$) due to instability of the polynomial trend. The use of a trend line try to make the process faster and any function could be obtained. In fact, the function should describe a very rapid improvement of K_{return} at early times.

An important parameter that determines different return permeability is associated to the particle distribution. For instance, the total surface area is the sum of the surface

area of all particles, but it is not true with particle diameter, which is only an unambiguous property if all particles have the same size. It makes differences if one chooses to base the mean size on the number of particles or on the volume of the particles as given by Lohne, Maximize Technical documentation, (2002). For the investigative purpose of this project, we based the particle distribution and total surface area on the mean diameter. We use Mud B lab results to estimate the specific return permeability for each segment (50 m) at field conditions as per Figure 24, then simulate drawdown and influx rate in NETool™. Damage zone shape is a truncated cone with inner boundary r_w and outer boundary r_i or radius of invasion. Each segment is 50 m width. We now proceed to upscale return permeability (Mud B) to field conditions.

3.6.4. Upscaling the return permeability and clean-up process

The main assumption in the entire project and the upscaling process is quoted as:

“Pore volume of the lab cylindrical core is similar to each field pore volume of the segmented cone as shown in the dash red zone of Figure 24”

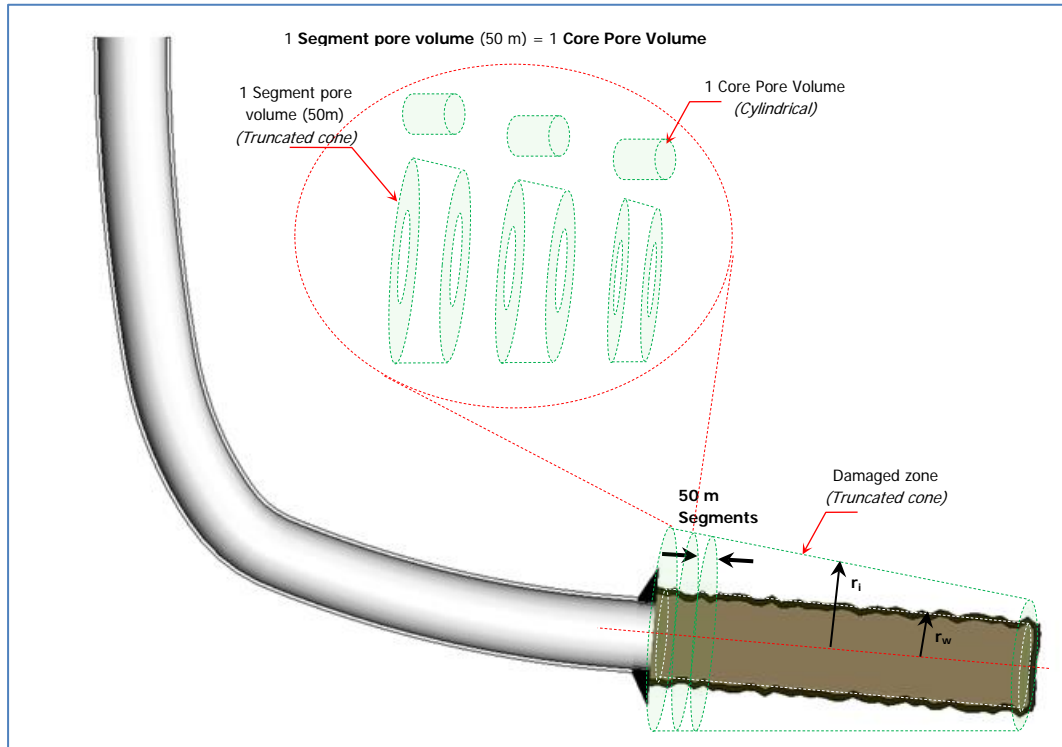


Figure 24. Damage region - Truncated cone

Using this statement we upscale the return permeability from the lab to the damage zone in the field. Lab linear flow is only different to radial field flow at early times during cake build up period; it means the flow resistance is mainly due to cake build up. But after that, fluid loss can be treated linear than radial at field conditions as reported by Han et al., (2005). It validates our assumption for return permeability upscaling from lab to field conditions. This process makes each calculation a time step and it is better explained by the Figure 25.

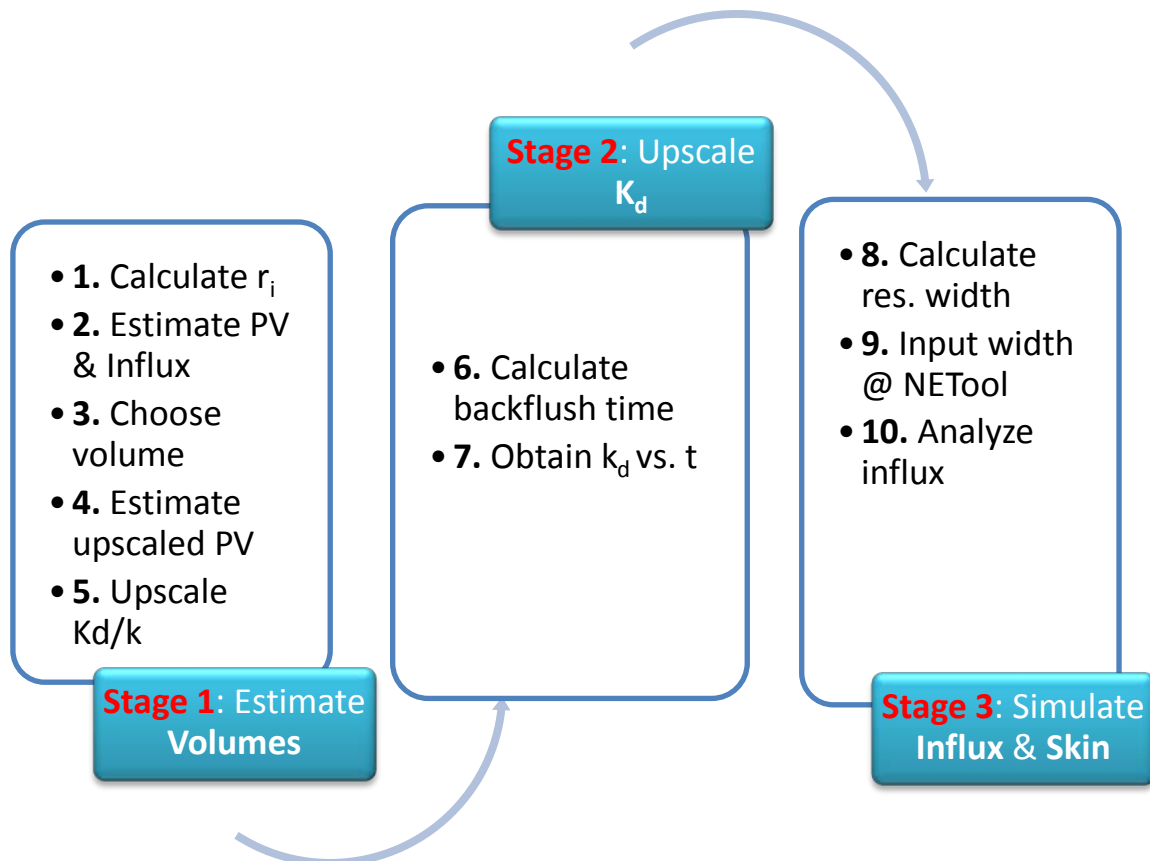


Figure 25. K_{return} upscaling process

The first stage start with the calculation of r_i (radius of invasion) of each 50 m segment (truncated cone from heel to toe). Then, we estimate PV-Pore volume [m^3] and influx rate per segment [m^3/d] (Influx rate is constant for ICD completion). We now choose a specific volume to be flushed back [m^3] (same for each segment) and we estimates upscale PV flushed back (Step 3/Step2). Finally in this stage, we upscale k_d/k from lab to field using Equation ($K_{\text{return}} = a \text{PV}^6 + b \text{PV}^5 + c \text{PV}^4 + d \text{PV}^3 + e \text{PV}^2 + f \text{PV}^1 + g$) for each truncated cone from heel to toe.

In the second stage, we determine the time it takes to flushed back the volume from Step 3. Then, we obtain K_{return} vs. time equation for heel and toe.

At third stage, we calculate the reservoir width using time from Step 6 (transient flow). Then, we input reservoir width into NETool Joshi model. The latest step leads us to analyze output from NETool - Influx rate, drawdown and skin. Detailed results are presented as follow:

- **Step 1 to 5**

Following the steps from 1 to 5 described in Figure 25, we get the variation of the return permeability at specific time for each particular segment of the entire horizontal section. Figure 26 show results for ICD completion at early times ($t < 15,9$ hr). At the toe, where the invaded zone is shallow and the invaded volume small, it takes a small volume of back-production to significantly improve the return permeability.

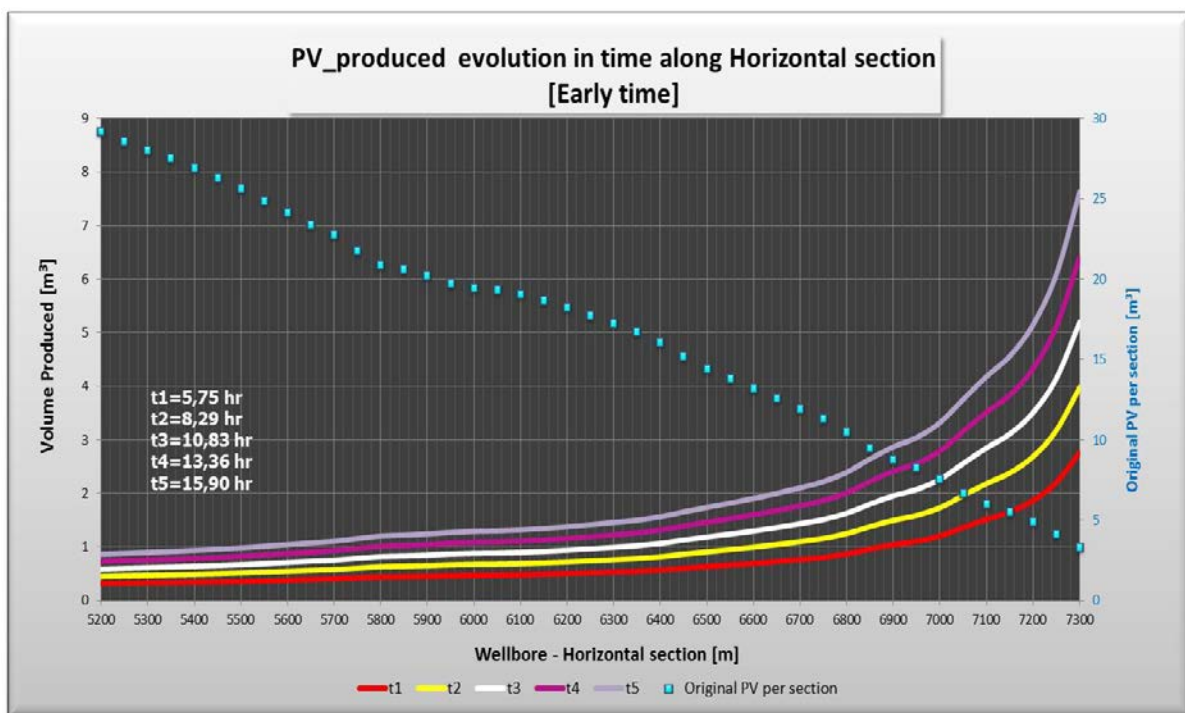


Figure 26. PV produced, evolution @ early times

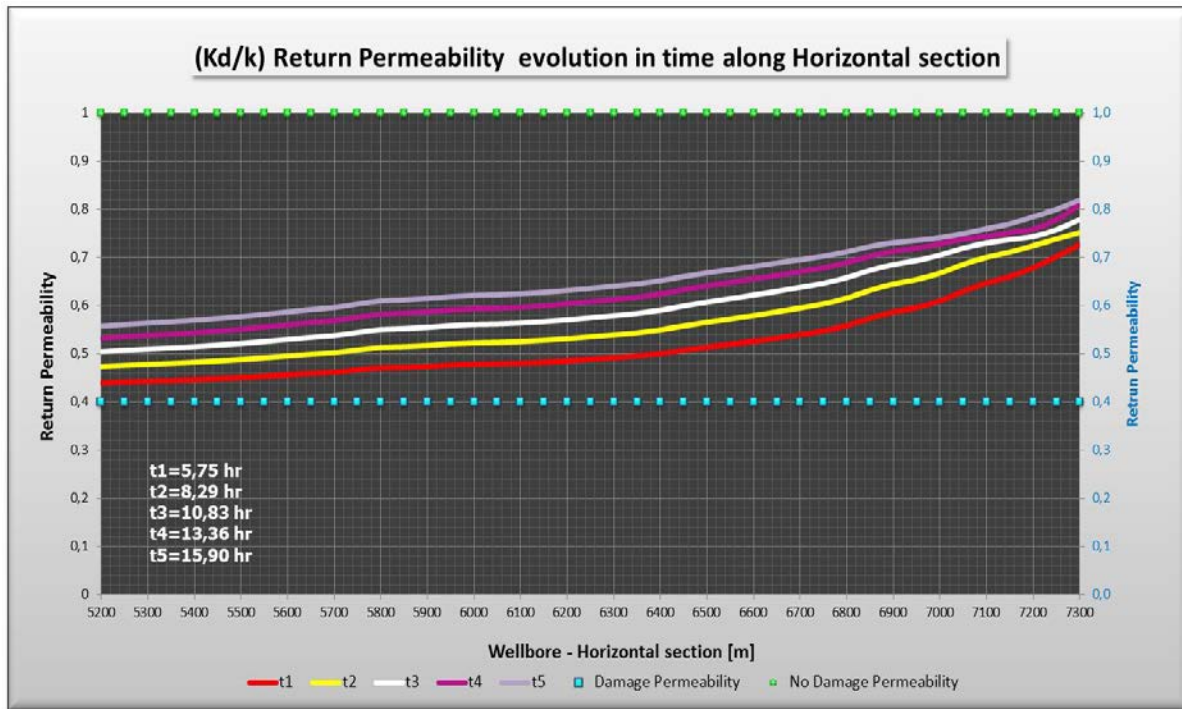


Figure 27. Return permeability evolution @ early times

For instance, the invaded volume for the 50 m segment at heel is $29,19 \text{ m}^3$. If flushed a volume of $9,08 \text{ m}^3$, we get 0,31 pore volume flushed. It is represented by the red line (left point at heel) in Figure 26. The process is performed for the entire horizontal section.

Using the six grade polynomial trend of the K_{return} function obtained at early times from Figure 23 (Mud B, red line), we get 0,44 return permeability (time step 5,75 hr). It corresponds to the red line (left point at heel) in Figure 27, and it is also performed for the entire horizontal section.

It leads to obtain a better return permeability at the toe as shown in Figure 27. For instance, at time step 5 the K_{return} is 0,82 at toe and 0,55 at heel. We also observe the higher recovery at the toe in short time due to the polynomial approach at early data.

Dashed blue line in Figure 27 represent the initial damage permeability before clean-up (obtained from "Maximize" simulation previously, it is assumed to be constant value of 0,40 along the horizontal section) and dashed green line represents the initial formation permeability or return permeability of 1. Even at early times the return permeability recovers in high values due to the logarithmic equation as shown by previous Figure 22 and 23. For late times, the produced pore volume and return permeability evolution is shown in Figure 28 and Figure 29. At time step 5 (48,19 hr), the toe has recovery the return permeability at values of 0,87 while the heel values

of 0,72. It is clear that recovery is slower at late times than early times due to the constant evolution instead of logarithmic/polynomial severity of the early times. If comparing Figure 27 with Figure 29, we observe the constant evolution of the return permeability along the horizontal section. Similarly, we observe the toe is cleaned up very nicely showing the advantage of the ICDs.

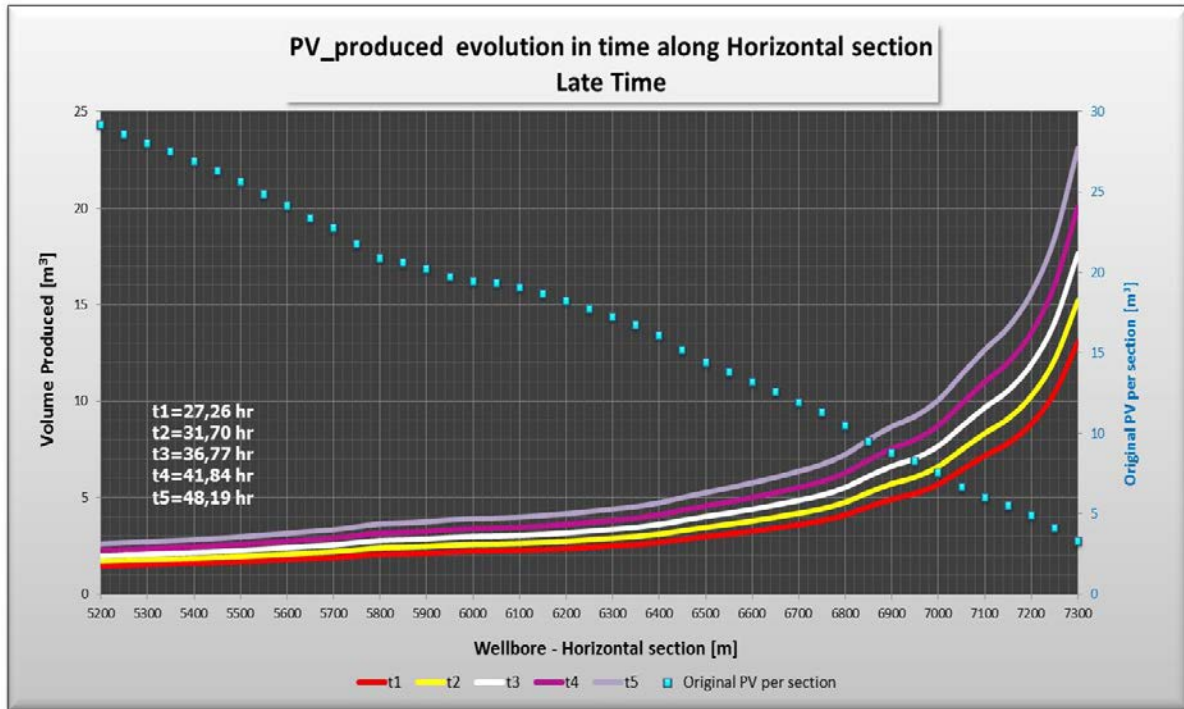


Figure 28. PV produced, evolution @ late times

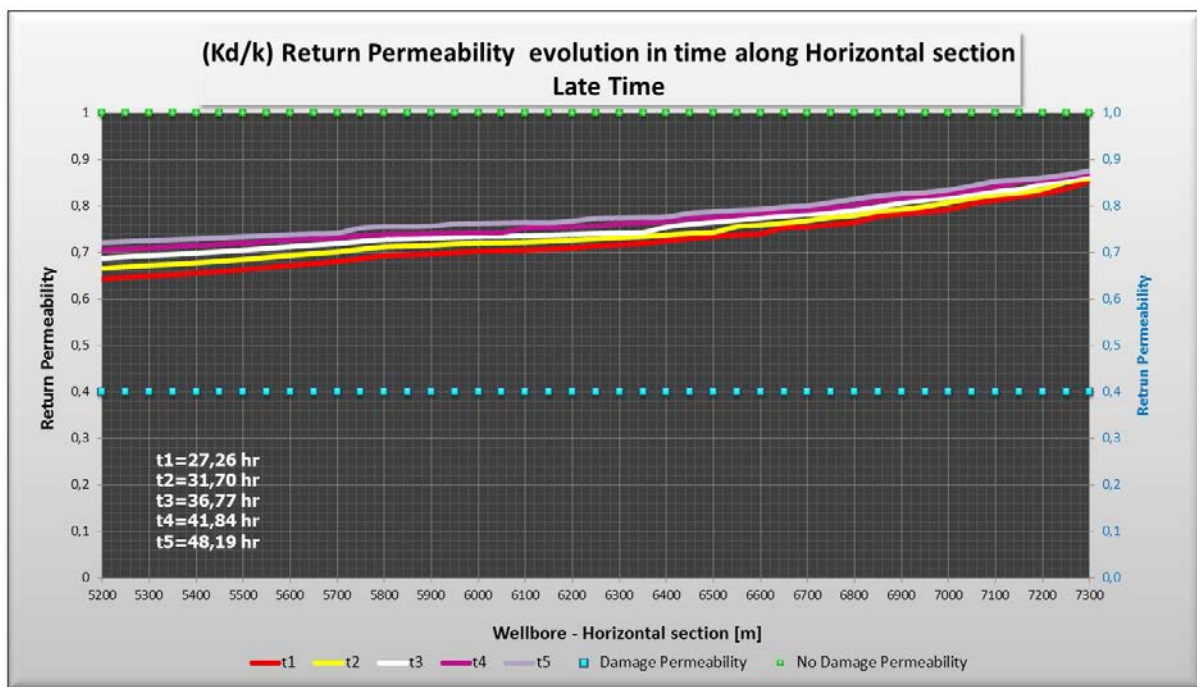


Figure 29. Return permeability evolution @ late times

- **Step 6 to 7**

From the upscaling process shown in Figure 25, we can calculate in step 7 a correlation between return permeability and clean-up time.

Extensive iterations of the lab data upscale to field conditions allow us to obtain a function of the return permeability at the heel and the toe for field conditions. They are shown in Equation 30, 31 and Figure 30. Note that this function is only representing one particular mud type, in our case, our mud conditions as shown in Table 4. This finding is a key element in the project and gives the benefits to an engineer to estimate a desired return permeability in a particular section of the well.

$$K_{return@heel} = 0,0714 \ln(t) + 0,6128$$

Equation 30. K_{return} @ Heel, evolution in time

$$K_{return@toe} = 0,1402 \ln(t) + 0,1772$$

Equation 31. K_{return} @ Toe, evolution in time

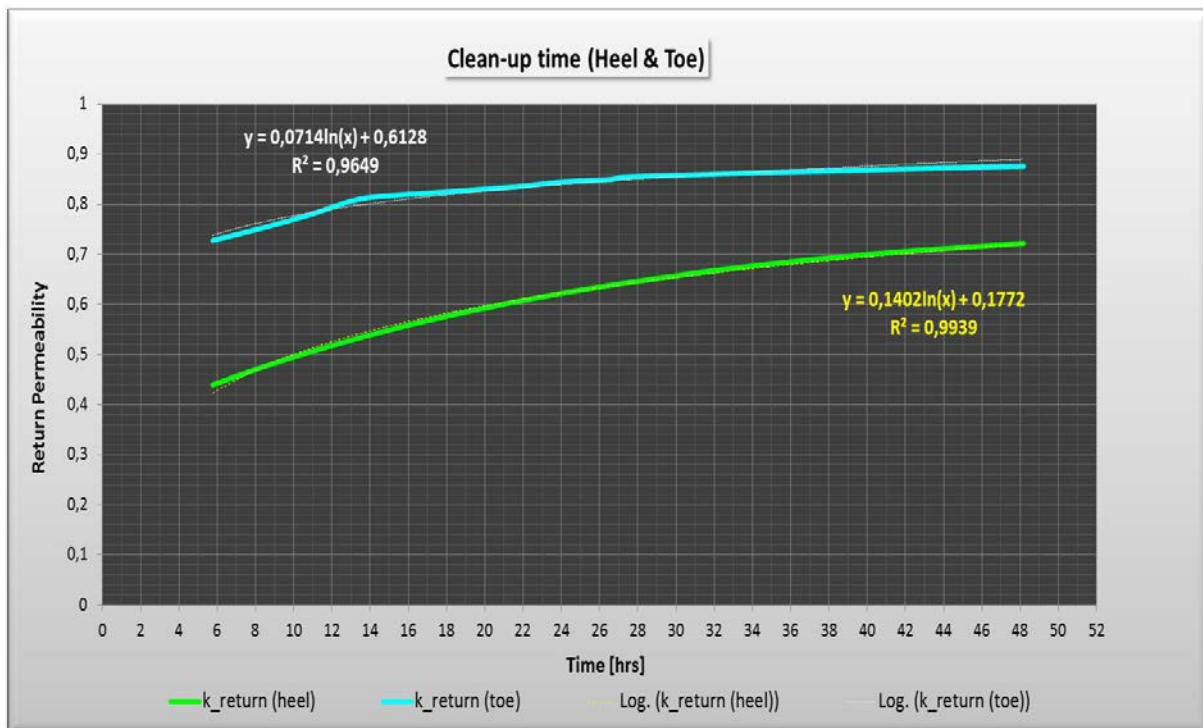


Figure 30. Clean-up time @ heel and toe based on K_{return}

Figure 30 represents one of the most important findings in this project. The return permeability at both well boundaries (heel & toe) can be estimated in time assuming the initial considerations of formation damage. The logarithmic trend line is shown in Figure 30 as well as R^2 values of the regression process indicating a good approximation of the simulated data. Note the curves try to become closer as time goes indicating the tendency of equalize the return permeability at both well boundaries.

Using Equations 30 and 31 we can estimate the time it takes to obtain a specific return permeability value in the field. For instance, in order to get 85% of return permeability for this particular Mud B, we must clean-up the toe during 27 hrs while the heel during 121 hrs. Heel values are very high due to the damaging condition of the mud assumed. For practical purposes, a non-damage condition of a well-designed mud may take less time. The equation represents our initial thesis regarding of the clean-up effects based on cumulative flow. The more flow pass through the specific damage zone, the better the return permeability and clean-up effect.

Continuing with step 6 in Figure 25, we calculate the exact time in which the chosen volume in Step 3 is flushed back (it physically represents the clean-up effect). $Time = volume/influx$, and influx rate per length calculated for ICD completion is 0,757 $m^3/d/m$, so for a 50 m segment the influx is 37,85 m^3/d . For instance, at heel the volume of damage zone (truncated cone) is 29,19 m^3 based on Equation 32.

$$Vol = \frac{\pi}{3} \phi (R_i^2 + R_i r_i + r_i^2) * \Delta h - (\pi r_w^2 * \Delta h * \phi)$$

Equation 32. Volume of truncated zone (Segmented damage region)

In Equation 32, R_i represents radius of invasion at segment start, r_i is the radius of invasion at segment end, r_w is the wellbore radius and Δh is assumed as 50 m segment. ϕ is the porosity. Total wellbore length is divided into 50 m segments. Truncated cones (damage zone) volumes are shown as dash blue line in Figure 26 (right vertical axis). If we choose a random volume of 15,41 [m^3] Time step t_1 is calculated as 15,41 [m^3] / 37,85 [m^3/d]. We, then get 9,77 hrs. Different time step are shown in Table 5. Return permeability reported in Table 5 is calculated using Equation 30 and 31. Note that Equation 32 considers 100% pore volume flushed.

Table 5. Time steps and reservoir width

Time Steps			Reservoir Width		
Time Step	Time [hrs]	Cum Vol Flushed back [m ³] per 50m segment	K _{return} @ heel	K _{return} @ toe	Reservoir width (LRF flow regime) [m]
t ₀	5,75	9,08	0,440	0,728	1921
t ₁	9,77	15,41	0,492	0,780	2742
t ₂	15,90	25,08	0,558	0,820	3680
t ₃	26,6	42	0,639	0,850	4909
t ₄	36,77	58	0,688	0,866	5833
t ₅	48,19	76	0,722	0,876	6727

Based on calculated time, we estimate the reservoir width for the Joshi model in NETool™ using Equation 22. This approach validates the transient pressure into the steady state simulation of NETool™. We do estimate transient pressure for LRF- Late radial flow that occurs when $t > 5,75$ hr, so the assumed time steps are inside this period.

▪ **Step 8 to 10**

Using reservoir width from Table 5 (Equation 22), we now input the Joshi PI model into NETool™. Likewise we input the return permeability (k_d/k) obtained at every individual segment along the wellbore (Figure 27 and 29) into NETool™ and obtain the drawdown for each particular time step as shown in Figure 31.

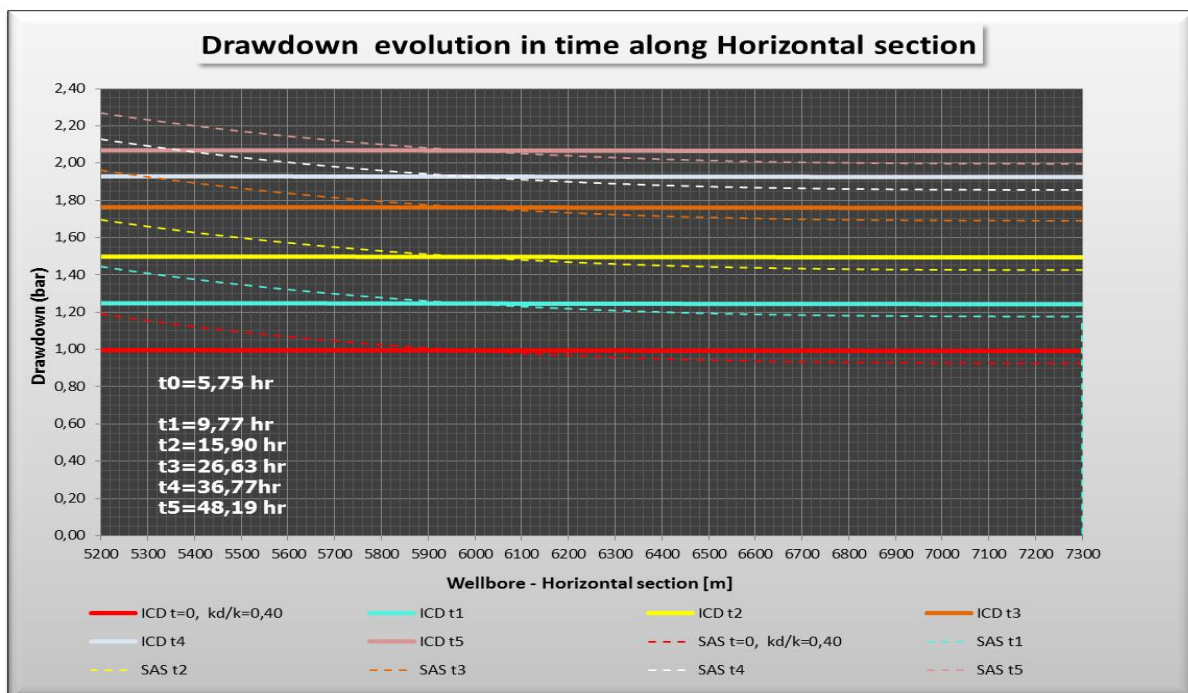


Figure 31. Drawdown evolution during clean-up: ICD vs. SAS

It is clear that ICD completion maintain a constant drawdown due to the choking effect of the nozzles, while SAS completion (dashed line) induces higher drawdown at heel. From $t_1=5,75 \text{ hrs}$ to $t_5=48,19 \text{ hrs}$ the drawdown is increased as expected.

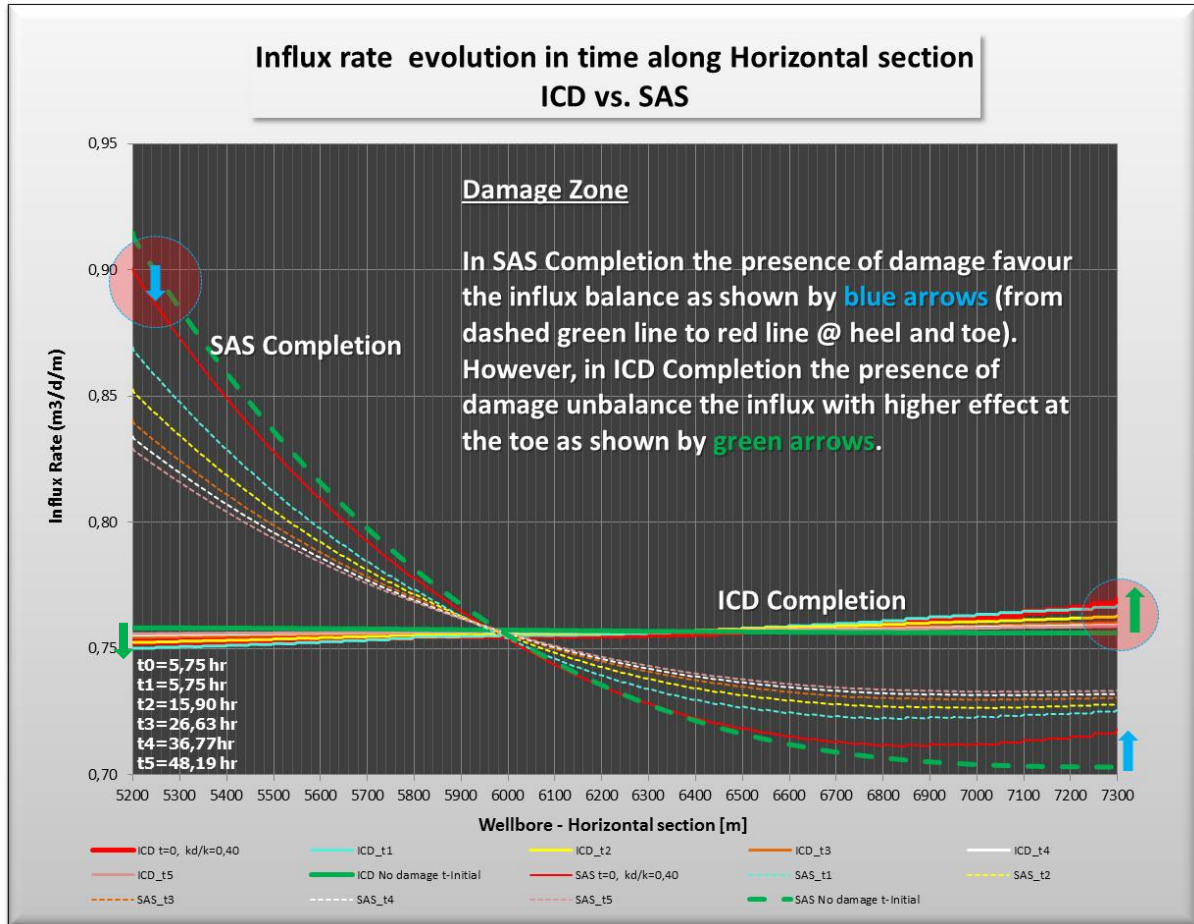


Figure 32. Influx rate evolution during clean-up: ICD vs. SAS

Figure 32 is another important graph in the project; it represents the evolution of the influx rate during clean-up time for both ICD and SAS completion (data obtained from NETool™). Our study is founded on the cumulative flow per segment that passes through as the key effect of cleaning efficiency while improving the return permeability. Five different time steps (Table 5) are orderly and even spaced to observe the removal of damage during clean-up process.

In the SAS Completion the presence of damage favors the influx balance as shown by blue arrows in Figure 32 (from dashed green line to red line @ heel and toe). It means that the truncated cone shape of the damage zone in the SAS completion will tend to slightly balance the influx rate; nevertheless the effect will not reach the stable ICD behavior of the influx rate as dictated by the almost horizontal green line.

However, in the ICD Completion the presence of damage unbalance the influx with higher effect at the toe as shown by green arrows in Figure 32.

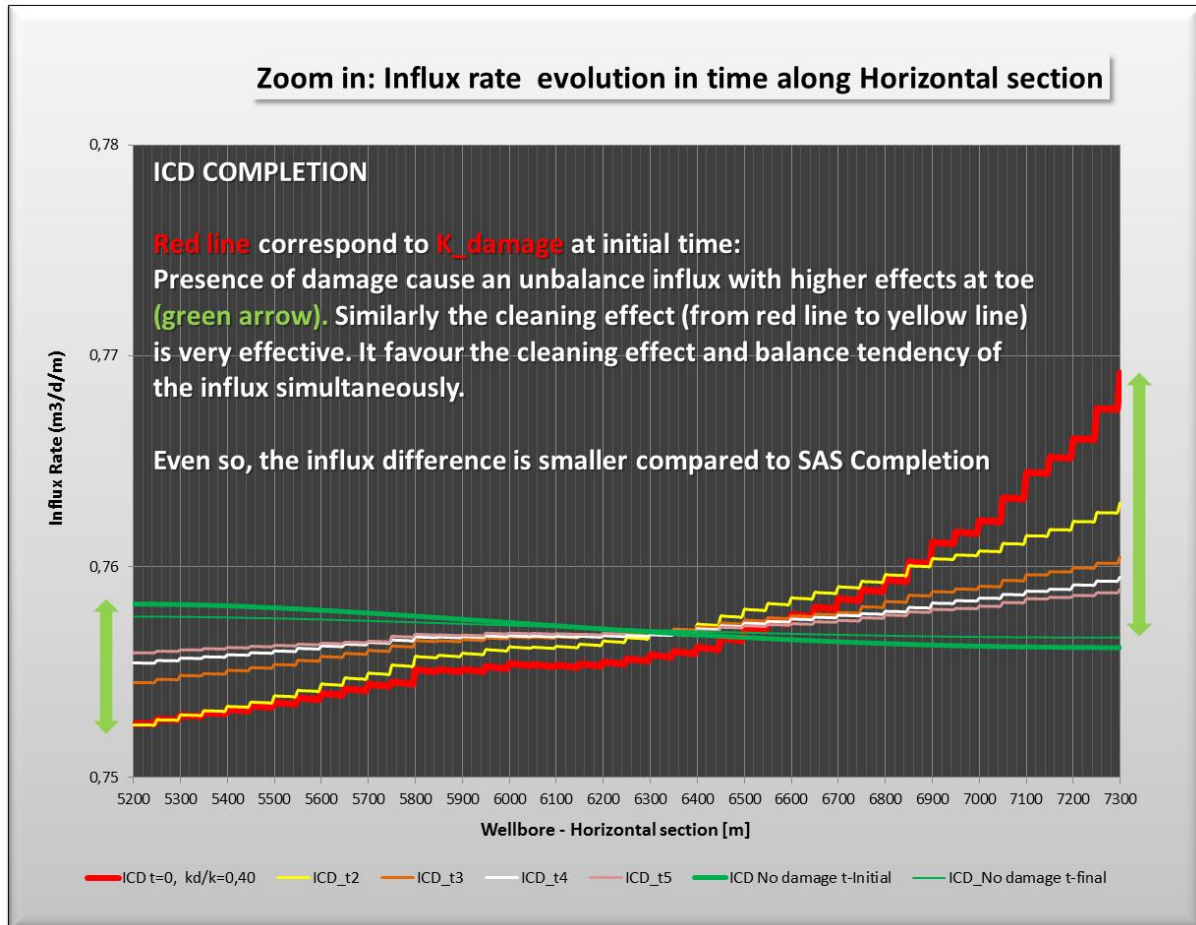


Figure 33. Detailed Influx rate evolution during clean-up: ICD

Data from Figure 32 is plotted in smaller scale in Figure 33 for better analysis of the damage zone into ICD completions. Red line corresponds to K_{damage} at initial time. Presence of damage causes an unbalance influx with higher effects at toe (green arrow). Similarly the cleaning effect (from red line to yellow line) is very effective at the toe, so it proves one of the greatest benefits of using ICD to improve and produce the toe section of horizontal wells. It favors the cleaning effect and balance tendency of the influx simultaneously.

Even so the influx difference is smaller compared to SAS Completion, the ICD offers a better stability of the influx during clean-up period. In the discussion session, both aspects (clean-up & balance influx) are separately analyzed based on the damage zone established in the model.

4. Discussion

4.1. SAS vs. ICD drawdown and influx rates

Results exposed in Chapter 3.3 clearly show the increase drawdown and influx at the heel in horizontal wells, even at low flow rates. One of the initial theses that appear in the project is that the midpoint of the well can be used as an average assumption of the total well drawdown pressure, and then use the Joshi equation to prove it. It motivate us to stablish a relationship between a calculated Joshi model using Excel compared to the results obtained in the NETool™ simulation (mid-point), and analyze the data results. Based on well data from Chapter 3, we obtain a value of 0,915 bar at 6250 m (midpoint). Using Equation 16 from Joshi horizontal well productivity model in field units, we calculate the pressure drop ΔP (bar) as follow:

$$\Delta P = \frac{141,2q_H\mu B_o * \ln \left[\frac{a + \sqrt{a^2 - \left(\frac{L}{2}\right)^2}}{\frac{L}{2}} \right] + \frac{h}{L} \ln\left(\frac{h}{2r_w}\right)}{k_o h / 14,5}$$

ΔP

$$= \frac{141,2 * 10000 * 0,5 * 1,5 * \ln \left[\frac{4667,6 + \sqrt{4667,6^2 - \left(\frac{6889,8}{2}\right)^2}}{\frac{6889,8}{2}} \right] + \frac{114,8}{6889,8} \ln\left(\frac{114,8}{2 * 0,354}\right)}{600 * 114,8 / 14,5}$$

$\Delta P = 0,9218 \text{ bar}$

It means that drawdown calculation at midpoint from NETool™ simulation is different - at the beginning - to the calculation using Equation 26. Figure 34 show the proximity of the data. Cyan line represents the drawdown for stand alone completion simulated from NETool™. Orange dashed line is the average value at midpoint 6250 m, it means 0,9152 bar and yellow line shows the calculation using Joshi formula 0,9218 bar (Equation 16). The red line represents a big size nozzle ICD, which do not stabilize the drawdown. Green and cyan dashed line represent small size nozzle ICD that stabilize drawdown.

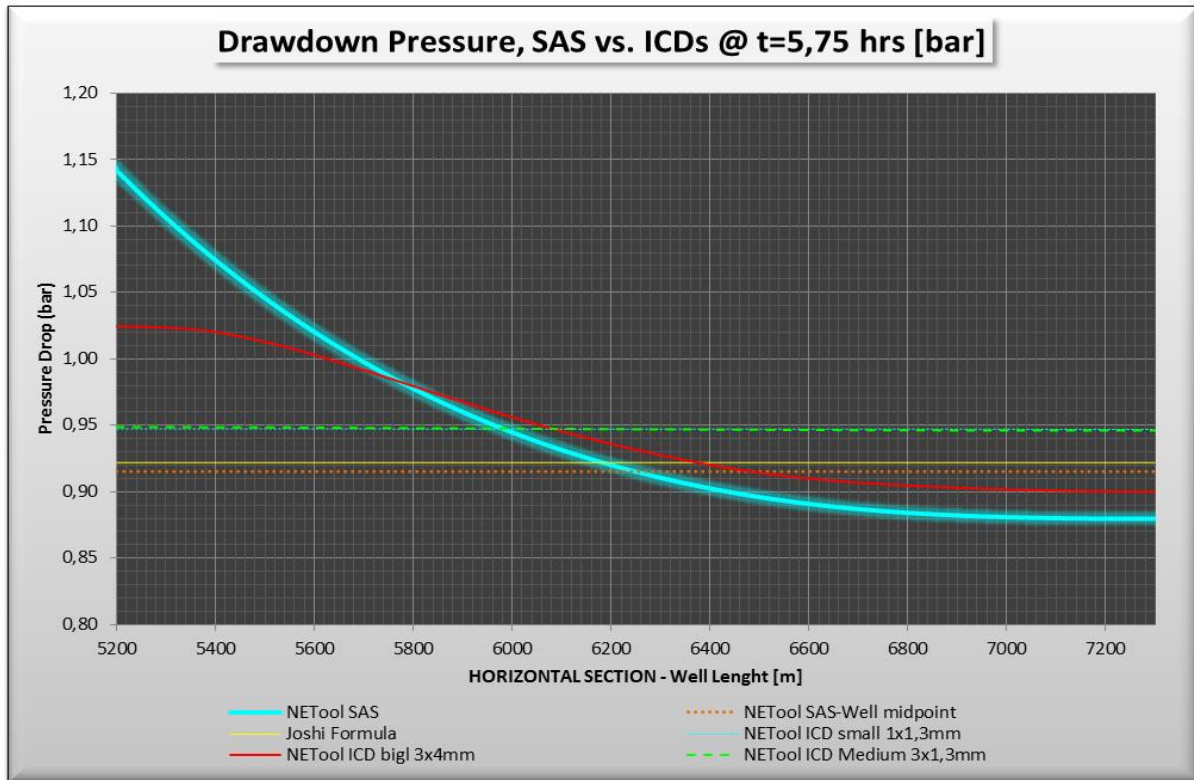


Figure 34. ICD and SAS Drawdown pressure

We observe that both SAS and ICD drawdown pressure do not match at well midpoint even the Joshi model. It indicates us that our study about clean-up process and its analysis cannot be focus on drawdown pressure, but instead, the influx rate is used for this analysis.

Plotting same data (from NETool™) as presented in previous Figure 34 at time step (5,75 hrs) for both SAS and ICD influx rate, we get Figure 35. Cyan line represents the SAS influx rate and yellow dashed line the big nozzle ICD design. Any nozzle size above the average optimum size will behave as stand alone completion, implicating non balance influx rate.

Clearly from Figure 35 we note that Joshi influx rate calculation, mid-point calculation and medium as well as small size nozzle ICD design behave all stable and very similar. It is a great point into the discussion and initial thesis about using influx rate to evaluate clean-up effects instead of drawdown pressure.

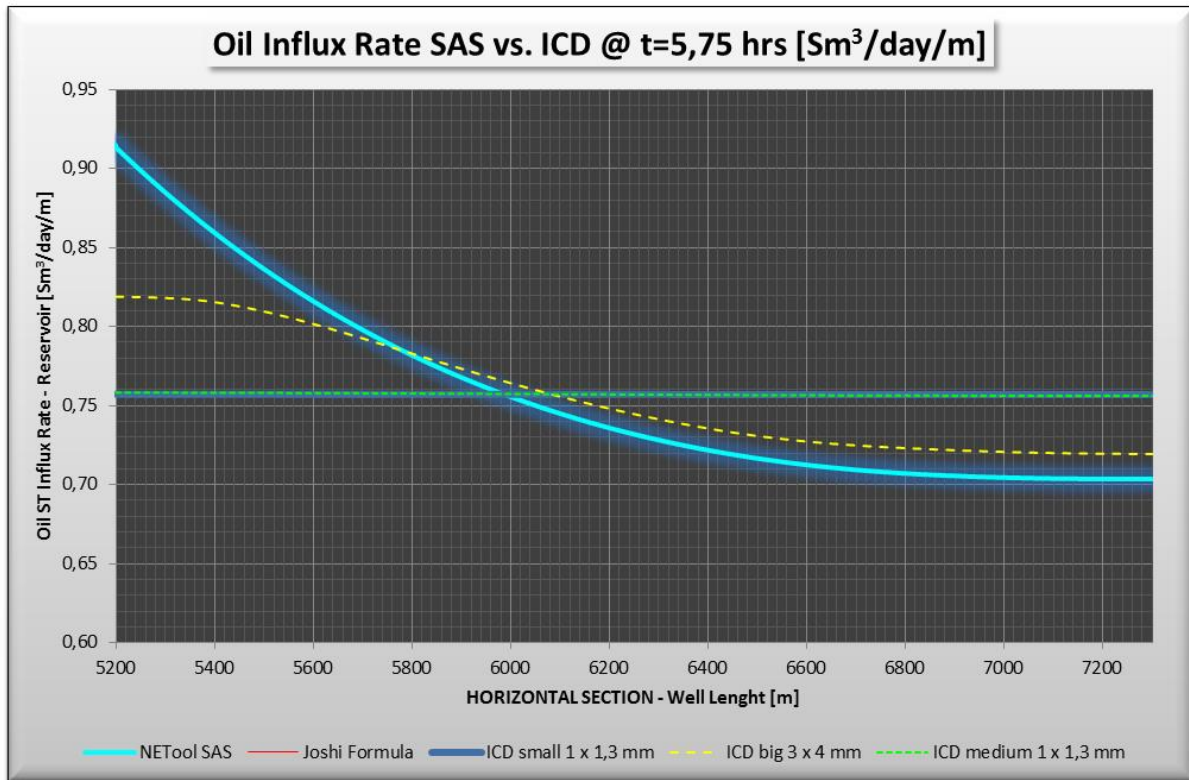


Figure 35. ICD vs. SAS Completion – influx rate

4.2. Flow regimes and transient pressure

For this particular well design, we have assumed clean-up process occurs during LRF – late radial flow regime. LRF boundary conditions are moving backward until reach the Joshi model limits, so it integrates the transition period ($5,75 > t > 9,77$) into late radial flow. In conclusion, our LRF analysis and clean-up period is modelled after $t > 5,75$ hr, which is logical from the operational point of view. For shorter horizontal wells, the model is valid at much early times. One of the key findings in the analysis is that wellbore length highly affects the late radial flow. It is dominated by square wellbore length (L_h^2). So, for this particular well length of 2100 m, the assumption of LRF flow regime is feasible.

As mentioned previously, the streamlines (blue arrows) from Figure 6 in the Joshi model match with streamlines (black arrows) at LRF in Figure 7, so it strengthens the initial assumption to establish late radial flow as the best flow regime wherein clean-up occurs.

Another important finding is related to lambda values conditions. Our model match the range of $1,35 < \lambda < 10,02$ calculated from Table 1, thus adding validity to the equating process of transient flow and Joshi model.

In general terms, errors of the model could be listed to the assumed period between 5,75 to 9,77 hr that is integrated into Late radial flow. Note also that ILF-intermediate linear flow end at 1,58 hr, thus there is a transition period until LRF start.

4.3. Final model analysis and benefits of ICD during clean-up

Results presented in Chapter 3.6.3 regarding of the return permeability logarithmic behavior in time are similar to the ones reported by Han et al., (2005) about return permeability variation in dimensionless distance along the core (Equation 6) following an exponential decay tendency. The statement presented by Han et al., (2005) basically mention that at same depth, the return permeability is higher at the limit of the damage zone, in other words, when radius of invasion is higher. Consequently, the return permeability is small at near wellbore vicinity when radius of invasion is same as wellbore radius.

We observe in our study that return permeability recovery is very rapid (at early times) in terms of pore volume produced. It indicates that our assumption of rapid clean-up at the very early stage of the process is valid, due to the great amount of particles that are accumulated near the wellbore compared to the ones far away from wellbore, following a similarity of the statement given by Han et al., (2005). Our observations indicate that return permeability can also follows a logarithmic/polynomial approach instead of an exponential decay. The better the muds particle sizing, the higher the recovery during early times.

In practice, an average value of return permeability is reported from core analysis. Likewise, we use an average return permeability for each segment along the wellbore after upscaling values from lab to field. It validates the average value assumption into NETool™ in order to model the damage zone.

Partial inaccuracies could come from the size the segments (50 m) are chosen in the present project. Main implication to assume this value is the reported information in the literature about losses for Tyrihans reservoir and well conditions.

In Chapter 3.6.3 some damage permeability values at very early time are shifted from 0,52 to 0,40 with no implications or high discrepancies. Values tend to follow the exponential decay function clearly showing the behavior of the return permeability. Similarly, the initial clean-up effect is high when the well is back flowed

or produced. We do use 0,40 return permeability at the beginning of the clean-up process in order to better explain its effect on influx rates calculated from NETool™. The assumption of a constant value of 0,4 damage permeability is reflected in the “U” shape of the red line in Figure 32 (SAS $t=0$, $k_d/k=0,4$). It means, that influx rate can be minimal not only at the toe but some significant distance closer to toe, leading to non-flushed zone due to presence of damage in SAS completion. It is a very common problem associated to horizontal well productivity.

Results obtained from Maximize software regarding of return permeability for Mud A and Mud B (Figure 23) shows R^2 values of the regression process. In Mud B the accuracy is reduced from 0,98 (Mud A) to 0,81 if a logarithmic approach is used. Return permeability values presented in this project are based on a polynomial trend line obtained for two different sets of data: early times and late times. It counts as part of the final error in calculations. The logarithmic tendency we adopt in the process is more accurate for highly damage drilling fluids. For those non-damage fluids, the logarithmic approach does not proper simulate the return permeability behavior at early times, and we do recommend following a polynomial or manual approach.

The main assumption presented in this project stating the same pore volume between the cores as the segmented truncated cone of the damage zone is valid from the proportionality analysis of the system. “Maximize” simulator calculate an average final value of the complete lab experiment. Function obtained after upscaling the results from lab to field conditions (Figure 30) follows a similar trend, in our case a logarithmic behavior in proportion. The assumption is founded on the fact that early filtration process in the field exhibits a flow resistance due to cake build up period mainly. It means that at very early times the flow through the core show a linear flow while at the field is radial. Notwithstanding, after cake is already built, the assumption of linear flow during fluid losses is valid for both lab and field conditions as given by Han et al., (2005).

One of the motivations of this project is to prove the claim that ICD completion offers an improved wellbore clean-up process and fewer concerns are imposed to the productivity reduction as given by Al-Khelaiwi et al., (2009). Findings are shown in Figure 36. Based on the formation damage factors and mechanism defined at the beginning of this project as well as the truncated cone shape of the damage zone established by the radius of invasion, we obtain curves of the time it takes to clean specific zone divided by 50 m segments.

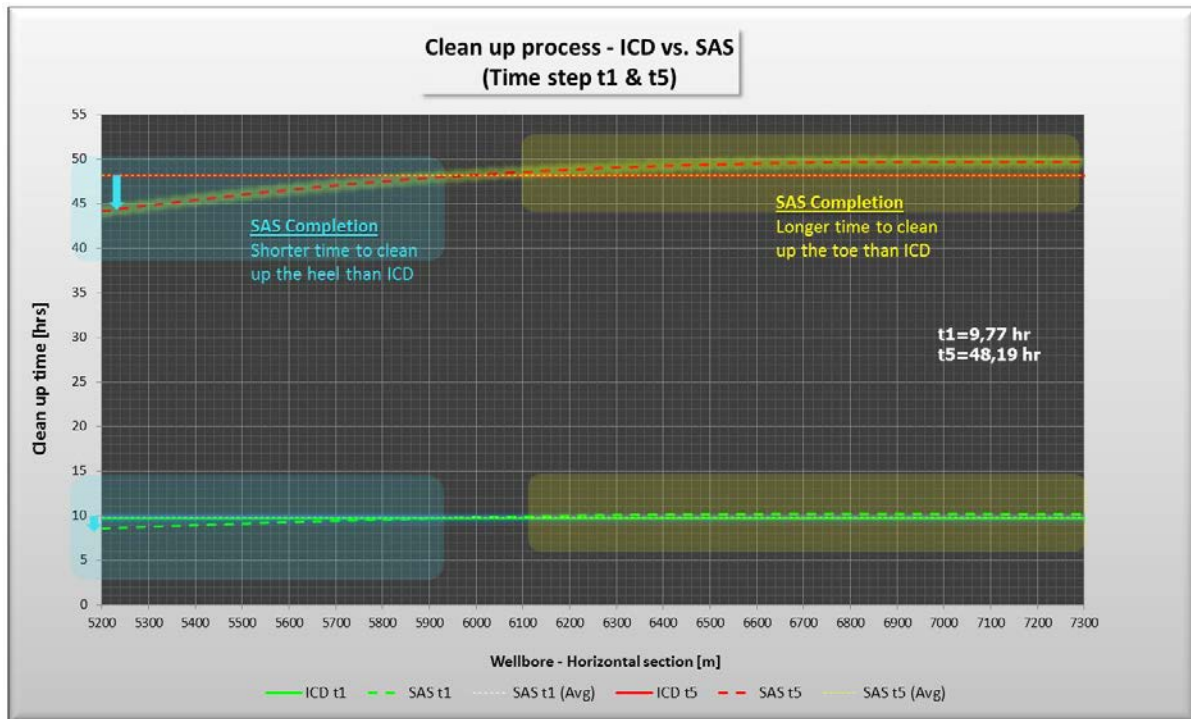


Figure 36. Clean-up time for SAS and ICD completion

In Figure 36 horizontal lines correspond to ICD completions while curved line to SAS completions. Green lines show effects at early times (t_1 : 9,77 hr) and red lines show effects at late times (t_5 : 48,19 hr).

Let's consider the first section at the heel at time step t_5 . For ICD completion, influx rates are obtained from NETool™ and we get 37,85 m³/d for the 50 m segment. At this point the volume flushed is 76 m³ into the conical shape of the damage zone, so we get $76 \text{ [m}^3\text{]} / 37,85 \text{ [m}^3\text{/d]}_{\text{segment}} * 24 \text{ [hr/d]} = 48,19 \text{ hr}$.

Notwithstanding; for SAS completion the influx is higher at heel. We obtain the influx from NETool™ when simulating damage zone in SAS completion. The value is 0,86 m³/d/m and then for a 50 m segment we get an average of 41,29 [m³/d]_{segment}. Carrying out same operation as before we get: $76 \text{ [m}^3\text{]} / 41,29 \text{ [m}^3\text{/d]}_{\text{segment}} * 24 \text{ [hr/d]} = 44,18 \text{ hr}$. This result shows that SAS completion take less time at heel to clean up properly, while it takes longer time at the toe.

Blue zones in Figure 36 shows less time to clean-up the heel for SAS completion and yellow zone longer time to clean-up the toe as compared to ICD. Around 700 m close to heel are cleaned up faster if completed with SAS completion. Why? We do believe the higher radius of invasion at heel due to longer time exposure during drilling require higher cumulative influx compared to the rest of the well. As a matter of fact, the undesired higher influx rate at the heel in SAS completion favors faster clean-up.

But, the longer time SAS completion takes to clean up the toe plus the rapid recovery of the return permeability at the toe while using ICD completion, lead us to conclude the preferential use of inflow control devices to clean up and produce the toe section in horizontal wells.

So, our initial thesis regarding of ICD completion shows as result that this devices effectively balance the ideal influx rate along the horizontal well and may allow higher production rates during clean-up process. It has extensively been proved on literature from operational to simulation sides as given by Aadnoy & Hareland, (2009); Sunbul et al., (2008); Akbari et al., (2014). However, in terms of damage removal based on cumulative flow, the return permeability is recovery faster if SAS completions, or in other words "higher flow area devices" are installed as shown in Figure 36. Note that this statement is based on observations of isotropic considerations. If analyzed from a whole prospective, including influx balance, higher clean-up rates and improved later productivity, the ICD completion may be preferred over SAS completion.

It is also supported by Figure 37, in which the skin removal is higher at the toe as indicated by the blue arrows. Rapid recovery of the return permeability is stimulated due to the balance influx and the small formation damage region (truncated cone at the toe). Figure 37 is calculated from NETool using the mentioned Hawkins skin formula. It also shows the higher recovery of the skin (and return permeability) at early times compared to late times. Thus, from a holistic view the ICD completion seems to be more beneficial.

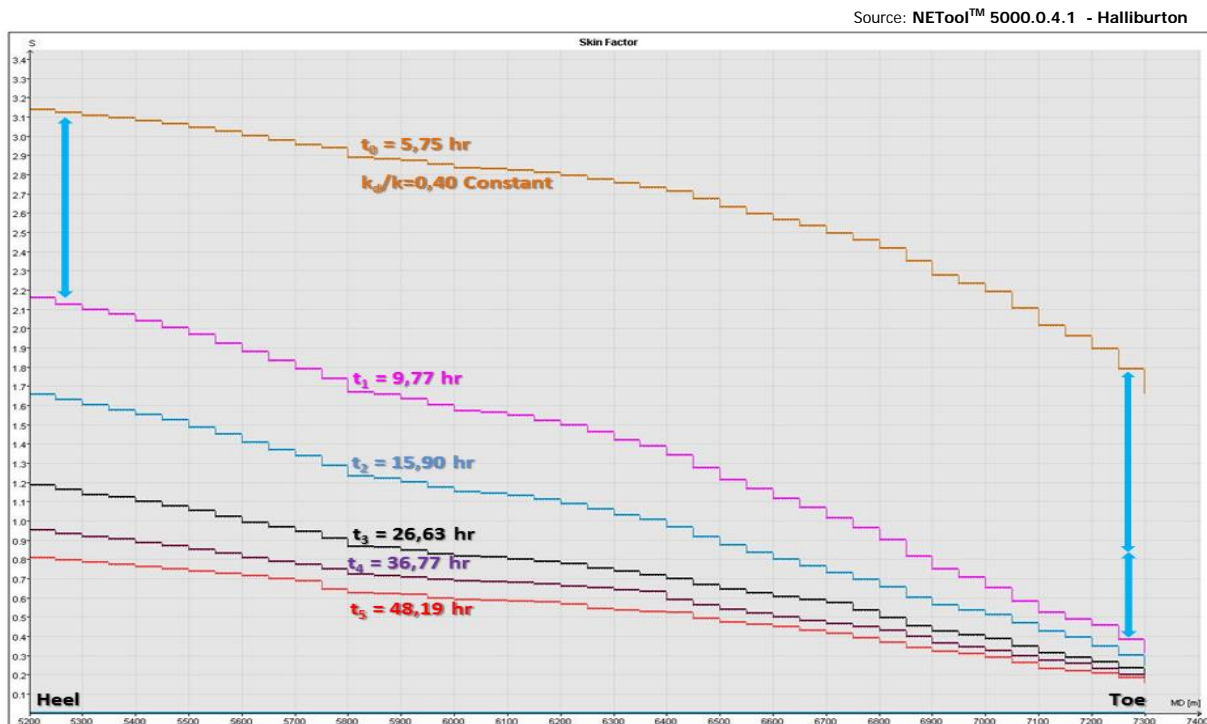


Figure 37. Skin removal during clean-up

The preferred higher influx rate (or higher flow area devices) at heel to remove damage can also be supported with the fact that ICV or inflow control valves are classified as the best completion type for clean-up process due to variable flow area compared to ICD static area as given by Al-Khelaiwi et al., (2009); Stone et al., (2014). For instance in multilateral wells, it has been proved by using tracers that not always ICD completion (alone) are a good option for clean-up process as given by Abay et al., (2013). Under some circumstances, ICD can be used in conjunction with ICV inflow control valves to improve the clean-up process in multilateral wells. Generally speaking, in highly heterogeneous reservoirs the clean-up process is improved by using inflow control valves as preferred completion type, followed by inflow control devices and lately stand alone completions.

Finally, this project offers the great advantage of determine the return permeability variation in time at field conditions, even for specific parts of the well like the heel or toe section. No lab experiments neither production logging data is associated to the model, so it can be very useful during planning stage. For instance if we use Mud B in this project, it takes 27 hr to get 0,85 of return permeability at the toe and 121 hr at the heel. Additionally, the best flow rates can be estimated for an optimal clean-up program considering the return permeability as the key evaluator of the clean-up efficiency. In our example using Mud B, if the flow rate is reduced 20% (from 1589,8 to 1271.8 m³/d) the same return permeability of 0,85 is obtained after a 25% increased time at both heel and toe.

5. Conclusions and recommendations

- The presented model is calibrated in time by using the transient flow equation into the Joshi horizontal well productivity model. It leads to an important interpretation of drawdown and influx rate variation in time, especially for those software results based on steady state flow. It reflects an advantage to some of the commercial static software in the market.
- Integration of lab experimental simulations into field conditions by using upscale process of return permeability, allow us to determine the clean-up effect of the total horizontal section flow. Evolution in time of the field return permeability at heel and toe section can be estimated even if lab experiments have not been performed yet.
- More than one drilling fluid can be evaluated using the current model in order to determine its impact on formation damage. By knowing the polymer and solid particles dimensions (mean size on the numbers of particles or on the volume of the particles) and properties, we can estimate the time it takes to recover a specific cut off value of return permeability.
- The skin variation in time can be obtained while integrating return permeability lab simulations and micro-nodal analysis around the wellbore. It can be an important value for reservoir simulation process. This integration process also include into the analysis the frictional pressure drop along the horizontal section as well as the upscale process of return permeability from lab to field conditions.
- Sensitivity studies of clean-up flow rates can be performed by using the model, so the duration of the clean-up process until reach an specific return permeability value can be estimated.
- Return permeability recovery is severe at the beginning of the clean-up process. It may be related to the fact that more particles are accumulated near the wellbore compared to those at the damage region limit (radius of invasion).
- Inflow control devices improve the clean-up efficiency due to the balancing effect of the influx rate, which indeed, stimulate the toe section to be produced and cleaned up. It is also demonstrated by the rapid evolution in time of the return permeability at the toe. Even so stand alone completion can take less time to clean up the heel due to higher influx rates; it can take more

time to clean up the toe section and in some cases, even not producing at all from that part of the well.

- The current model can be improved by using the measured radius of invasion or damage region obtained from logging data. It adds a more precise analysis of the damage region dimension instead of assuming a straight line between two points.
- Integration of additional damaging factor into the presented model could lead to an improved result to determine the clean-up efficiency of horizontal wells. Similarly, the integration of the current model into a reservoir simulator describing near wellbore phenomenon can be valuable to validate and improve the proposed model.

6. References

- Aadnoy, B. S., & Hareland, G. (2009). Analysis of Inflow control devices. *SPE 122824. Presented at the SPE Offshore Europe Oil & Gas conference and Exhibition held in Aberdeen, UK. 8-11 Sep 2009.*
- Aasen, J. (2016). PET 600. Well Completion curriculum - Productivity of horizontal wells. Department of Petroleum Engineering, UiS.
- Absolute Completion Technologies - Inflow control* . (2016, 03 26). Retrieved from <http://absolutect.com/flow-control/>
- Akbari, M., Gonzalez, J., & Macklin, N. (2014). Considerations for optimum inflow control devices (ICDs) selection and placement in horizontal sections. *SPE 171281. Presented at the Russian oil and gas exploration and production technical conference and exhibition held in Moscow, Russia. 14-16 Oct 2014.*
- Al-Kadem, M., AlMuhaish, A., Lee, B. O., & Least, B. (2015). First autonomous ICD installation in Saudi Arabia modeling a field case. *SPE 177997. Presented at the Saudi Arabia technical symposium and exhibition held in Al-khobar, Saudi Arabia. 21-23 Apr 2015.*
- Al-Khelaiwi, F., Muradov, K., Davies, D., & Olowoleru, D. (2009). Advanced Well Flow Control Technologies can Improve Well Cleanup. *SPE 122267. Prepared for the 2009 European Formation Damage Conference, The Netherlands 27-29 May 2009 .*
- Augustine, J. R. (2002). An investigation of the economic benefit of inflow control devices on horizontal well completions using a reservoir-wellbore coupled model. *SPE 78293. Presented at the 13th European petroleum conference held in Aberdeen, Scotland, UK. 29-31 Oct 2002.*
- Babu, D., & Odeh, A. (1989). Productivity of a Horizontal well. *SPE 18298. Presented at the Annual Technical conference and exhibition held in Houston, US. 2-5 Oct 1989.*
- Bellarby, J. (2009). *Well Completion Design* (1st. ed.). Amsterdam, The Netherlands: Elsevier.
- Bennion, B. (1999). Formation Damage-The impairment of the invisible, by the inevitable and uncontrollable, resulting in an inderterminate reduction of the unquantifiable. *Journal of Canadian Petroleum Technology 38(2). February 1999, 11-17.*
- Bensnes Torbergsen, H.-E., & Aadnoy, B. (2010). *Application and design of passive inflow control devices on the Goliat oil producer wells. MSc. Thesis. UiS-University of Stavanger. Faculty of Science and Technology - Petroleum Engineering.*
- Besson, J. (1990). Performance of Slanted and horizontal wells on an anisotropic medium. *SPE 20965. Presented at the European Conference held in La Hague, The Netherlands, 22-24 Oct 1990.*
- Breitmeier, J. M., Tosch, W. C., Adewumi, M. A., & Miller, M. N. (1989). Investigation of radial invasion of mud filtrate in porous media. *SPWLA-1989-S. Presented at the Thirtieth annual logging symposium. 11-14 Jun 1989.*

- Civan, F. (2007). *Reservoir Formation Damage: Fundamentals, modeling, assesment and mitigation* (2nd ed.). Burlington, USA: Elsevier.
- David, L., Russell, L., & Wenwu, H. (2014). Deciphering Return permeabilities. *SPE 168119. Presented at SPE International symposium and Exhibition on formation damage control held in Lafayette, USA, 26-28 Feb 2014.*
- Ding, Y., Longeron, G., Renard, G., & Audibert, A. (2002). Modeling of both near-wellbore damage and natural cleanup of horizontal wells drilled with a water-based mud. *SPE 73733. Presented at SPE International symposium and exhibition of Formation damage control held in Lafayette, 20-21 Feb 2012.*
- Economides, M., Brand, C., & Frick, T. (1996). Well configurations in anisotropic reservoirs. *SPE 27980. Presented at the University of Tulsa centennial petroleum engineering symposium held in Tulsa, 29-31 Aug 1996.*
- Egerman, P., Lamy, F., & Longeron, D. (2002). A New Methodology To Derive Both Relative Permeability And Effective Permeability Reduction Profile From Numerical Simulations Of Formation Damage Experiments. *SPWLA-2002-v43n4a2. Society of Professional Well Log Analysts. Presented at SCA Symposium Proceedings, Edinburgh, Sept. 17-19,2001.*
- Garcia , L. A., Coronado, M. P., Russell, R. D., Garcia, G. A., & Peterson, E. R. (2009). The first passive inflow control device that maximizes productivity during every phase of a well's life. *IPTC 13863. Presented at the International petroleum technology conference held in Doha, Qatar, 7-9 Dec 2009.*
- Gimre, J., Aadnoy, B. S., & Sukkestad, T. (2012). *Efficiency of ICV/ICD Systems. MSc. Thesis. UiS- University of Stavanger. Faculty of Science and Technology - Industrial Economy/Reservoir and Project Management.*
- Halvorsen, M., Elseth, G., & Naevdal, O. (2012). Increased oil production at Troll by autonomous inflow control with RCP valves. *SPE 159634. Presented at the Annual technical conference and exhibition held in San Antonio, Texas, USA, 8-10 Oct 2012.*
- Han, L., Lohne, A., Stevenson, B., & Stavland, A. (2005). Making sense of return permeability data measured in the Laboratory. *SPE 94715. Presented at the SPE European formation damage conference held in Scheveningen, The Netherlands, 25-27 May 2005.*
- Jones, C., Morgan, Q., Beare, S., Awid, A., & Parry, K. (2009). Design, testing, qualification and application of orifice type inflow control device. *IPTC 13292. Presented at the International Petroleum technology conference held in Doha, Qatar. 7-9 Dec 2009.*
- Joshi, S. (1988). Augmentation of well productivity with slant and horizontal wells. *SPE 15375. Journal of Petroleum Technology.*
- Kamal, M. M. (2009). *Transient Well Testing* (Vol. 23). Richardson, TX - USA: Society of Petroleum Engineers.

- Kasa, N., Hamouda, A., Midttveit, O., & Siamos, A. (2011). *Production performance analysis of well with different inflow technologies*. MSc. Thesis. UiS-University of Stavanger. Faculty of Science and Technology - Petroleum Engineering.
- Kuchuk, F. J. (1995). Well testing and interpretation for horizontal wells. *SPE 25232*. Presented at the Annual Technical conference and exhibition, Dallas, 6-9 Oct 1991.
- Landmark NETool Technical Manual. (2014). *NETool 5000.0.4.x Technical Manual*. Houston, Texas: Halliburton.
- Least, B., Greci, S., Huffer, R., Rajan, R., & Golbeck, H. (2014). Steam flow test for comparing performance of nozzle, tube, and fluidic diode autonomous ICDs in SAGD wells. *SPE 170083*. Presented at the Heavy oil conference-Canada held in Alberta, Canada, 10-12 Jun 2014.
- Lohne, A. (2002). Maximize Technical documentation. *Report RF-2004/044*, 56.
- Lohne, A., Han, L., van der Zwaag, C., van Velzen, H., Mathisen, A.-M., Twynam, A., et al. (2010). Formation-Damage and Well Productivity Simulation. *SPE 122241*. Presented at the 8th European Formation Damage conference, Scheveningen, The Netherlands, 27-29 May 2009.
- Mathiesen, V., Werswick, B., & Aakre, H. (2014). The next generation inflow control, the next step to increase oil recovery on the Norwegian continental shelf. *SPE 169233*. Presented at the Bergen one day seminar held in Grieghallen, Bergen, Norway. 2 Apr. 2014.
- Odeh, A., & Babu, D. (1990). Transient flow behaviour of horizontal wells: Pressure drawdown and buildup analysis. *SPE 18802*. *SPEFE (1)*:7-15.
- Ozkan, S. E., Hacıislamoglu, M., & Raghavan, R. (1995). Effect of conductivity on horizontal well pressure behaviour. *SPE 24683*. *SPE Advance technology Series 3 (1)*.
- Rana, R., & Sharma, M. (2001). The relative importance of solids and filtrate invasion on the flow initiation pressure. *SPE 68949*. Presented at the European Formation damage conference held in The Hague, The Netherlands, 21-22 May 2001.
- Schlumberger - Inflow control devices*. (2016, 03 26). Retrieved 2016, from http://www.slb.com/services/completions/sand_control/sandscreens/inflow_control_device_s.aspx
- Schlumberger oilfield glossary. (2016). *Schlumberger oilfield glossary*. Retrieved 03 26, 2016, from <http://www.glossary.oilfield.slb.com/>
- Stone, T., Wardell-Yerburgh, P., Dyer, S., Mikhailov, D., Kotlyar, L., Neylon, K., et al. (2014). Flow control valves and inflow control devices optimized for wellbore cleanup and production. *IPTC 18002*. Presented at the International Petroleum technology conference held in Kuala Lumpur, Malaysia. 10-12 Dec 2014.
- Sunbul, A., Lauritzen, J., Hembling, D., Majdpour, A., Raffn, A., Zeybek, M., et al. (2008). Case histories of improved horizontal well clean up and sweep efficiency with nozzle based inflow control devices (ICD) in Sandstone and Carbonate reservoir. *SPE 120795*. Presented at the Saudi Arabia section technical symposium held in Al-khobar, Saudi Arabia. 10-12 May 2008.

- Suri, A., & Sharma, M. M. (2005). Clean up of internal filter cake during flowback. *PhD. Dissertation. Presented to the Faculty of the Graduate School of The University of Texas at Austin, 389.*
- van der Zwaag, C., Omland, T., & Vandbakk, T. (2012). Dynamic filtration: Seepage losses on Tyrihans. *SPE 151678. Presented at the SPE International symposium and Exhibition on Formation damage control held in Lafayette, USA, 15-17 Feb 2012.*
- Zain, Z., & Sharma, M. (2001). Mechanism of mudcake removal during flowback. *SPE 74972. Presented at the International Symposium on Formation damage, Lafayette, USA. 23-24 Feb 2001.*

Appendix A

ILF – Intermediate Linear Flow regime Equation

In case the clean-up period occurs during ILF-Intermediate linear flow regime, the pressure can be calculated as given by Kamal, (2009) in Equation 33.

$$P_{wD} \approx \sqrt{\frac{k}{k_y}} \left[\sqrt{\pi t_D} + \frac{1}{2L_D} (S_z + S) \right]$$

$$\Delta P_{wf} = \frac{8.128qB\mu}{L_h h \sqrt{\phi C_t k_y}} \sqrt{t} + \frac{141.2qB\mu}{L_h \sqrt{k_y k_z}} (S_z + S)$$

Equation 33, ILF pressure transient

Where,

k → Permeability, [mD]

k_x → Permeability in x direction, [mD]

k_y → Permeability in y direction, [mD]

k_z → Vertical permeability [mD]

P_{wD} → Dimensionless pressure

t_D → Dimensionless time

L_D → Dimensionless length

S_z → Pseudo skin

ΔP_{wf} → Pressure drop, [psi]

q → Flow rate, (bpd)

B → Volumetric factor, $\left[\frac{\text{bbl}}{\text{STB}} \right]$

μ → Viscosity, [cP]

S → Skin

ϕ → Porosity, fraction

t → Time, [hr]

L_h → Horizontal well length

h → Thickness, [ft]

Boundary conditions are imposed to pressure transient solution in time scales as follow:

$$\frac{160\phi C_t \mu L_h^2}{k_x} \geq t \geq \max \left\{ \frac{1800Z_w \phi C_t \mu}{k_z}; \frac{1800(h - Z_w)^2 \phi C_t \mu}{k_z} \right\}$$

Equation 34, ILF Time limit in pressure transient

Where,

$C_t \rightarrow$ Total compressibility, [psi⁻¹]

$Z_w \rightarrow$ Distance to mid height, [ft]

ILF flow regime happens when an important condition is achieved, and it is given by Equation 35. The graphical analysis needs at least half log scale to be valid.

$$L_h \geq 20h \sqrt{\frac{k}{k_z}}$$

Equation 35, ILF condition

Condition expressed in Equation 35 may not always be achieved as practical, so ILF flow regime can even be assumed as given by Odeh & Babu, (1990).

Pseudo skin due to partial penetration in the vertical plane corresponds to the term S_z in Equation 33. Pseudo skin is calculated using Equation 36.

$$S_z = -\ln\left(\frac{r_w}{h}\right) + \frac{1}{4}\ln\left(\frac{k_y}{k_z}\right) - \ln\left(\sin\frac{\pi Z_w}{h}\right) - 1,838$$

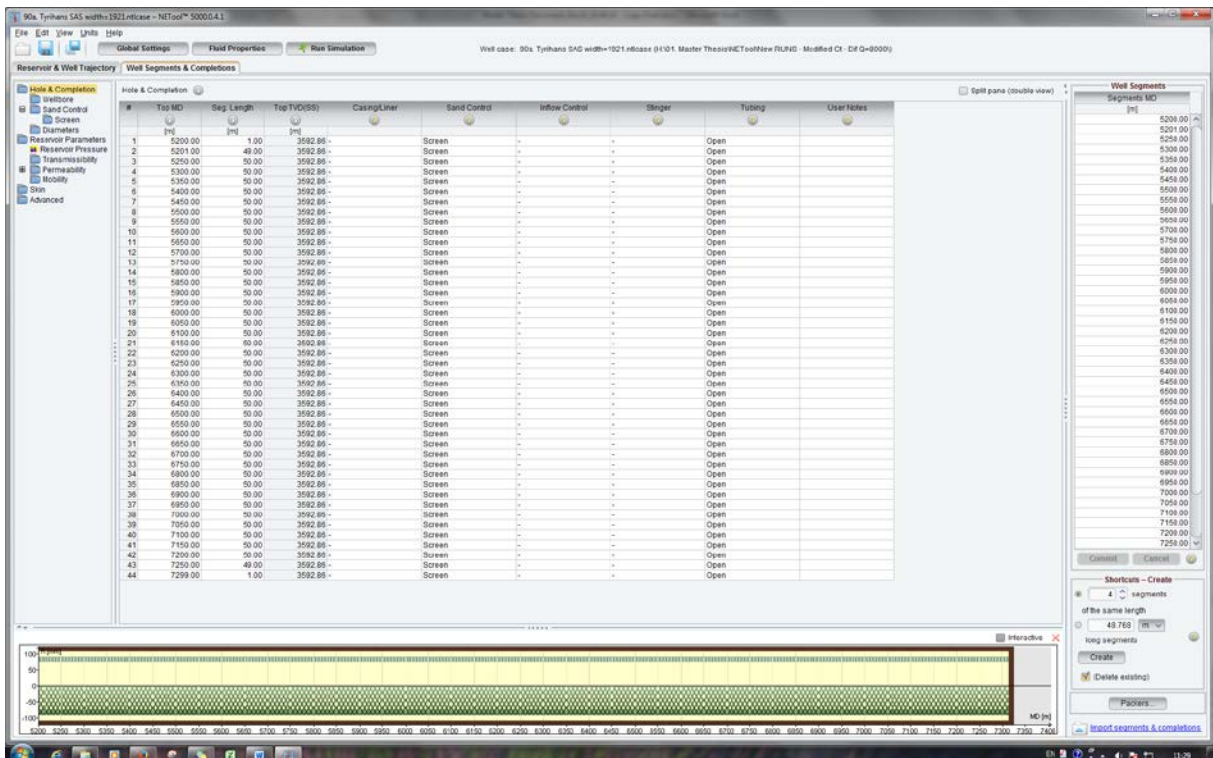
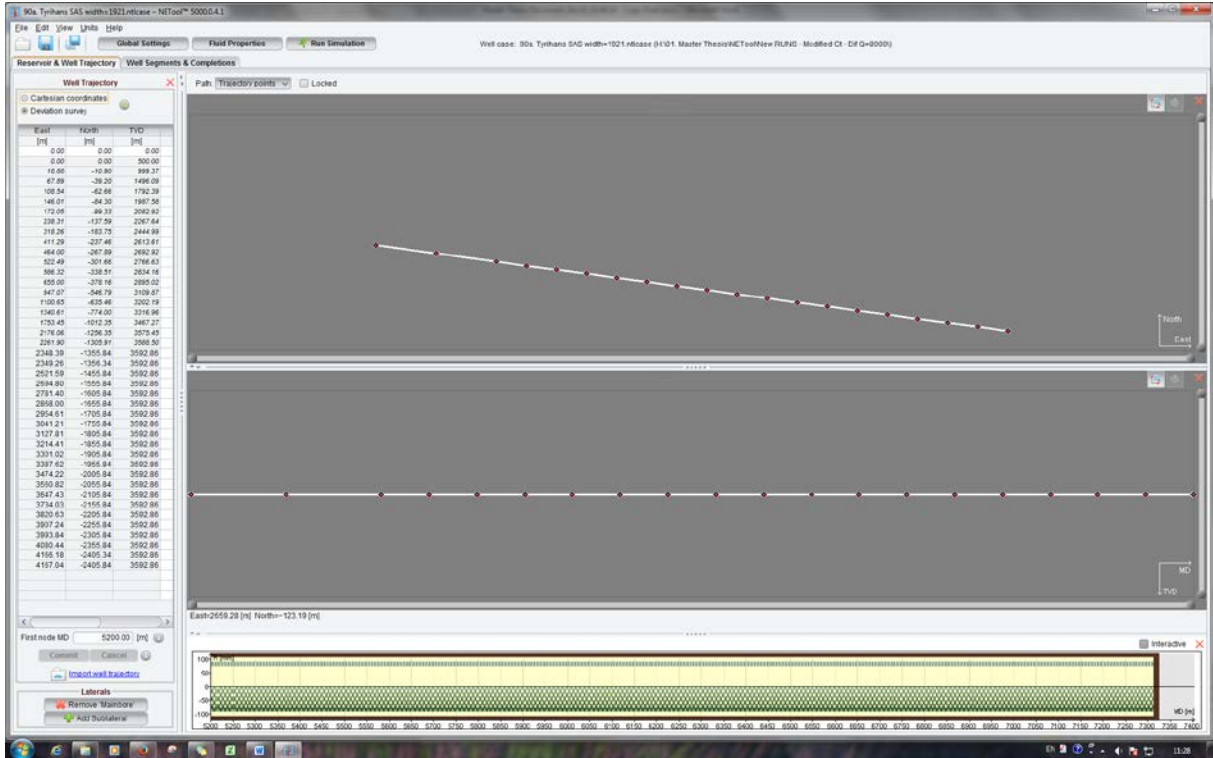
Equation 36, Pseudo skin – ILF

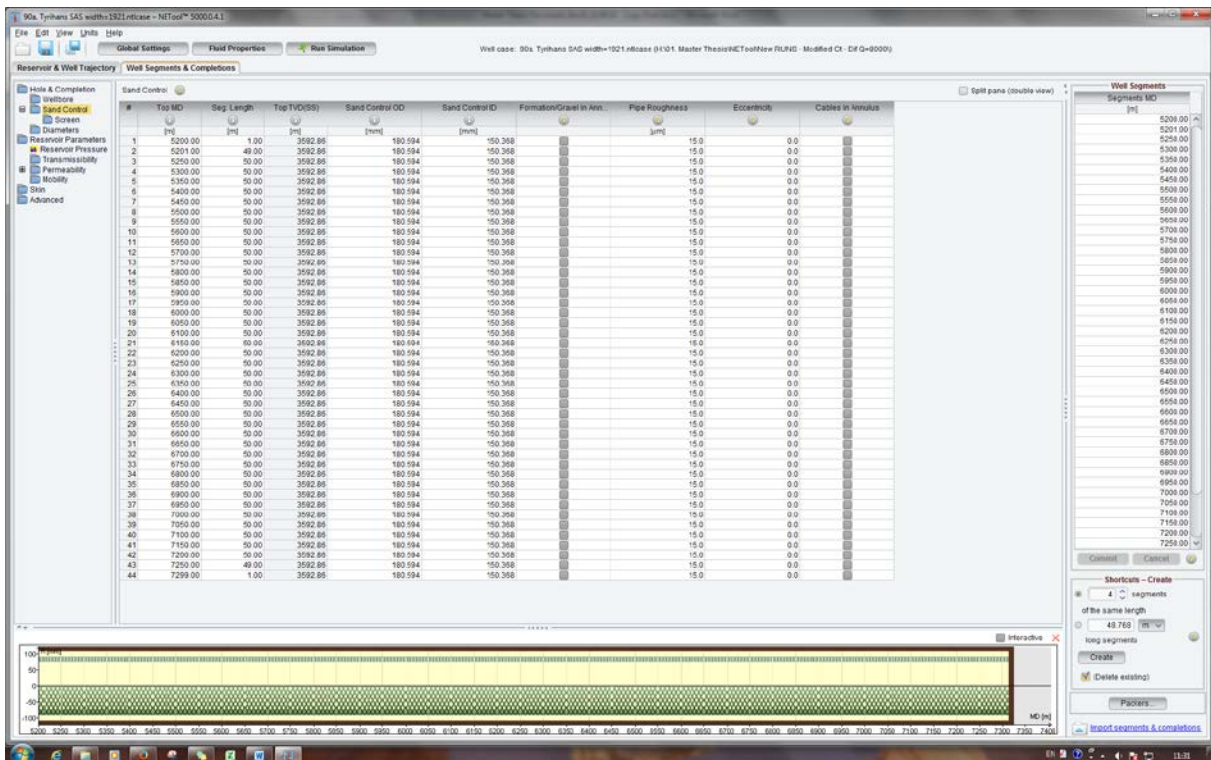
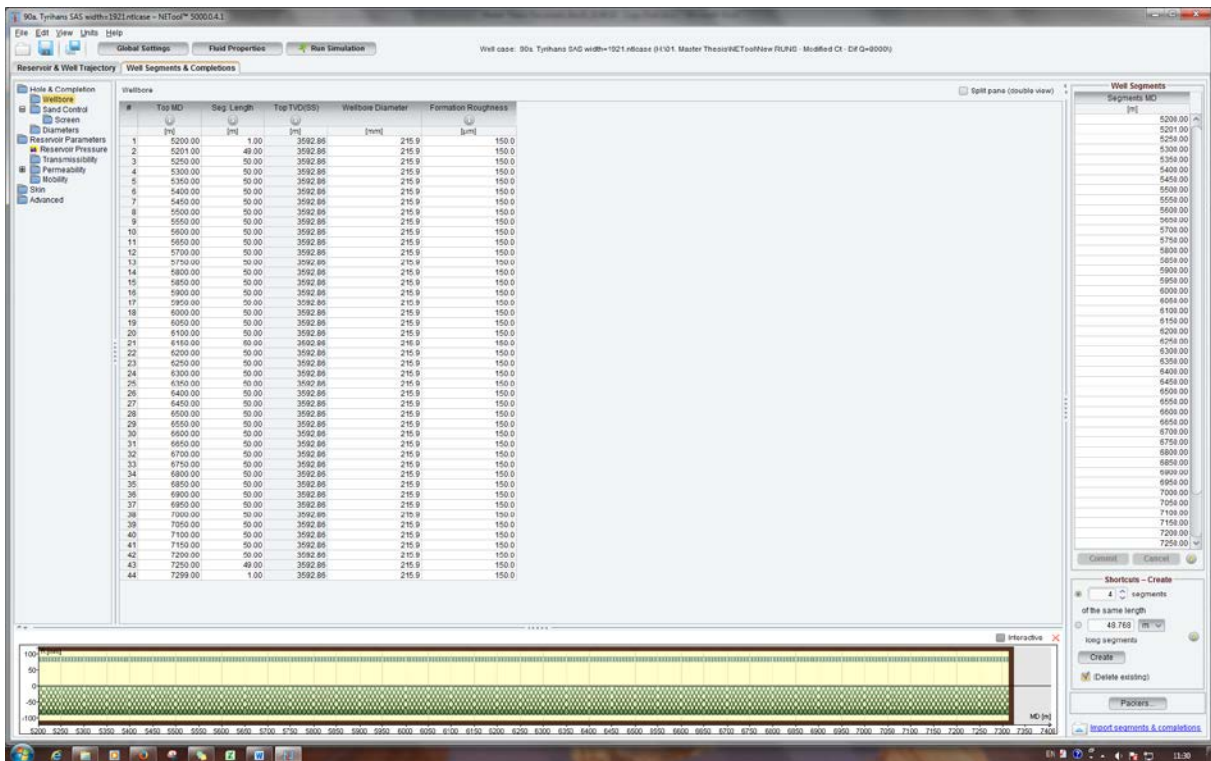
Where,

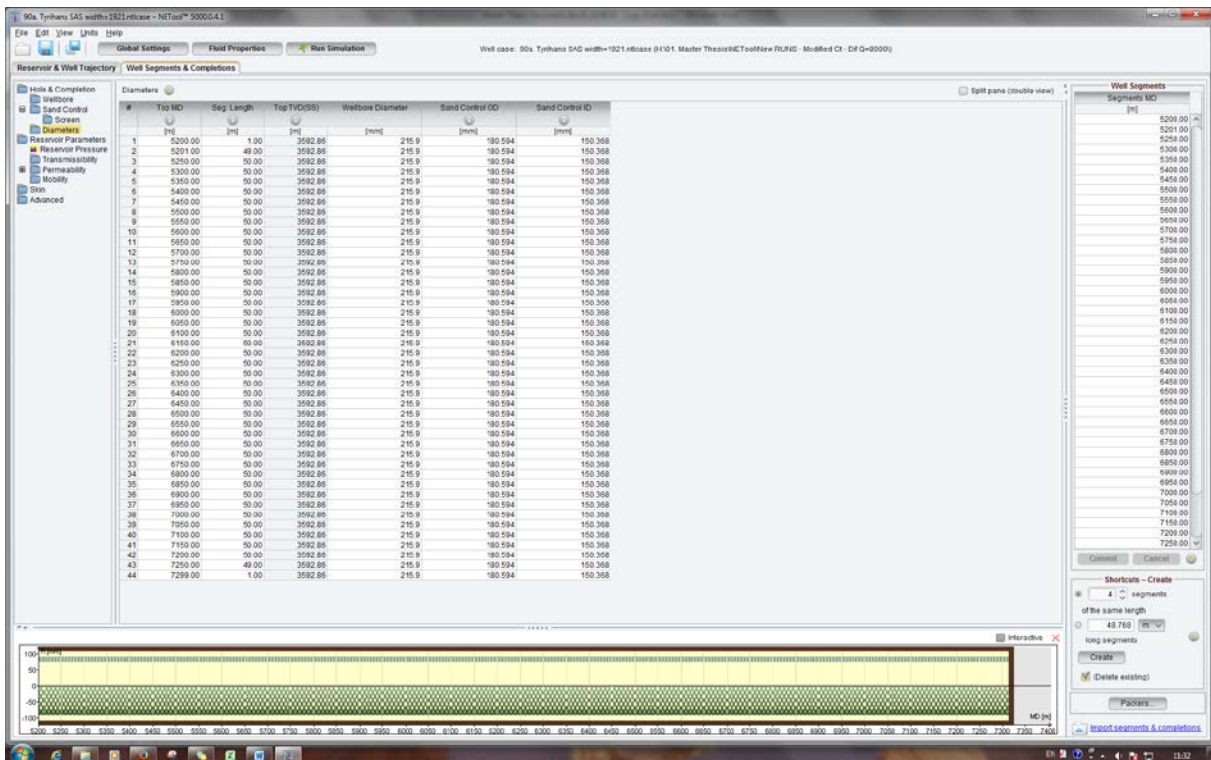
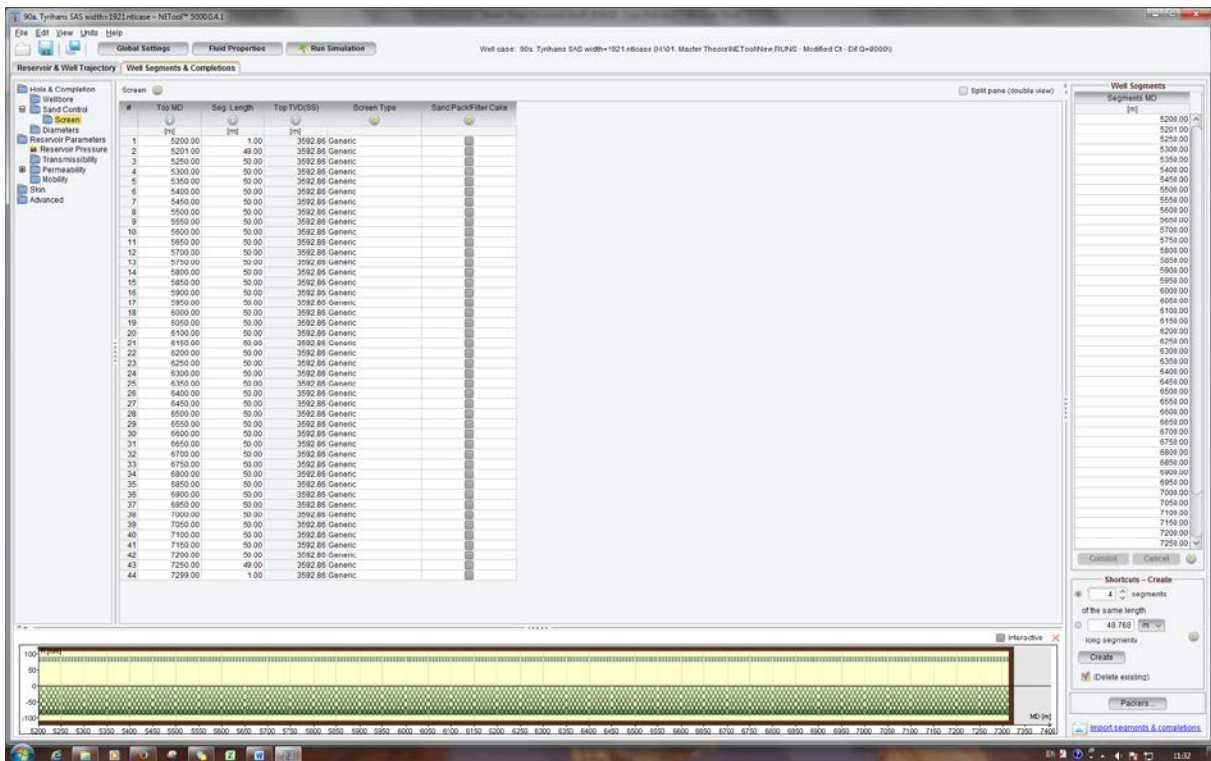
$r_w \rightarrow$ Wellbore radius, [ft]

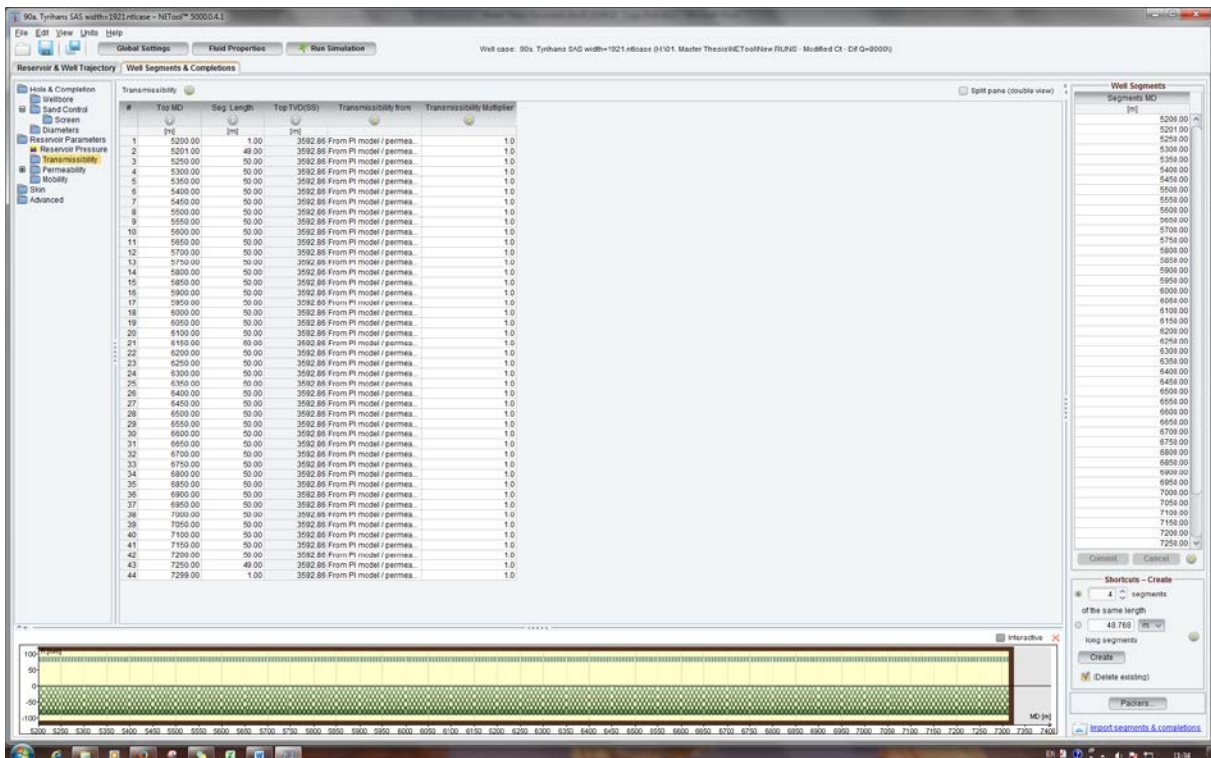
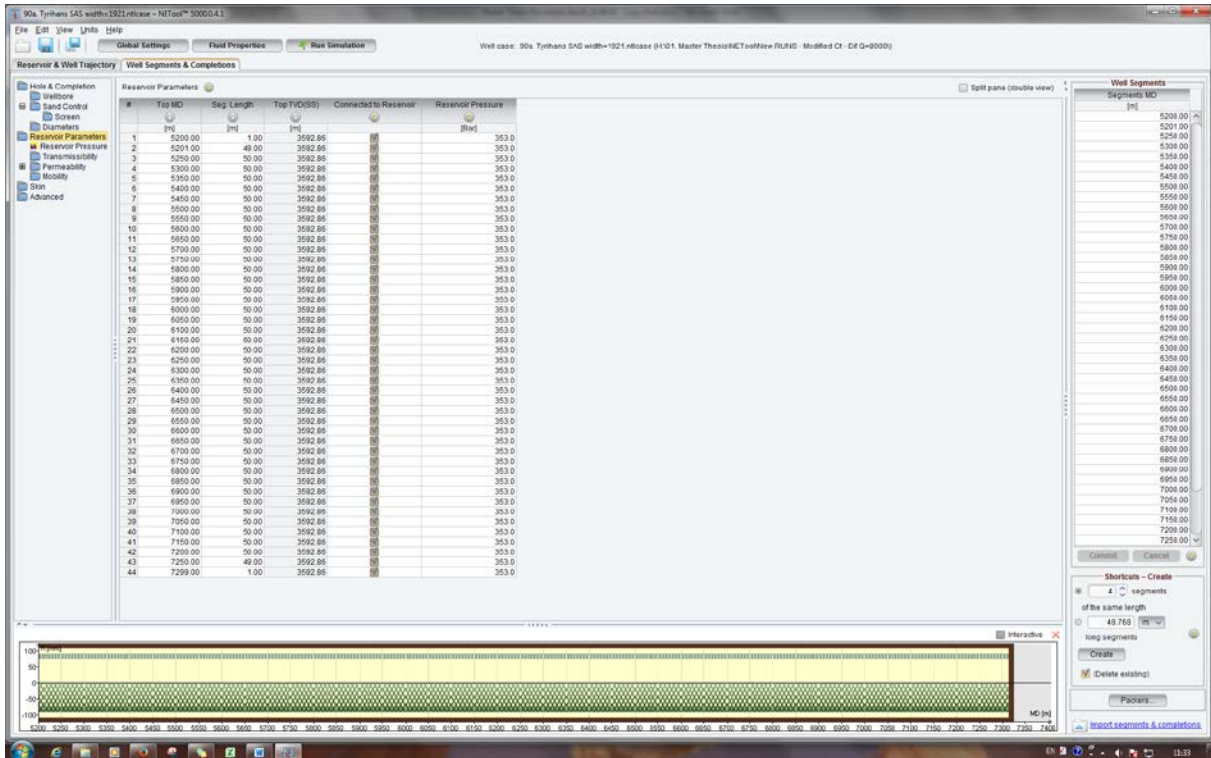
Appendix B

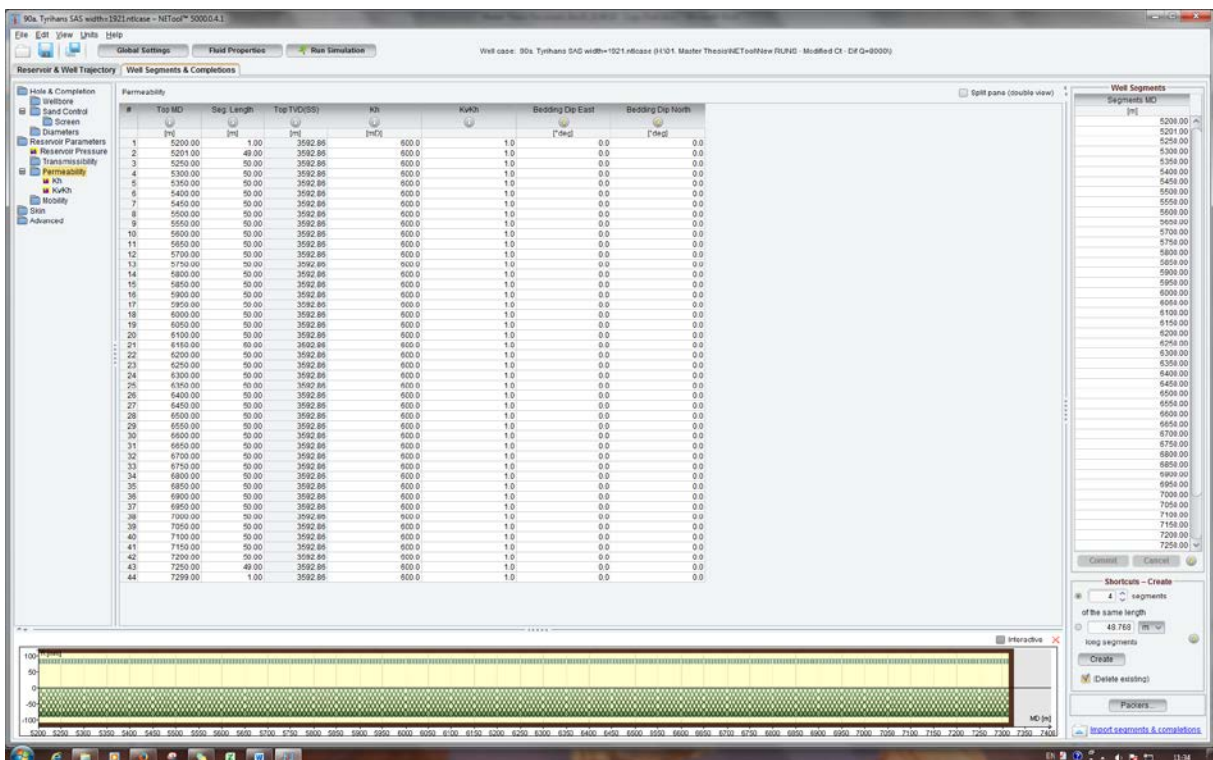
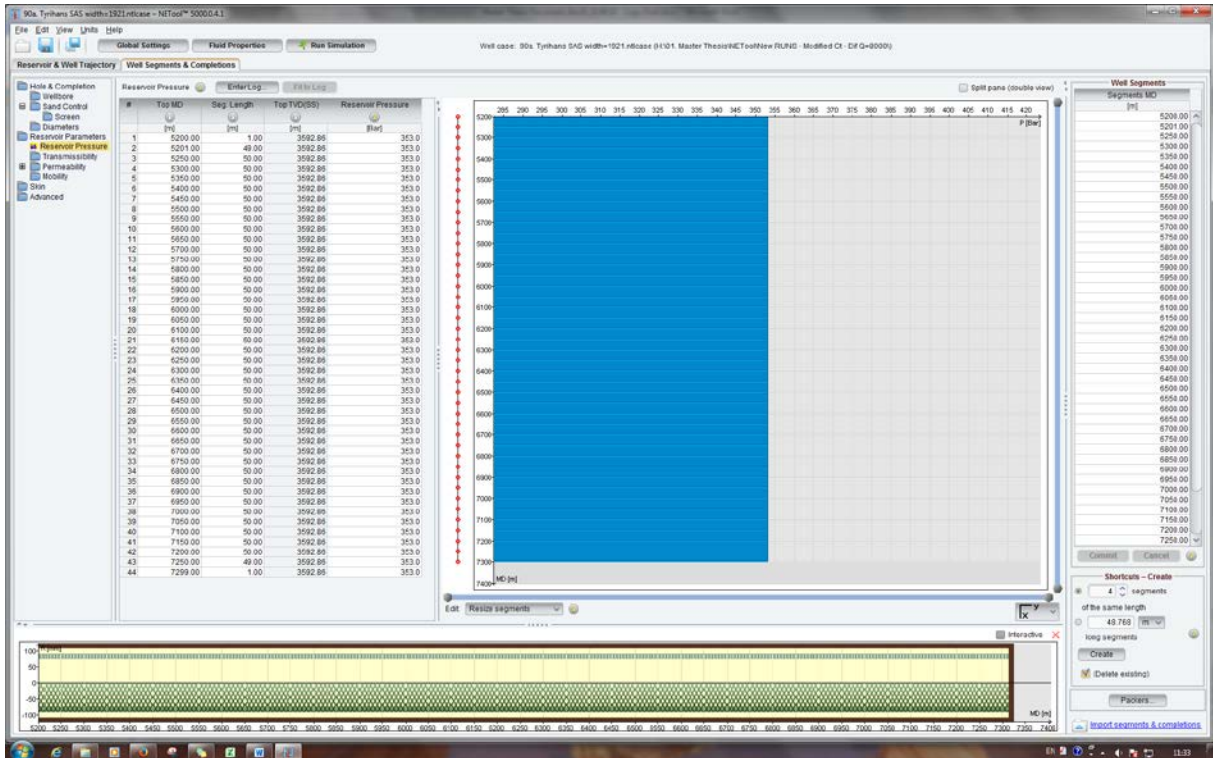
NETool™ – SAS Completion Setup

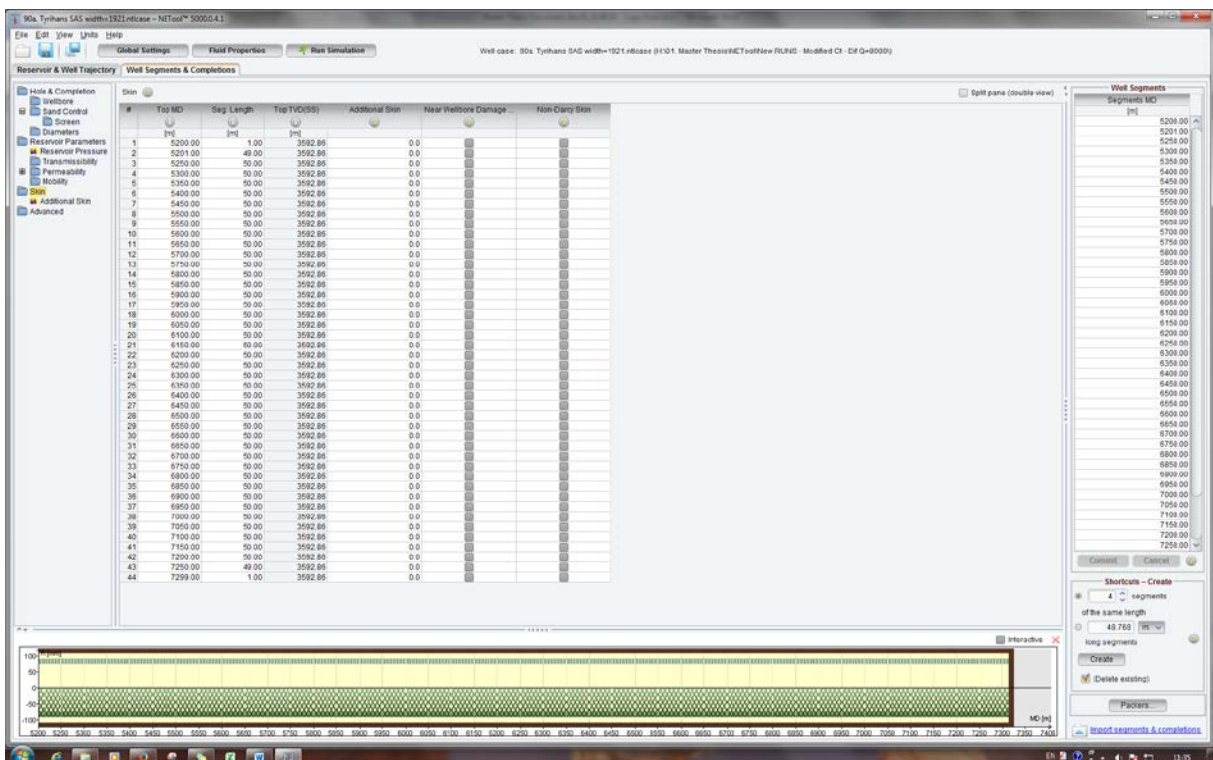
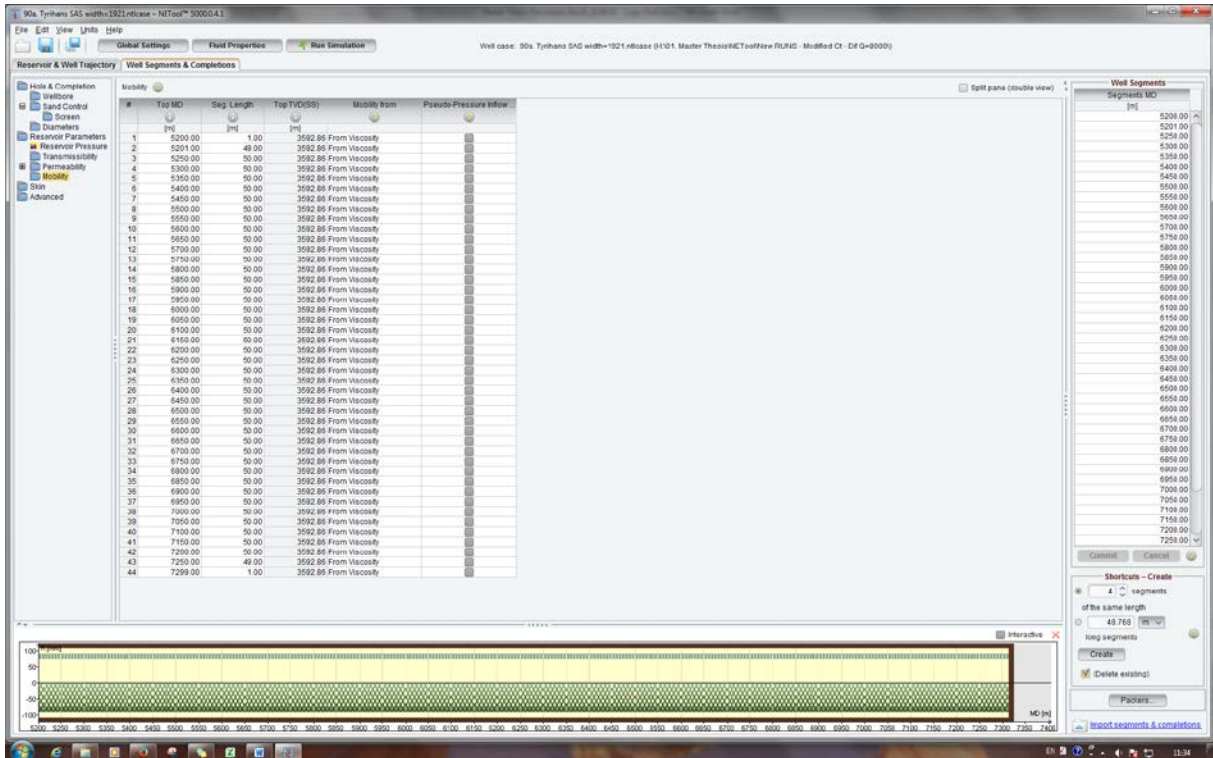


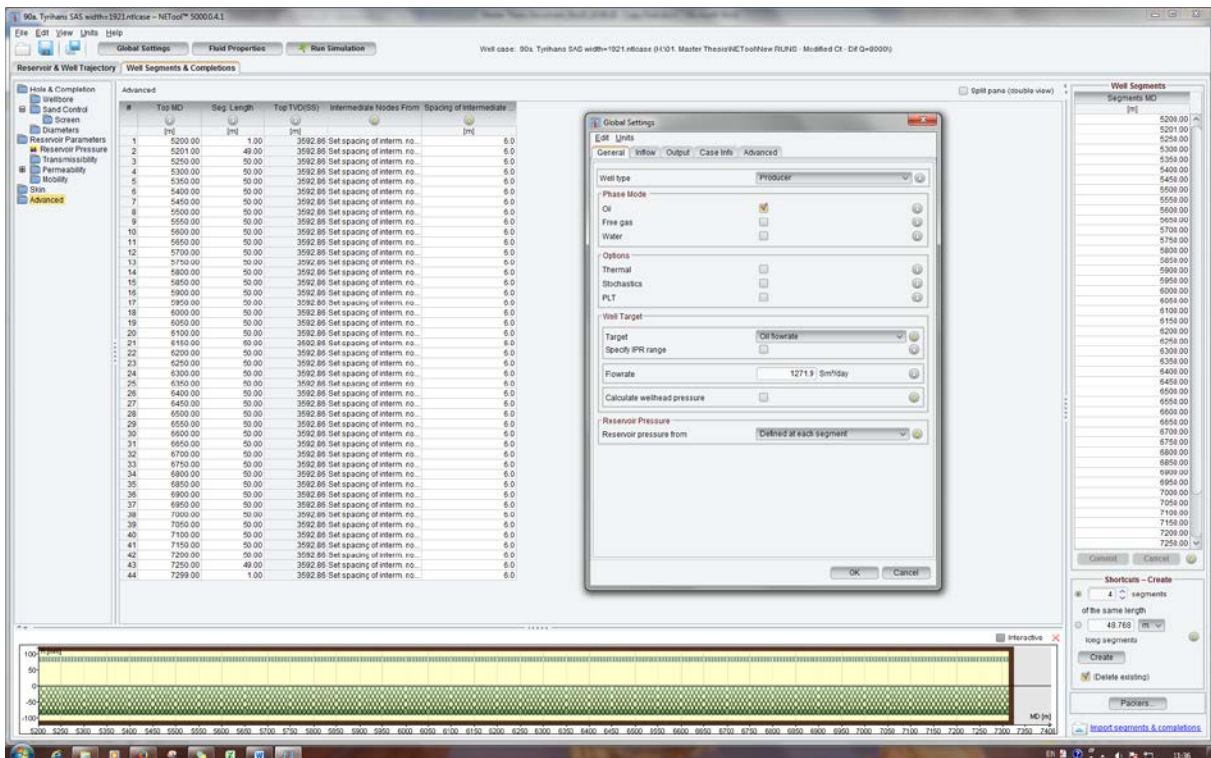
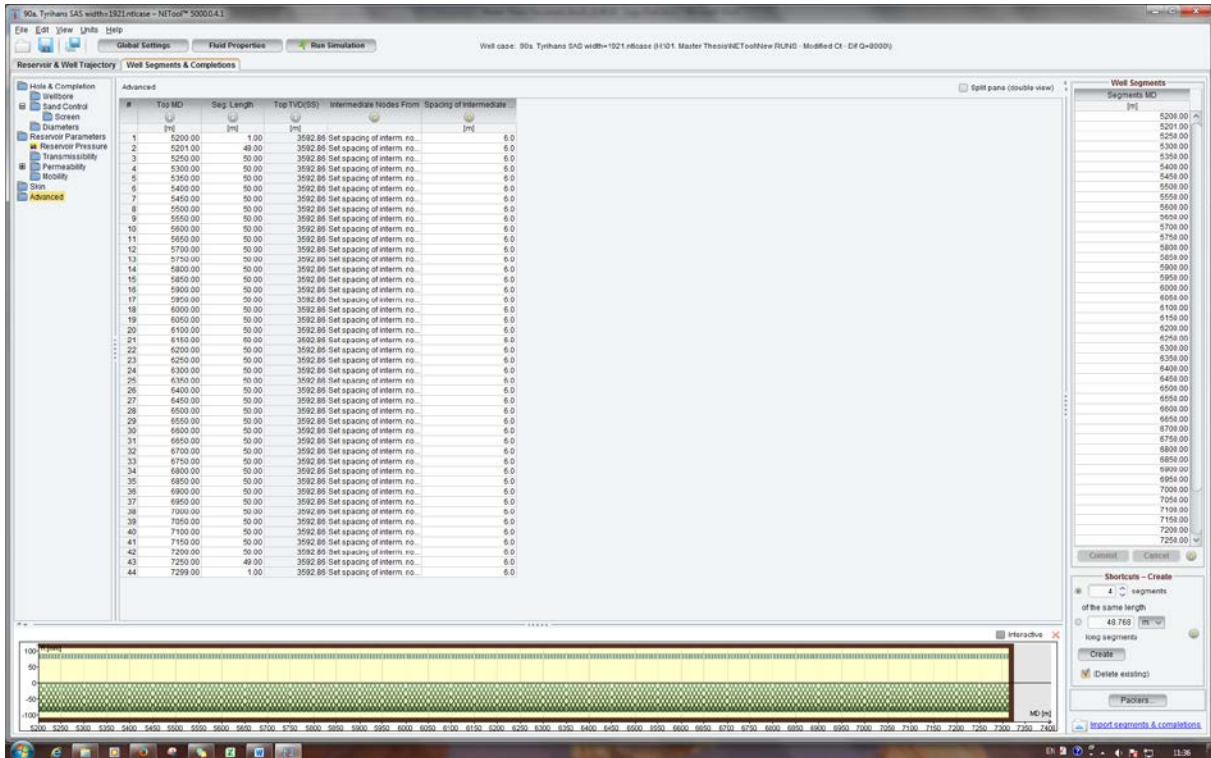












Reservoir width: 1921 m

The screenshot shows the NETool interface for a well case named '90s_Tyhans SAS width=1921mCase - NETool™ 5000.04.1'. The 'Global Settings' dialog box is open, showing the 'Advanced' tab. The 'PI Model' is set to 'Joint (horizontal well only)'. The 'Well PI multiplier' is set to 1.0. The 'Horizontal PI Model Settings' section shows 'Reservoir thickness' as 34.8991 m and 'Reservoir width' as 1921.8 m. The 'Well Segments' table on the right lists 44 segments, each 49.00 m long, with a total length of 4976.00 m. The 'Well Segments' table is as follows:

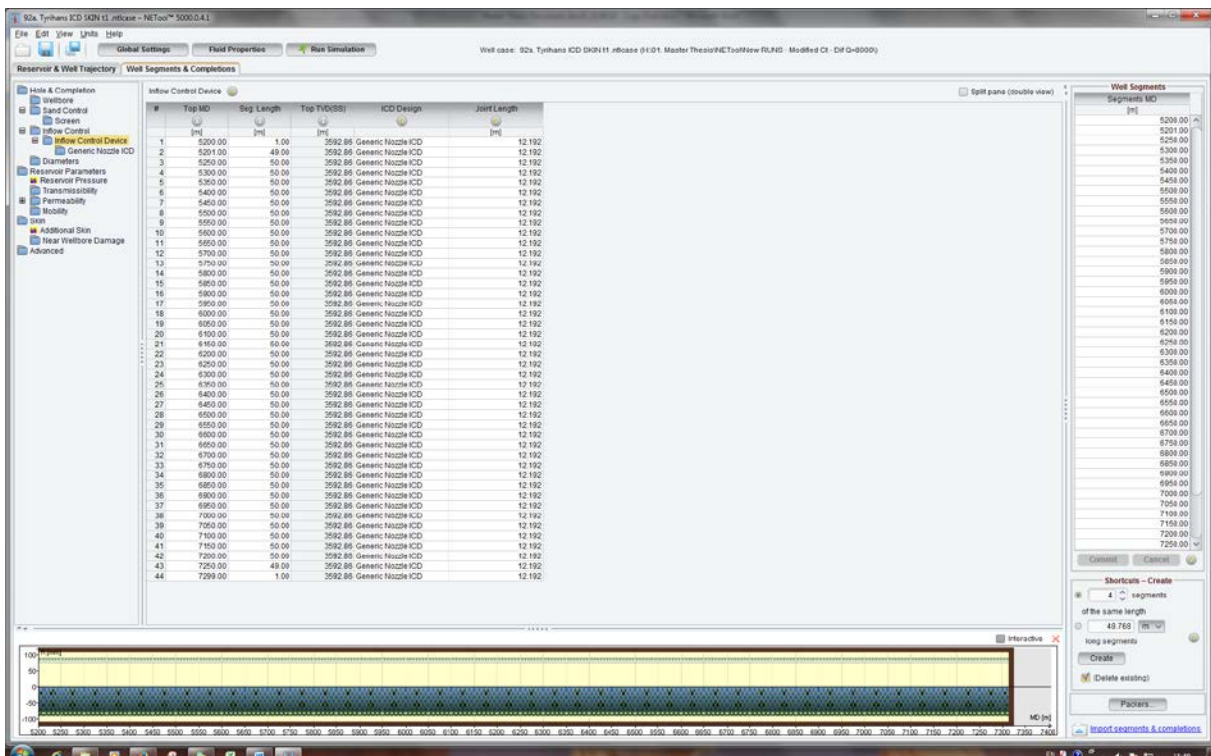
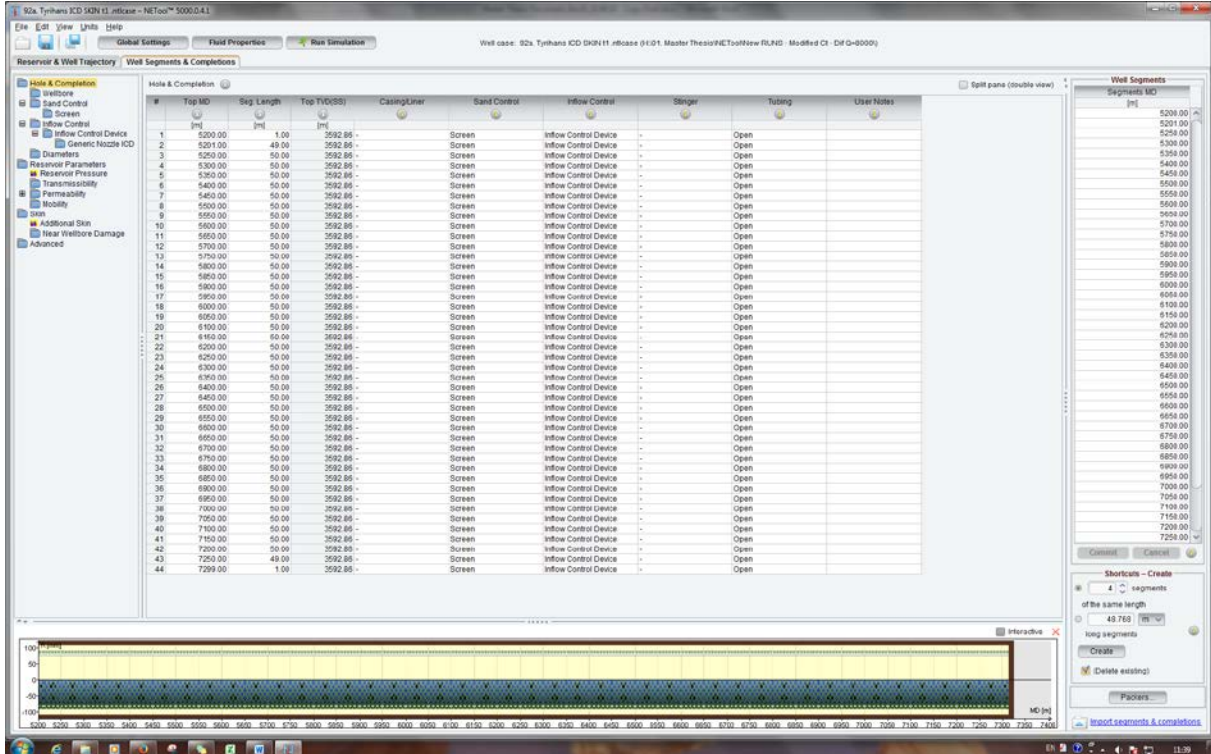
Segment ID	Top MD [m]	Seg. Length [m]	Top TVD(SS) [m]	Intermediate Nodes From [m]	Spacing of Intermediate [m]
1	5200.00	49.00	3592.89	Set spacing of intern. no.	6.0
2	5201.00	49.00	3592.89	Set spacing of intern. no.	6.0
3	5202.00	49.00	3592.89	Set spacing of intern. no.	6.0
4	5300.00	50.00	3592.89	Set spacing of intern. no.	6.0
5	5300.00	50.00	3592.89	Set spacing of intern. no.	6.0
6	5400.00	50.00	3592.89	Set spacing of intern. no.	6.0
7	5400.00	50.00	3592.89	Set spacing of intern. no.	6.0
8	5500.00	50.00	3592.89	Set spacing of intern. no.	6.0
9	5500.00	50.00	3592.89	Set spacing of intern. no.	6.0
10	5600.00	50.00	3592.89	Set spacing of intern. no.	6.0
11	5600.00	50.00	3592.89	Set spacing of intern. no.	6.0
12	5700.00	50.00	3592.89	Set spacing of intern. no.	6.0
13	5700.00	50.00	3592.89	Set spacing of intern. no.	6.0
14	5800.00	50.00	3592.89	Set spacing of intern. no.	6.0
15	5800.00	50.00	3592.89	Set spacing of intern. no.	6.0
16	5900.00	50.00	3592.89	Set spacing of intern. no.	6.0
17	5900.00	50.00	3592.89	Set spacing of intern. no.	6.0
18	6000.00	50.00	3592.89	Set spacing of intern. no.	6.0
19	6000.00	50.00	3592.89	Set spacing of intern. no.	6.0
20	6100.00	50.00	3592.89	Set spacing of intern. no.	6.0
21	6100.00	50.00	3592.89	Set spacing of intern. no.	6.0
22	6200.00	50.00	3592.89	Set spacing of intern. no.	6.0
23	6200.00	50.00	3592.89	Set spacing of intern. no.	6.0
24	6300.00	50.00	3592.89	Set spacing of intern. no.	6.0
25	6300.00	50.00	3592.89	Set spacing of intern. no.	6.0
26	6400.00	50.00	3592.89	Set spacing of intern. no.	6.0
27	6400.00	50.00	3592.89	Set spacing of intern. no.	6.0
28	6500.00	50.00	3592.89	Set spacing of intern. no.	6.0
29	6500.00	50.00	3592.89	Set spacing of intern. no.	6.0
30	6600.00	50.00	3592.89	Set spacing of intern. no.	6.0
31	6600.00	50.00	3592.89	Set spacing of intern. no.	6.0
32	6700.00	50.00	3592.89	Set spacing of intern. no.	6.0
33	6700.00	50.00	3592.89	Set spacing of intern. no.	6.0
34	6800.00	50.00	3592.89	Set spacing of intern. no.	6.0
35	6800.00	50.00	3592.89	Set spacing of intern. no.	6.0
36	6900.00	50.00	3592.89	Set spacing of intern. no.	6.0
37	6900.00	50.00	3592.89	Set spacing of intern. no.	6.0
38	7000.00	50.00	3592.89	Set spacing of intern. no.	6.0
39	7000.00	50.00	3592.89	Set spacing of intern. no.	6.0
40	7100.00	50.00	3592.89	Set spacing of intern. no.	6.0
41	7100.00	50.00	3592.89	Set spacing of intern. no.	6.0
42	7200.00	50.00	3592.89	Set spacing of intern. no.	6.0
43	7200.00	49.00	3592.89	Set spacing of intern. no.	6.0
44	7299.00	1.00	3592.89	Set spacing of intern. no.	6.0

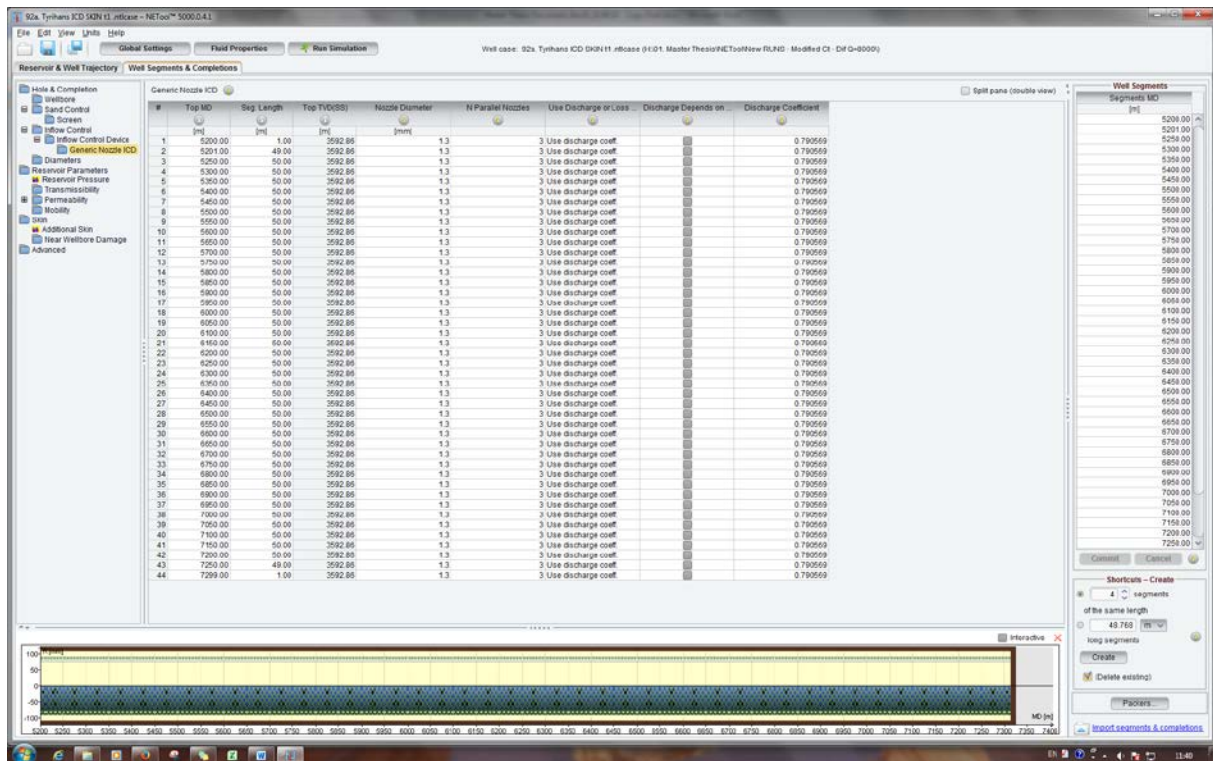
The screenshot shows the NETool interface for the same well case. The 'Global Settings' dialog box is open, showing the 'Advanced' tab. The 'PI Model' is set to 'Joint (horizontal well only)'. The 'Well PI multiplier' is set to 1.0. The 'Horizontal PI Model Settings' section shows 'Reservoir thickness' as 34.8991 m and 'Reservoir width' as 1921.8 m. The 'Well Segments' table on the right lists 44 segments, each 49.00 m long, with a total length of 4976.00 m. The 'Well Segments' table is as follows:

Segment ID	Top MD [m]	Seg. Length [m]	Top TVD(SS) [m]	Intermediate Nodes From [m]	Spacing of Intermediate [m]
1	5200.00	49.00	3592.89	Set spacing of intern. no.	6.0
2	5201.00	49.00	3592.89	Set spacing of intern. no.	6.0
3	5202.00	49.00	3592.89	Set spacing of intern. no.	6.0
4	5300.00	50.00	3592.89	Set spacing of intern. no.	6.0
5	5300.00	50.00	3592.89	Set spacing of intern. no.	6.0
6	5400.00	50.00	3592.89	Set spacing of intern. no.	6.0
7	5400.00	50.00	3592.89	Set spacing of intern. no.	6.0
8	5500.00	50.00	3592.89	Set spacing of intern. no.	6.0
9	5500.00	50.00	3592.89	Set spacing of intern. no.	6.0
10	5600.00	50.00	3592.89	Set spacing of intern. no.	6.0
11	5600.00	50.00	3592.89	Set spacing of intern. no.	6.0
12	5700.00	50.00	3592.89	Set spacing of intern. no.	6.0
13	5700.00	50.00	3592.89	Set spacing of intern. no.	6.0
14	5800.00	50.00	3592.89	Set spacing of intern. no.	6.0
15	5800.00	50.00	3592.89	Set spacing of intern. no.	6.0
16	5900.00	50.00	3592.89	Set spacing of intern. no.	6.0
17	5900.00	50.00	3592.89	Set spacing of intern. no.	6.0
18	6000.00	50.00	3592.89	Set spacing of intern. no.	6.0
19	6000.00	50.00	3592.89	Set spacing of intern. no.	6.0
20	6100.00	50.00	3592.89	Set spacing of intern. no.	6.0
21	6100.00	50.00	3592.89	Set spacing of intern. no.	6.0
22	6200.00	50.00	3592.89	Set spacing of intern. no.	6.0
23	6200.00	50.00	3592.89	Set spacing of intern. no.	6.0
24	6300.00	50.00	3592.89	Set spacing of intern. no.	6.0
25	6300.00	50.00	3592.89	Set spacing of intern. no.	6.0
26	6400.00	50.00	3592.89	Set spacing of intern. no.	6.0
27	6400.00	50.00	3592.89	Set spacing of intern. no.	6.0
28	6500.00	50.00	3592.89	Set spacing of intern. no.	6.0
29	6500.00	50.00	3592.89	Set spacing of intern. no.	6.0
30	6600.00	50.00	3592.89	Set spacing of intern. no.	6.0
31	6600.00	50.00	3592.89	Set spacing of intern. no.	6.0
32	6700.00	50.00	3592.89	Set spacing of intern. no.	6.0
33	6700.00	50.00	3592.89	Set spacing of intern. no.	6.0
34	6800.00	50.00	3592.89	Set spacing of intern. no.	6.0
35	6800.00	50.00	3592.89	Set spacing of intern. no.	6.0
36	6900.00	50.00	3592.89	Set spacing of intern. no.	6.0
37	6900.00	50.00	3592.89	Set spacing of intern. no.	6.0
38	7000.00	50.00	3592.89	Set spacing of intern. no.	6.0
39	7000.00	50.00	3592.89	Set spacing of intern. no.	6.0
40	7100.00	50.00	3592.89	Set spacing of intern. no.	6.0
41	7100.00	50.00	3592.89	Set spacing of intern. no.	6.0
42	7200.00	50.00	3592.89	Set spacing of intern. no.	6.0
43	7200.00	49.00	3592.89	Set spacing of intern. no.	6.0
44	7299.00	1.00	3592.89	Set spacing of intern. no.	6.0

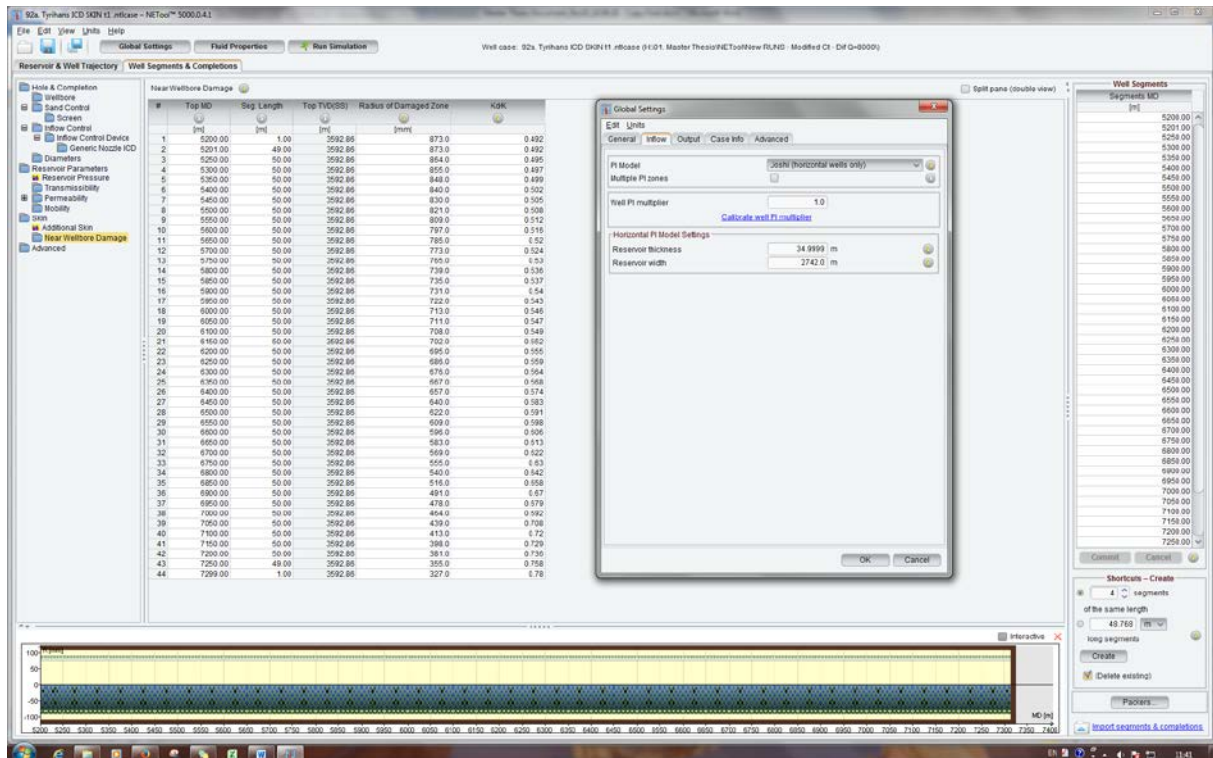
Appendix C

NETool™ – ICD Completion Setup





Return Permeability – Damage zone (Reservoir width: 2742 m)



Appendix D

MAXIMIZE Software Setup

01.Tyrihans Mud 7mic NEW

5. Components | 6. Simulation parameters | 7. Well / boundaries
 1. Runtype | 2. Grid properties | 3. Initialization | 4. Rock properties

Model description parameters

Run description
 Coreflood. Linear geometry.

Model type
 Core - Linear
 Field - Radial
 Field - Rectangular

Import grid properties from file
 Property file:

Grid resolution (number of blocks)
 Low resolution
 Medium resolution
 High resolution
 User defined
 In main flow direction (Nx): 40
 In the y-direction (Ny): 1
 Number of layers (Nz): 1

Units
 Default lab
 Default field
 User defined

01.Tyrihans Mud 7mic NEW

5. Components | 6. Simulation parameters | 7. Well / boundaries
 1. Runtype | 2. Grid properties | 3. Initialization | 4. Rock properties

Core dimensions and properties, Nx = 40, Ny = 1, Nz = 1

Total dimensions
 Core length (cm) 8
 Well radius (cm) 0
 Core diameter (cm) 3.8
 Filtercake diameter 3.4

Grid orientation
 Depth to top layer (cm) 0
 Angle (°) between X-axis and horizontal direction, clockwise 0

Properties
 Kabs (mD) 600
 Porosity (fraction) 0.25

